Analysis and Control of Multiscale Dynamics in Regional Electricity and Heat Supply Systems

Hikaru Hoshino

Analysis and Control of Multiscale Dynamics in Regional Electricity and Heat Supply Systems

A Dissertation

Presented to the Graduate School of Engineering

of Kyoto University

in Partial Fulfillment of the Requirements for the Degree of

Doctor of Philosophy

by

Hikaru Hoshino

February 2017

Abstract

Classification of dynamic phenomena (dynamics) is essential to analysis and control of electric power systems. While various dynamics evolve on a wide range of scales in space and time, it is necessary to extract the dynamics of interest through relevant mathematical modeling. For this purpose, such multiscale dynamics are classified in terms of their physical characteristics: wave, electromagnetic, electromechanical, and thermodynamic phenomena. Conventionally, this classification has been consistent with the temporal and spatial scales on which effective tools of analysis and control are developed. Namely, electric power systems have been based on the underlying principle of *scale separation*.

While electric power systems have played the most prominent role in delivering energy services, several studies have indicated that design of the next-generation energy systems cannot be looked as an isolated issue regarding electricity supply. This point of view is described by e.g. Energy Systems Integration (ESI). In this integration, multiple type of energy such as electricity, heat, and natural gas are managed consistently by utilizing interconnections between various energy systems. For example, the so-called Combined Heat and Power (CHP) technology, which exploits waste heat as a by-product of conversion of fuel into electricity, induces interaction between electric power systems and district heating and cooling networks. Due to such a interaction, energy conversion and transfer under ESI are governed by various physical laws on different scales. The dynamical principle for managing these interactions is remaining to be discussed and understood.

This dissertation takes a bottom-up approach to the problem and focuses on multiscale dynamics occurring in regional electricity and heat supply systems, which appear as district heating and cooling networks with CHP plants. Conventionally, a CHP plant has been operated on a slow time scale of heat supply and has not contributed to the fast control of power systems. However, several novel operations are now proposed for compensating variable outputs of renewable energy sources and contributing to demand response. This induces a dynamic interaction between electromechanical and thermody-

namic phenomena. For this, we introduce a rudimentary two-site system, which comprises electric and heat subsystems interconnected by two CHP plants. This dissertation conducts analysis and control of multiscale dynamics of simultaneous supply of electricity and heat through simple mathematical models of the two-site system.

In the first half of this dissertation, we analyze multiscale dynamics occurring in the two-site system. First, a stability analysis of the electric subsystem is performed to revisit the effectiveness and limitation of the conventional scale separation of power system dynamics. The conventional methods of stability analysis are applicable to evaluate the effect of the heat subsystem if the dynamics of the heat subsystem are negligible due to scale separation. If this is not the case, it is shown that the electric subsystem is possibly destabilized due to transient dynamics of the heat subsystem. Then, we analyze multiscale property of dynamics occurring in general steam supply networks. The purpose of the analysis is to derive a simple lumped-parameter model describing the system-wide dynamics of interest. To verify the correctness of the derived model, we discuss its structural stability based on the concept of Normally Hyperbolic Invariant Manifold (NHIM) in singular perturbation theory. The existence of the manifold implies a separation principle for steam supply systems, which is analogue to that for electric power systems.

The second half addresses problems of controller synthesis to achieve coordinated operation of CHP plants in the two-site system. For regional electricity and heat supply, the following two basic control objectives are considered. One is to maintain the steady energy balance between demand and supply. The other is to regulate energy flows in the system for achieving transient energy supply driven by market or energy-efficiency policies. Because the control objectives require a large change of operating conditions of CHP plants, our aim is to synthesize nonlinear control systems that are applicable to a wide range of operating conditions. With this aim, we perform structural analyses of the state-space model of the two-site system based on geometric nonlinear control theory. Here, the existence of the NHIM clarified above plays an essential role in the structural analysis for controller synthesis. Based on this, it is shown that the two different objectives can be achieved by a single control scheme without changing its structure.

Acknowledgments

I am deeply grateful to my adviser and mentor, Professor Takashi Hikihara, for his support and guidance over the last six years including my Ph.D. duration. He offered invaluable observations, constructive opinions, and encouragement. He provided me with insightful comments based on his research experience on applications of nonlinear dynamics into engineering. His comments broadened my outlook on engineering science.

I would like to appreciate my mentor, Associate Professor Yoshihiko Susuki (Osaka Prefecture University; OPU) for his continuous support and guidance over the last one year at OPU and the former five years at Kyoto University. He introduced me to research areas of power & energy systems and nonlinear dynamics, provided thoughtful suggestions, and improved my writing skills. I am grateful to his patience and generosity.

I would like to be grateful to Dr. Takkuen John Koo (Hong Kong Applied Science and Technology Research Institute) for his collaboration. He provided me with an opportunity to stay in Hong Kong and introduced me to nonlinear control. His observations and opinions during and after the stay were crucial to the work on parts of the dissertation.

I would like to extend my gratitude to the members of my dissertation committee: Professor Hiroshi Yamakawa and Professor Tetsuji Matsuo who listened to me explaining the materials consisting of the dissertation, and offered their insightful comments and encouragement.

I would like to acknowledge all the laboratory members for providing me with a comfortable research environment. In particular, present and former staffs including Assistant Professor Ryo Takahashi, Assistant Professor Takafumi Okuda, Professor Nobuo Satoh (Chiba Institute of Technology), and Ms. Keiko Saito, offered helpful comments and valuable discussions, as well as encouragement. I would like to thank Ms. Yoshiko Deguchi for the administrative support. I would like to thank all the students of the laboratory, which include Dr. Tsuguhiro Takuno, Dr. Masataka Minami, Dr. Atsushi Yao, Dr. Madoka Yao, Dr. Alexandros Kordonis, Dr. Yanzi Zhou, Mr. Shinya Nawata, Mr. Fredrik Raak,

Mr. Yoshihiko Yamaguchi, Mr. Takuya Kajiyama, Mr. Kohei Nagaoka, Mr. Yohei Kono, Mr. Tsukasa Saito, and Mr. Shiu Mochiyama for their supports and encouragement.

I would like to appreciate Professor Atsushi Ishigame (Osaka Prefecture University) and the members of his research group for providing me with a research environment at OPU and offering valuable discussions.

This work was partly supported by Kyoto University and CREST Project "Creation of Fundamental Theory and Technology to Establish a Cooperative Distributed Energy Management System and Integration of Technologies Across Broad Disciplines Toward Social Application" of Japan Science and Technology Agency.

I would like to thank my parents, Tsutomu and Hiroko Hoshino, for their constant support and encouragement. Finally, I would like to thank my wife Natsu Hoshino for her care and continuous support.

Contents

Notations and acronyms

Frequently used notations

Notation	Usage	Meaning
$\mathbb{R}$		Set of real numbers
$\mathbb{Z}$		Set of integer numbers
i		Unit imaginary number
$\mathbb{T}$		Unit torus
$\|\|\cdot\|\|$	$\|\|\boldsymbol{x}\|\|$	Euclid norm of a vector $\boldsymbol{x}$
ϵ		Positive perturbation parameter
$\mathcal{O}$		Large O notation of order symbols
$\frac{\mathrm{d}}{\mathrm{d}t}$, $\dot{}$	$\frac{\mathrm{d}\boldsymbol{x}}{\mathrm{d}t}$, $\dot{\boldsymbol{x}}$	Time derivative of $\boldsymbol{x}$
$\frac{\partial}{\partial \boldsymbol{x}}$, D	$\frac{\partial \boldsymbol{f}}{\partial \boldsymbol{x}}$, $\mathrm{D}\boldsymbol{f}(\boldsymbol{x})$	Partial derivative of $\boldsymbol{f}$ with respect to $\boldsymbol{x}$ (Jacobian Matrix)
L	$L_f h$	Lie derivative of h with respect to $\boldsymbol{f}$
$\top$	$\boldsymbol{x}^\top, \mathsf{A}^\top$	Transpose of a vector $\boldsymbol{x}$ or matrix A
$\mathbf{1}$		All-one vector
$\mathbf{0}$		All-zero vector
$\mathrm{Ker}(\cdot)$	$\mathrm{Ker}(\mathsf{A})$	Kernel space of liner mapping A
$\mathrm{Im}(\cdot)$	$\mathrm{Im}(\mathsf{A})$	Image space of linear mapping A

det	det$\mathsf{A}$	Determinant of a matrix A
X		State space or phase space
$\boldsymbol{\phi}(t, \cdot)$	$\boldsymbol{\phi}(t, \boldsymbol{x}_0)$	Trajectory of a dynamical system starting from $\boldsymbol{x}_0$ at $t = 0$

List of acronyms

Acronym	Meaning
AC	Alternative Current
AVR	Automatic Voltage Regulator
CHP	Combined Heat and Power
DHC	District Heating and Cooling
ESI	Energy Systems Integration
NHIM	Normally Hyperbolic Invariant Manifold
PSS	Power System Stabilizer
SEP	Stable Equilibrium Point
UEP	Unstable Equilibrium Point
ACEJ	Advanced Cogeneration and Energy Utilization Center Japan
ASME	American Society of Mechanical Engineers
IEEE	Institute of Electrical and Electronics Engineers
IEEJ	Institute of Electrical Engineers of Japan
IEICE	Institute of Electronics, Information and Communication Engineers
ISCIE	Institute of Systems, Control and Information Engineers
JSME	Japan Society of Mechanical Engineers
SHASE	Society of Heating, Air-Conditioning and Sanitary Engineers of Japan
SIAM	Society for Industrial and Applied Mathematics

Chapter 1

Introduction

This dissertation investigates multiscale dynamics in regional electricity and heat supply systems in order to provide an insight into a problem of Energy Systems Integration (ESI) [43, 100]. In this integration, multiple types of energy such as electricity, heat, and natural gas are managed together to satisfy specifications of stability, reliability, and efficiency of energy supply. As will be reviewed in Sec. 1.1, electricity has been managed with the so-called *scale separation* of power system dynamics [114, 84]. However, under ESI, no dynamical principle has been discussed and understood in literature for managing multiple types of energy. In Sec. 1.2, we discuss prior work regarding ESI and specify the purpose of this dissertation. Section 1.3 is devoted to technical details of regional electricity and heat supply systems. Based on this, in Sec. 1.4, we introduce a *two-site system* as a rudimentary model for the current bottom-up approach to analysis and control of multiscale dynamics emergent due to ESI. Section 1.5 summarizes the contents of this dissertation.

1.1 Scale separation of power system dynamics

Classification of dynamic phenomena (dynamics) is essential to analysis and control of electric power systems [77, 84, 133]. Because the systems have complex structures comprising subsystems for generation, transmission, distribution, and consumption of electricity, various dynamics evolve on a wide range of scales in space and time. In order to develop effective tools for analysis and control of the systems, it is necessary to describe the dynamics of interest though a relevant mathematical modeling. For this, the dynamics are classified according to their cause, consequence, time frame, physical characteristics,

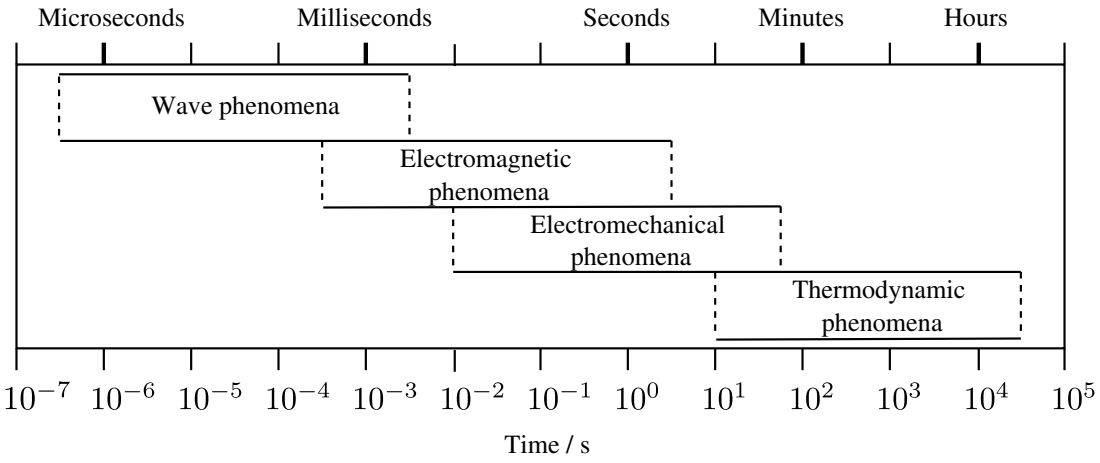

Figure 1.1: Time frame of the basic power system dynamic phenomena [84].

or the places where they occur [77, 114, 84].

A common and important classification of the dynamics is based on physical characteristics. In [84], the dynamics are classified into *wave*, *electromagnetic*, *electromechanical*, and *thermodynamic* phenomena. As stated in [84], this classification is consistent with the time frame shown in Fig. 1.1. A similar concept is presented in [114, 6]. The fastest phenomena in Fig. 1.1 are the wave phenomena that occur in high-voltage transmission lines and correspond to the propagation of electromagnetic waves caused by lightning strikes or switching operations. Much slower phenomena are the electromagnetic dynamics that take place in machine windings following a disturbance, operation of a protection system, or the interaction between electric machines and transmission lines. These are followed by the electromechanical dynamics of rotating masses of generators and motors. The slowest phenomena are the thermodynamic changes which result from boiler control in steam power plants.

The above classification based on the time frame is essential to analysis and control of electric power systems. The classification is also related to the places where the dynamics occur within the system [84]. When we look at Fig. 1.1 from the left to right, the associated components of power systems vary: from three-phase transmission circuits, generator windings, generator rotors, and to boilers of steam power plants. Based on this fact, it is possible to extract the dynamics of interest exhibited by each component in the system. For example, as mentioned in [77], analysis of power system stability is mainly connected with electromechanical dynamics of the rotors of generators, and many analysis tools have been developed by assuming that other phenomena are negligible. Furthermore, by the

above fact, it is possible to construct a hierarchical control structure of the systems. Indeed, the control systems of voltage and frequency have a typical hierarchical structure, where a local controller acts faster and a global controller does slower. Thus, the modern power systems have been based on the underlying principle of scale separation.

This scale separation is not a new concept in power systems but recently has attracted a lot of interest from an alternative viewpoint. In the context of dynamical systems theory [128], several methods of reduced-order modeling are developed based on singular perturbation methods [66, 72] or time-scale modeling [26, 72]. In [114], dynamic models of synchronous machines with standard control systems are provided with a particular emphasis on model origins, development, and specifications. In [26, 27], the above developed methods are applied to identify and aggregate a coherent area where multiple machines exhibit similar rotor swings after a disturbance. According to [27], the coherency identification stems from the work of R. Podmore [106] in the early 1970s and was established by P. Kokotović [73] and co-workers [131, 13, 130, 26] in the rate 1970s. Recently, as stated in [57, 27], the identification based on scale separation has become rather important due to the need for aggregating data of synchrophasor measurements [67] in the context of the so-called Smart Grids perspective [36, 20].

1.2 Energy systems integration

While electric power systems have played the most prominent role of delivering energy services, various studies have indicated that design of the next-generation energy systems cannot be looked as an isolated issue regarding electricity supply [43, 83, 100, 87]. This point of view is described by e.g. *Energy Systems Integration (ESI)* [100] and has recently attracted a lot of interest in engineering and science. The energy systems mentioned here include not only renewable energy sources, batteries, and controllable loads connected to electric power systems but also other fuel infrastructures such as natural gas networks and oil pipelines, as well as thermal heating and cooling systems. The ESI aims to utilize interconnections between these energy systems on a wide range of scales in space and time for satisfying specifications of stability, reliability, and efficiency of energy supply.

The concept of ESI originates from combined modeling and analysis of electric power systems and natural gas infrastructures: see e.g. [5, 90, 94, 116, 21, 80]. This is motivated by the fact that the restructuring of power industries has introduced new risks associated

with security and reliability of natural gas infrastructures [94, 116]. In this case, the interaction between the two types of systems is established by gas-fired (combined-cycle) power plants. In [5, 21, 80], operational optimization and performance evaluation have been conducted for integrated electricity and natural gas infrastructures. In particular, a security-constrained scheduling is investigated in [80] with taking into account the transient characteristics of natural gas flow. It is shown in [80] that the use of steady-state natural gas flow models would result in impractical or suboptimal solutions in a short-term scheduling problem because natural gas and electric power flows usually travel through networks via different speeds and thus illustrate distinct physical characteristics.

In order to generalize the above results and to verify the effectiveness of ESI, several concepts have been proposed for modeling interconnections between energy systems: energy-services supply systems [45], energy hubs [43], distributed multi-generation and multi-energy systems [25, 87], and smart energy systems [83]. These concepts involve thermal heating and cooling systems interconnected with other infrastructures via Combined Heat and Power (CHP) [28, 56] and heat pump [29, 102] technologies. A CHP plant utilizes waste heat as a by-product of the conversion of fuel (natural gas, hydrogen, etc.) into electricity. A heat pump recovers heat by consuming electricity or fuel. Based on these concepts, operational optimization and performance evaluation have been conducted. In particular, analysis based on the concept of energy hubs is a well-known approach, and a general framework for steady-state analysis and optimization of energy systems was proposed by M. Geidl and G. Andersson in 2007 [42]. Their studies have shown the potential for reduction of overall energy cost and emissions through ESI.

While the above studies successfully showed the effectiveness of ESI in a steady state, the dynamical principle of management of multiple types of energy is remaining to be discussed and understood for the purpose of designing secure and reliable energy systems and synthesizing their control systems. In general, it is well-known that analysis of security and reliability of interconnected infrastructures[1] is an interwind issue [94, 116, 50, 19, 62]. For the analysis, there are many ways for modeling the structure and behavior of an interconnected infrastructure depending on the extent to which physical and dynamic characteristics are described: see e.g. [35, 62, 61]. While detailed models are superior in reproducing the detailed behavior of the system, they usually require unfeasible computa-

[1]Here, the term "infrastructure" includes communication networks studied in [19] and railway networks in [62], as well as energy systems in [94, 116, 50].

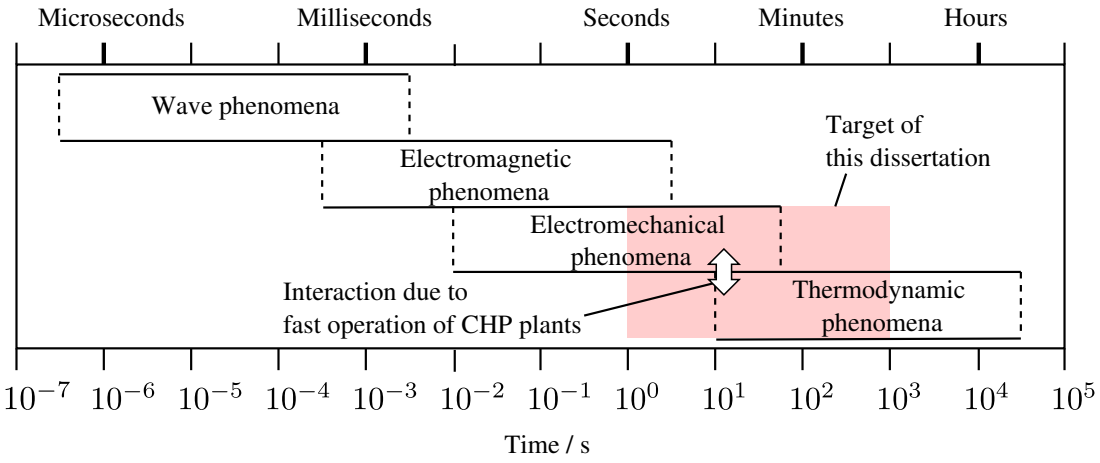

Figure 1.2: The time frame of dynamics investigated in this dissertation. We address dynamic interaction between electromagnetic and thermodynamic phenomena appearing in regional electricity and heat supply systems due to fast operation of CHP plants.

tional time for the analysis and are too complicated to reveal the system-wide dynamics of interest. In contrast, while topological (graph theoretic) models inspired by network theory [96] are computationally fast and captures structural properties of the system, it is pointed out in [35, 51] that this approach does not always capture the mechanisms of relevant behavior of the system. Although several studies [91] have identified relationships between physical and topological properties of electric power systems, no dynamical principle has been revealed for management of multiple types of energy under ESI.

This dissertation takes a bottom-up approach to the above problem and focuses on multiscale dynamics occurring in a rudimentary model of ESI. The model, which will be introduced in Sec. 1.4, appears as a typical example of regional electricity and heat supply systems, where a CHP plant induces interaction between subsystems of electricity and heat. In particular, as shown in Fig. 1.2, we discuss the dynamic interaction between electromechanical and thermodynamic phenomena on the time scale of seconds to tens of seconds. The dynamic interaction is emergent[2] due to fast operations of CHP plants recently proposed in e.g. [118, 41, 135]: see Sec. 1.3 for details. In this dissertation, we analyze and control the multiscale dynamics based on geometric singular perturbation theory [76]. Particularly, regarding the modeling problem mentioned above, we show in Chapter 3 that it is possible to derive a reduced-order model capturing graph theoretic

[2]Several studies are reported to discuss the interaction appearing in the plant-level dynamics in combined cycle power plants [31, 64] and steam power plants [3]. This dissertation discusses the system-level dynamics in regional electricity and heat supply systems as explained in Sec. 1.3.

property of the system as well as the multiscale property of the original dynamics.

1.3 Regional electricity and heat supply systems

This section provides a technical background of regional electricity and heat supply systems and discusses the role of a CHP plant from the perspective of ESI. A key technical feature of a CHP plant is that it can not generate electricity and heat independently. Thus, the ratio of electricity and heat outputs of a CHP plant, simply called as *electricity-to-heat ratio* [86, 117], is an important parameter that characterizes the interaction between subsystems of electricity and heat. Conventionally, the effect of the interaction has been extensively studied for a slow time scale of hours, days, or seasons in a year. For example, a design problem of a CHP plant is addressed in [136, 112, 65] for selecting the prime-mover type[3] and determining their nominal output based on the annual load curves of electricity and heat. In [60, 11], a operational optimization problem is solved for determining the hourly schedule of generation of a CHP plant in a day.

Recently, several novel operations of a CHP plant are proposed to provide *ancillary services* [70, 109][4] of electric power systems. In [41, 99], a CHP plant is utilized for tracking a secondary frequency control (Load Frequency Control) signal. Also, a CHP plant can be utilized for compensating variable outputs of renewable energy sources [118, 135, 92] and for contributing to demand response [98, 85, 71]. Such a operation of a CHP plant induces an interaction between electricity and heat supply systems on a faster time scale than the conventional operations. Particularly, the operation studied in [135] is as fast as on the time scale of seconds to tens of seconds (minutes). Since the heat output of a CHP plant under such an electricity-oriented operation varies depending on the electricity-to-heat ratio, the operation induces uncertainty in the heat output and imbalance between heat supply and demand.

To resolve the imbalance of heat due to the above operations, a promising approach is to absorb the energy imbalance by a district heating and cooling (DHC) system [95, 99]. Here, for the following discussion, we briefly review the two practical examples of DHC systems shown in Fig. 1.3. First, Fig. 1.3a shows an example in Shibaura region

[3]For regional scale systems, gas turbine, gas engine, and diesel engine are utilized as a prime mover.

[4]While some ancillary services result in the delivery of electricity, they are called "ancillary" because their importance stems from the potential to deliver energy upon request rather than the amount of the delivered electricity. While there are many definitions of the services (see [70, 109]), this dissertation focuses on the demand-side ancillary services [70] providing active power.

in Japan [2, 121]. In the region, there are six (office and commercial) buildings, and steam and cold water are supplied from main and sub-stations. The main-station has seven boilers (total of 120 GJ/h) and two CHP plants (930 kW for each) for generating electricity and steam (0.88 MPa). The sub-station has two CHP plants (930 kW for each) and is connected to the main-station through a steam pipeline. In the summer season, the generated steam is utilized by absorption chillers [117] to supply cold water. Next, Fig. 1.3b shows a schematic diagram of an electricity and heat supply system studied in [82]. The system is based on a district heating system in Barry Island region in UK [134, 105]. In this case, hot water (70 °C) is supplied for space heating and domestic hot water of two civil buildings, three hundred residential houses, and fifty shops. In Fig. 1.3b, several houses and shops are lumped together, and the electricity and heat networks are fed by three CHP plants. The total demand is 1.6 MW for electricity and 2.164 MW for heat [82].

One important benefit of a DHC system is that excess or deficit heat in one place can be transfered to another. Indeed, in the DHC system in Fig. 1.3a, the CHP plants are selected so that the total heat output does not exceed the minimum heat demand in the DHC system[5], and the deficit heat is compensated by the boilers of the main-plant [2]. Furthermore, by a coordinated operation of multiple CHP plants, it is possible to regulate total heat output as well as electricity output: see Sec. 1.4 in details. In this direction, an optimal dispatching problem is addressed in [82] for the system in Fig. 1.3b, where the electricity and heat generated from the all sources are unknown and their electricity-to-heat ratios are known. In this dissertation, we explore a coordinated operation (control) of multiple CHP plants with taking into account the dynamic characteristics of electricity and heat supply in order to discuss ancillary services on a fast time scale of seconds to minutes.

1.4 Two-site system: A rudimentary model

In this section, we introduce a rudimentary model of ESI in order to perform analysis and control of multiscale dynamics emerging due to the fast operation of CHP plants mentioned in Sec. 1.3. The system comprises two CHP plants, and we call it as a *two-site*

[5]This is intended to maximize the energy saving effect of the operation of the CHP plants by preventing the excess heat [2]. Also, the capacity of the CHP plants is designed so as not to exceed the electricity demand.

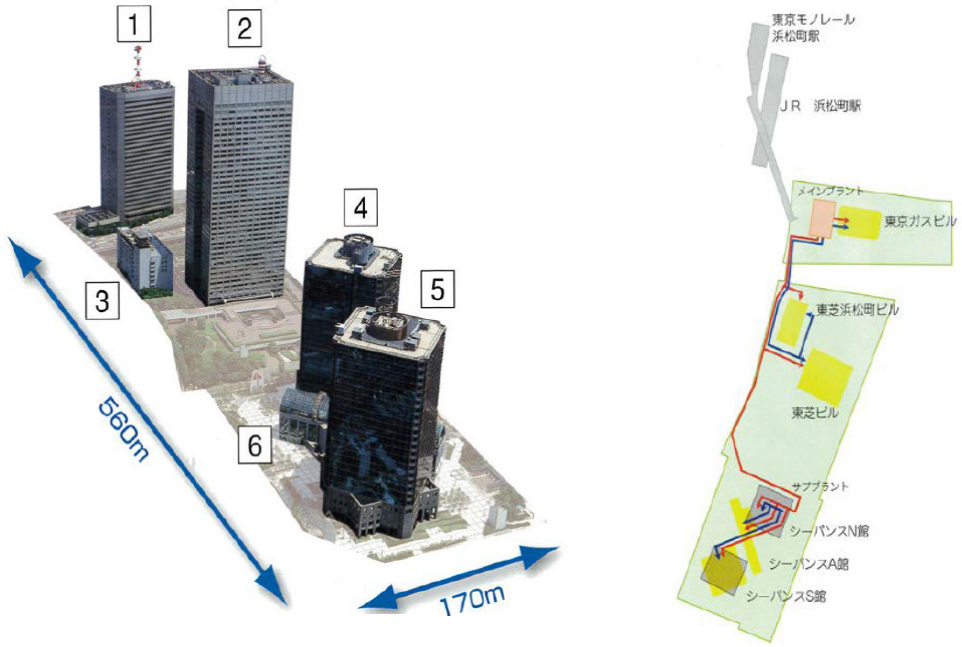

(a) Example in Shibaura region [2]

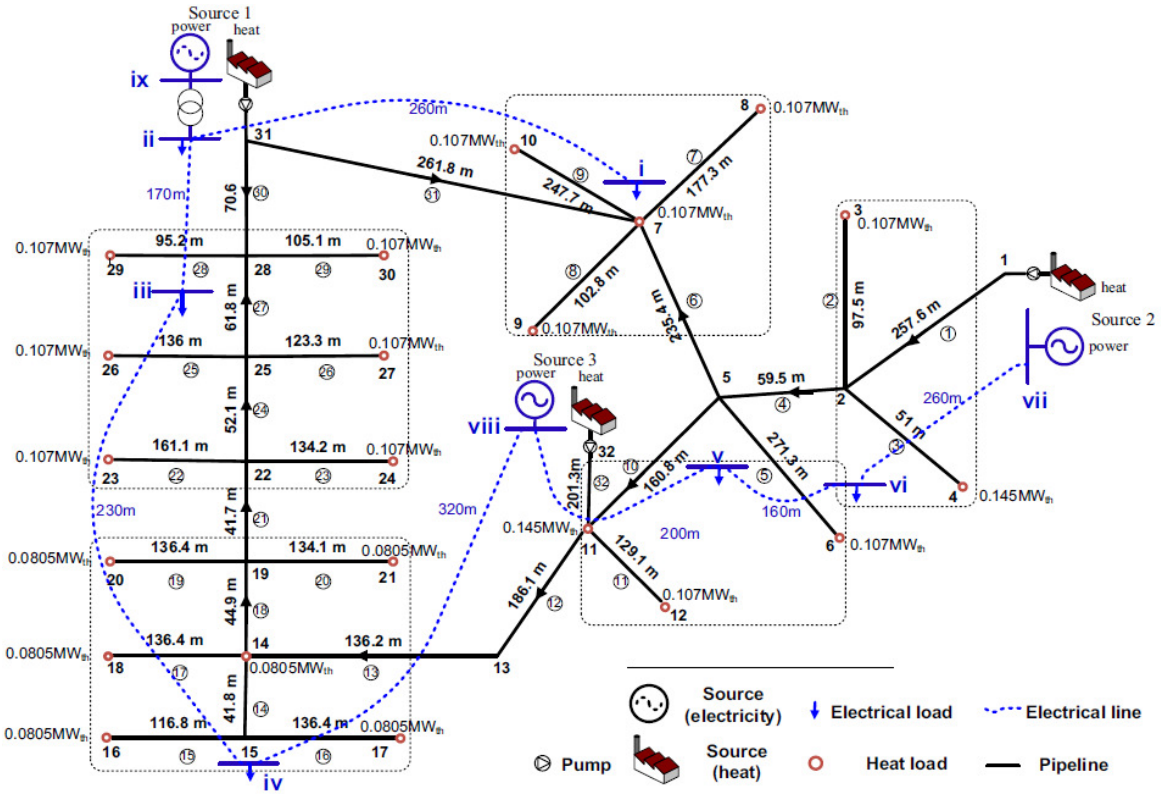

(b) Example in Barry Island region [82]

Figure 1.3: Practical examples of district heating systems with CHP plants.

system. While realistic systems may comprise more than two sites, it is of basic importance to clearly describe fundamental concepts of analysis and control for the system. In the context of electric power systems, the system can be regarded as an extension of the so-called double machine-infinite bus system, for which static and dynamic characteristics have been studied in [10, 9, 124, 125, 47]. In terms of heat supply, the system is minimal in the sense that the heat transfer between different sites can be considered.

Figure 1.4 shows the schematic diagram of the two-site system. The concept of *site* stands for a unit of energy system that consists of a CHP plant, a (lumped) electric load, and a (lumped) heat load. Its practical example is a commercial, civil, or large residential building with own CHP plant as reviewed in Sec. 1.3. It is assumed that the CHP plant is based on gas turbine-generator, and its capacity is on the order of MW for electricity and of GJ/h for heat. The electricity-to-heat ratio of the CHP plants can be different for each of the two sites in the system[6]. The two sites are connected to a commercial power grid through a transmission line[7], and it is possible to supply the excess electricity to the grid. The two sites are also interconnected by a pipeline for steam or hot water. No additional components such as renewable energy sources, batteries, boilers, hot-water storages, and heat pumps are considered[8] in order to clearly apprehend the dynamical consequence of operation of the CHP plants.

For the analysis and control in the rest of this dissertation, we will introduce two subsystems based on their physical characteristics: *electric subsystem* and *heat subsystem*. For this, Fig. 1.5 shows the diagram of energy flows in the two-site system. The CHP plant at each site comprises gas turbine, synchronous generator, and heat recovery boiler [117]. At each site $\#i$ for $i = 1, 2$, the fuel flow $P_{\mathrm{g}i}$ to the gas turbine can be controlled via a fuel valve. As a result of the fuel combustion, the mechanical power $P_{\mathrm{m}i}$ is produced and transmitted to the generator in each CHP plant. The heat flow, denoted by $Q'_{\mathrm{a}i}$, is also recovered from the exhaust gas and absorbed by a heat recovery boiler. In this dissertation, we describe the energy conversion by the following equation:

$$\begin{bmatrix} P_{\mathrm{m}i} \\ Q'_{\mathrm{a}i} \end{bmatrix} = \begin{bmatrix} \eta_{\mathrm{e}i} \\ \eta_{\mathrm{h}i} \end{bmatrix} P_{\mathrm{gas}i}, \tag{1.1}$$

[6]The two CHP plants are identical in Chapters 2 and 3, and have different electricity-to-heat ratio in Chapters 4 and 5 as will be explained later.

[7]While we call the connecting network as a "transmission" line, for the grid interconnection of a CHP plant, 6.6 kV "distribution" network through a 66 kV/6.6 kV transformer is usually utilized [117].

[8]With the modeling and analysis in this dissertation, it is possible to include these components to the lumped electric and heat loads if the dynamics of the components are negligible.

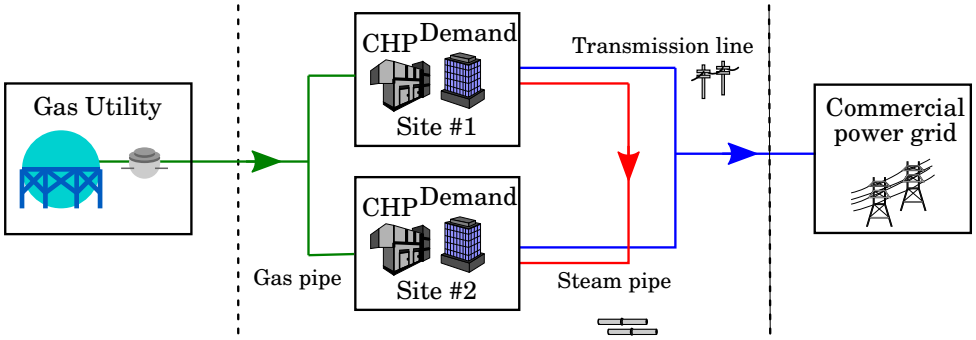

Figure 1.4: Schematic diagram of the two-site system studied in this dissertation. Each site consists of a CHP plant with gas turbine-generator, an electric load, and a heat load. The two sites are connected to a commercial power grid through a transmission line and are interconnected by a pipeline for steam or hot water.

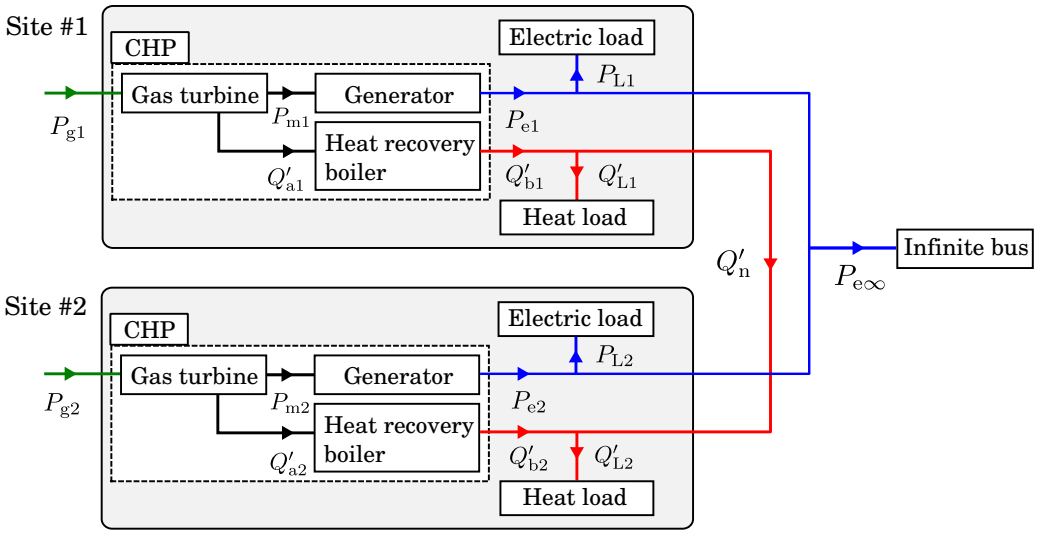

Figure 1.5: Energy flow diagram of the two-site system. The dimension of the variables in the figure is [W] = [J/s]. The arrows show the positive directions of the energy flows.

where η_{ei} and η_{hi} stand for the thermal efficiency and coefficient of heat recovery, respectively. The electric power P_{ei} and heat flow Q'_{bi} are then supplied to the electric and heat loads, as well as the commercial power grid. The grid is modeled by an infinite bus [77], which is a voltage source with constant amplitude, frequency, and phase. Here, the *electric subsystem* comprises the generators, electric loads, transmission line, and the infinite bus in Fig. 1.5. The *heat subsystem* comprises the heat recovery boilers and heat loads, and pipeline. The two subsystems are interconnected via the gas turbines in the CHP plants.

Here, as mentioned in Sec. 1.3, it is possible to consider a coordinated operation of

CHP plants to regulate the total outputs of electricity and heat simultaneously. As a preliminary result, in this section, we discuss the coordinated operation in the two-site system under a steady state. In addition, without any loss in energy conversion and transfer, the steady energy balance between demand and supply is described by

$$P_{\mathrm{m}1} + P_{\mathrm{m}2} = P_{\mathrm{e}1} + P_{\mathrm{e}2} = P_{\mathrm{L}1} + P_{\mathrm{L}2} + P_{\mathrm{e}\infty}, \tag{1.2a}$$

$$Q'_{\mathrm{a}1} + Q'_{\mathrm{a}2} = Q'_{\mathrm{b}1} + Q'_{\mathrm{b}2} = Q'_{\mathrm{L}1} + Q'_{\mathrm{L}2}. \tag{1.2b}$$

where $P_{\mathrm{L}i}$ and $Q'_{\mathrm{L}i}$ stand for the consumptions in the electric and heat loads, and $P_{\mathrm{e}\infty}$ for the electric power to the infinite bus. Here, for the electricity supply, $P_{\mathrm{e}\infty}$ is an important quantity for the ancillary services mentioned in Sec. 1.3. From Eqs. (1.2a) and (1.1), $P_{\mathrm{e}\infty}$ is given by

$$P_{\mathrm{e}\infty} = -(P_{\mathrm{L}1} + P_{\mathrm{L}2}) + \frac{\eta_{\mathrm{e}1}}{\eta_{\mathrm{h}1}} Q'_{\mathrm{a}1} + \frac{\eta_{\mathrm{e}2}}{\eta_{\mathrm{h}2}} Q'_{\mathrm{a}2}. \tag{1.3}$$

Furthermore, by introducing the parameter Q'_{n} representing the heat transfer rate between the two sites, the energy balance (1.2b) is rewritten as follows:

$$Q'_{\mathrm{a}1} = Q'_{\mathrm{L}1} + Q'_{\mathrm{n}}, \quad Q'_{\mathrm{a}2} = Q'_{\mathrm{L}2} - Q'_{\mathrm{n}}. \tag{1.4}$$

Thus, under a steady state, the electric power $P_{\mathrm{e}\infty}$ is parameterized by Q'_{n} as follows:

$$P_{\mathrm{e}\infty} = -(P_{\mathrm{L}1} + P_{\mathrm{L}2}) + \left(\frac{\eta_{\mathrm{e}1}}{\eta_{\mathrm{h}1}} Q'_{\mathrm{L}1} + \frac{\eta_{\mathrm{e}2}}{\eta_{\mathrm{h}2}} Q'_{\mathrm{L}2} \right) + \left(\frac{\eta_{\mathrm{e}1}}{\eta_{\mathrm{h}1}} - \frac{\eta_{\mathrm{e}2}}{\eta_{\mathrm{h}2}} \right) Q'_{\mathrm{n}}. \tag{1.5}$$

Equation (1.5) implies that by operation of the CHP plants with different values of $\eta_{\mathrm{e}i}/\eta_{\mathrm{h}i}$, it is possible to vary the electric power $P_{\mathrm{e}\infty}$ while maintaining the steady energy balance.

From Eq. (1.5), we now specify two types of coordinated operation of the CHP plants. The two operations can be distinguished by the manner in which the regulation of $P_{\mathrm{e}\infty}$ affects the heat supply system. If the two CHP plants are operated so as to satisfy Eq. (1.5), then the steady energy balance between demand and supply is maintained. This is achieved by the heat transfer between the two sites to compensate excess or deficit heat caused by regulating the electric output of a CHP plant. The other is to regulate the heat transfer rate Q'_{n} as well as the electric power $P_{\mathrm{e}\infty}$. Under this operation, the steady energy balance is not maintained if the two energy flows (Q'_{n} and $P_{\mathrm{e}\infty}$) do not satisfy Eq. (1.5). While the operation is not necessary feasible on the infinite time interval, it is important for achieving temporal energy supply driven by market and energy-efficiency policies. In this dissertation, we synthesize a controller for the two coordinated operations in Chapters 4 and 5.

1.5 Overview of the dissertation

This dissertation is devoted to analysis and control of multiscale dynamics occurring in the two-site system. The rest of this section explains the contents of this dissertation.

In Chapter 2, we revisit the effectiveness and limitation of the conventional scale separation of power system dynamics through stability analysis of the electric subsystem of the two-site system. As mentioned in Sec. 1.1, power system stability has been mainly connected with electromechanical dynamics, and the associated methods of analysis have been developed by assuming that mechanical power supplied to generators is constant. In this chapter, we formulate a stability problem of the electric subsystem with the so-called swing equation model [77, 84] by modifying the description of the mechanical power to represent the effect of the heat subsystem. It is shown that the conventional methods of stability analysis such as energy function method [114, 23] are applicable to the current stability problem if the dynamics of the heat subsystem are negligible due to scale separation. If this is not the case, the dynamic interaction between the two subsystem needs to be taken into account. In this direction, we conduct a time-response analysis of the derived model and discuss an instability phenomenon due to a change of operating conditions of CHP plants of the two-site system.

Chapter 3 analyzes multiple time scale dynamics of the heat subsystem to derive a simple model describing the dynamic interaction with the electric subsystem. We study a problem of mathematical modeling for dynamics occurring in general steam supply networks[9], in which multiple boilers (including a heat recovery boiler within a CHP plant) are connected via a steam pipe network. The dynamics of interest are originally described by the model for *fast* steam flows over a pipe network coupled with the model for *slow* internal dynamics of boilers. For a single boiler or single plant, much work has been reported on *lumped-parameter* modeling [12, 69, 127, 18], while for dynamics of steam flows in pipes, partial differential equations or *distributed-parameter* models [101, 4, 81, 126] are normally used. In this chapter, we derive a simple lumped-parameter model through physically relevant approximations. The correctness of the derived model is verified by theoretical and numerical analyses of the model in terms of multiscale property of steam supply. Specifically, we discuss the structural stability of the derived model based on the concept of Normal Hyperbolic Invariant Manifold (NHIM) [129, 97, 76]. Furthermore, the

[9]Here, we do not restrict the discussion to the two-site system, and the result of Chapter 3 is applicable to the general n-site system.

existence of the NHIM suggests a separation principle for steam supply systems, which is analogue to that for electric power systems.

Chapters 4 and 5 address synthesis problems of control systems to achieve the coordinated operation of CHP plants described in Sec. 1.4. The following two control objectives are considered. One is to maintain the steady energy balance of demand and supply characterized by Eq. (1.5). The other is to regulate energy flows for achieving transient energy supply driven by market or energy-efficiency policies. Since these objectives require a large change of operating conditions of CHP plants, our aim is to synthesize a nonlinear control system that is applicable to a wide range of operating conditions. With this aim, we perform structural analysis of the state-space model of the two-site system based on geometric nonlinear control theory [59, 113, 68]. The analysis is conducted by the method of *input-output linearization*. The method is different from the usual Jacobian linearization of a nonlinear system and is a process of making the input-output response exactly linear by deriving a suitable coordinate transformation. The coordinate transformation converts the system into the so-called *normal form* representing inherent structure of the system. It is shown that the existence of the NHIM clarified in Chapter 3 plays essential role in the structural analysis and controller synthesis of the two-site system.

In Chapter 4, we synthesizes a state-feedback controller for maintaining the energy balance. The controller determines the signals of fuel inputs to the CHP plants to render an equilibrium point of the state-space model asymptotically (exponentially) stable. As illustrated in Chapters 2 and 3, energy imbalance causes not only short-term dynamics of generators in the electric subsystem but also long-term dynamics of boilers in the heat subsystem. With this observation of the multiscale dynamics, it is shown that the state-space model becomes a minimum phase system when we choose its output as the electric power flow interchanged with the infinite bus and the averaged pressure level, which parameterizes the slow dynamics along the NHIM. This fact implies that a standard stabilizing controller is directly obtained with the input-output linearization.

Chapter 5 addresses an output tracking control problem for the energy flows in the two-site system. When the outputs are given as the energy flows, the model becomes a non-minimum phase system. The non-minimum phase property is characterized by the existence of an invariant manifold in the zero dynamics of the model, which is associated with the NHIM in Chapter 3. Then, based on the structural analysis, we synthesize a tracking controller for the energy flows by redefining the outputs and utilizing a slowly

time-varying reference of the outputs used in Chapter 4. As a result, the different control objectives in Chapters 4 and 5 are achieved by a single control scheme without changing its structure. By managing this control scheme with a high-level planner, which selects the control objectives, a new hierarchical management architecture can be considered for shaping the multiscale dynamics in the two-site system.

Chapter 6 concludes this dissertation with a brief summary and future research directions. The ideas of analysis and control are not restricted to the particular two-site example in this dissertation. One future direction is to apply the ideas to other types of integrated energy systems. Another direction is to propose a hierarchical management structure for shaping multiscale dynamics due to ESI. The author believes that this dissertation contains significant contributions towards the next-generation energy system.

Chapter 2

Stability of the electric subsystem

This chapter revisits the scale separation of power system dynamics through stability analysis of the electric subsystem affected by the heat subsystem. In general, *power system stability* [77, 84] is an important factor of security [84, 133] of power systems, and is broadly defined as the ability of a power system to maintain an acceptable operating condition after being subjected to a disturbance. In particular, the so-called *rotor angle stability* [77, 84] is the ability of interconnected synchronous machines in a power system to maintain their synchronism. In this chapter, we focus on the rotor angle stability of generators in the electric subsystem. Specifically, we will formulate a stability problem in which electromechanical dynamics of the generators are directly affected by the heat subsystem through the gas turbines. It will be shown that the conventional methods of stability analysis such as *energy function method* [114, 23] are applicable if the dynamics of the heat subsystem are negligible. With this aim, the classical *swing equation* model [77, 114, 84] is utilized to represent the electromechanical dynamics and is generalized by introducing a new parameter to represent the effect of the heat subsystem.

The rotor angle stability is classified in the following two categories [77, 84]: *small-signal stability* and *transient stability*. The small-signal stability is the ability of a power system to maintain synchronism under a small disturbance. The stability can be understood as the *linear stability* [128] of an equilibrium point of an underlying nonlinear dynamical system. Here, we conduct the linear stability analysis to identify the feasible range of steady operating conditions of the two-site system, where the synchronized operation of the generators is achieved. We then analyze the *basin of attraction* [128] of the equilibrium point for each steady operating condition. The analysis is closely related to the transient stability [24, 23], which is the ability of a power system to maintain synchro-

nism under a large disturbance, and depends on the initial condition of the underlying dynamical system. The basin portraits of a dynamical system model of the two-site system are visualized under several fixed values of the set points of the CHP plants. The visualization is then used for considering the responses of the system under a situation where the scale separation does not hold between the dynamics of the electric and heat subsystem.

2.1 Stability concepts of dynamical systems theory

This section briefly reviews several concepts of stability in dynamical systems theory [128] that are utilized for analysis of power system stability [84, 23]. A dynamical system plays an important role as a *mathematical model* of dynamics of interest occurring in a real system. It is often derived from not only the structure of the system but also fundamental physical laws governing the elements of the system. When we formulate a dynamical system model, it is necessary to determine *state variables* and *state space*. The state variables are the minimum set of variables $x_1, x_2, \ldots, x_n$ that uniquely determine the operating condition of the system, and written as a vector $\boldsymbol{x} = [x_1, x_2, \ldots, x_n]^\top$, where the symbol $\top$ stands for the transpose of a vector or matrix. The *state space*, denoted by X, is the space of the state variables and is also referred to as *phase space*.

In this chapter, we consider a dynamical system that is modeled as an ordinary differential equation of the form

$$\frac{\mathrm{d}\boldsymbol{x}}{\mathrm{d}t} = \boldsymbol{f}(\boldsymbol{x}), \tag{2.1}$$

with $\boldsymbol{x} \in X$ and $t \in \mathbb{R}$, where X is an open set in $\mathbb{R}^n$, and the independent variable t is often referred to as time. The symbol $\mathrm{d}/\mathrm{d}t$ stands for the derivative with respect to time. The function $\boldsymbol{f} : X \to \mathbb{R}^n$ is assumed to satisfy the conditions of existence and uniqueness of a solution [128]. A solution curve $\bar{\boldsymbol{x}}(t)$ of Eq. (2.1) is referred to as a *trajectory*, and the trajectory starting from $\boldsymbol{x}_0$ at $t = 0$ is denoted by $\boldsymbol{\phi}(\boldsymbol{x}_0, t)$.

The stability property of an trajectory is characterized by the following definitions of *Lyapunov*[1] *stability* and *asymptotic stability*.

[1]The name "Lyapunov" is also spelled as "Liapunov", and the both are used depending on the authors [128]. In this dissertation, we will spell as "Lyapunov" because it is frequently used in the context of power system engineering [114, 84].

Definition 2.1 (Lyapunov stability [128]). *A trajectory $\bar{\boldsymbol{x}}(t)$ of (2.1) is said to be stable if, for any $\varepsilon > 0$, it is possible to choose a constant $\delta = \delta(\epsilon) > 0$ such that, for any other solution $\boldsymbol{y}(t)$ of (2.1) satisfying $||\bar{\boldsymbol{x}}(t_0) - \boldsymbol{y}(t_0)|| < \delta$, the following inequality $||\bar{\boldsymbol{x}}(t) - \boldsymbol{y}(t)|| < \varepsilon$ holds for $t > t_0$, $t_0 \in \mathbb{R}$, where $||\cdot||$ stands for Euclidean norm.*

Roughly speaking, the concept of Lyapunov stability states that the trajectory $\bar{\boldsymbol{x}}(t)$ is stable if any other solution starting close to $\bar{\boldsymbol{x}}(t)$ at a given time t_0 remains close to $\bar{\boldsymbol{x}}(t)$ for all later times. Furthermore, to describe the cases where nearby solutions converge to $\bar{\boldsymbol{x}}(t)$ as $t \to \infty$, the following concept of asymptotic stability is utilized.

Definition 2.2 (Asymptotic stability [128]). *A trajectory $\bar{\boldsymbol{x}}(t)$ of (2.1) is said to be asymptotically stable if it is Lyapunov stable and for any other solution $\boldsymbol{y}(t)$ of (2.1), there exists a constant $b > 0$ such that if $||\bar{\boldsymbol{x}}(t_0) - \boldsymbol{y}(t_0)|| < b$, then $\lim_{t\to\infty} ||\bar{\boldsymbol{x}}(t) - \boldsymbol{y}(t)|| = 0$.*

A trivial trajectory $\bar{\boldsymbol{x}}(t) = \bar{\boldsymbol{x}} = const.$ is referred to as *equilibrium point*. Since an equilibrium point $\bar{\boldsymbol{x}}$ is a solution of Eq. (2.1) that does not change in time, it satisfies

$$\boldsymbol{f}(\bar{\boldsymbol{x}}) = 0. \tag{2.2}$$

When we apply the above concepts of stability to a problem of power system stability, a dynamical system model of a power system is usually derived such that a steady operating condition is described by an equilibrium point. Disturbances affecting the power system are modeled by changes in its parameters or by initial conditions apart from the equilibrium point [84].

To determine the stability of an equilibrium point, analysis based on linear approximation have been widely used in practical problems [88]. Here, we emphasize that, under a certain condition, the linear stability indicates the orbit (trajectory) structure near an equilibrium point affected by a small disturbance in terms of model parameters as well as initial conditions [88, 128]. To determine the stability of a trajectory $\bar{\boldsymbol{x}}(t)$, we consider a solution near $\bar{\boldsymbol{x}}(t)$ by

$$\boldsymbol{x} = \bar{\boldsymbol{x}}(t) + \boldsymbol{y}. \tag{2.3}$$

By substituting Eq. (2.3) into Eq. (2.1), and Taylor expanding about $\bar{\boldsymbol{x}}(t)$, we have

$$\frac{\mathrm{d}\boldsymbol{x}}{\mathrm{d}t} = \frac{\mathrm{d}\bar{\boldsymbol{x}}(t)}{\mathrm{d}t} + \frac{\mathrm{d}\boldsymbol{y}}{\mathrm{d}t} = \boldsymbol{f}(\bar{\boldsymbol{x}}(t)) + \mathrm{D}\boldsymbol{f}(\bar{\boldsymbol{x}}(t))\boldsymbol{y} + \mathcal{O}(||\boldsymbol{y}||^2), \tag{2.4}$$

where $\mathrm{D}\boldsymbol{f}$ stands for the derivative of $\boldsymbol{f}$, and $\mathcal{O}$ for the large O notation of order symbols. By using the fact that $\mathrm{d}\bar{\boldsymbol{x}}(t)/\mathrm{d}t = \boldsymbol{f}(\bar{\boldsymbol{x}}(t))$, Eq. (2.4) becomes

$$\frac{\mathrm{d}\boldsymbol{y}}{\mathrm{d}t} = \mathrm{D}\boldsymbol{f}(\bar{\boldsymbol{x}}(t))\boldsymbol{y} + \mathcal{O}(||\boldsymbol{y}||^2). \tag{2.5}$$

Equation (2.5) describes the evolution of a solution near $\bar{\boldsymbol{x}}(t)$. For stability analysis, the behavior of solutions arbitrary close to $\bar{\boldsymbol{x}}(t)$ is of concern. It is thus reasonable to study the associated linear system given by

$$\frac{\mathrm{d}\boldsymbol{y}}{\mathrm{d}t} = \mathrm{D}\boldsymbol{f}(\bar{\boldsymbol{x}}(t))\boldsymbol{y}. \tag{2.6}$$

If $\bar{\boldsymbol{x}}(t)$ is an equilibrium point, i.e. $\bar{\boldsymbol{x}}(t) = \bar{\boldsymbol{x}}$, then $D\boldsymbol{f}(\bar{\boldsymbol{x}}(t)) = D\boldsymbol{f}(\bar{\boldsymbol{x}})$ is a matrix with constant entries, and the stability of the solution $\boldsymbol{y} = 0$ of Eq. (2.6) is determined by the eigenvalues of the Jacobian matrix $D\boldsymbol{f}(\bar{\boldsymbol{x}})$. The following theorem states that the stability of the solution $\boldsymbol{y} = 0$ implies the stability of $\bar{\boldsymbol{x}}(t) = \bar{\boldsymbol{x}}$ under a certain condition.

Theorem 2.3 (Stability in the linear approximation [88, 128])**.** *If all of the eigenvalues of* $\mathrm{D}\boldsymbol{f}(\bar{\boldsymbol{x}})$ *have negative real parts, then the equilibrium point* $\bar{\boldsymbol{x}}$ *of Eq. (2.1) is asymptotically stable. Also, if at least one of the eigenvalues of* $\mathrm{D}\boldsymbol{f}(\bar{\boldsymbol{x}})$ *has a positive real part, then the equilibrium point* $\bar{\boldsymbol{x}}$ *is unstable.*

The above theorem provides a sufficient condition for the asymptotic stability of an equilibrium point. Furthermore, it is stated by the so-called *Hartman-Grobman theorem* [128] that if all of the eigenvalues of the associated linear system have nonzero real parts, then the orbit structure near the equilibrium point is essentially the same as that of the linear system. Such an equilibrium point is referred to as a *hyperbolic* equilibrium point and persists under a perturbation of vectorfield [128]. In the rest of this chapter, we simply call an equilibrium point where the associated Jacobian matrix has eigenvalues with negative real parts as Stable Equilibrium Point (SEP). In the context of power system stability, a steady operating condition represented by an SEP will be maintained under a small disturbance in terms of model parameters as well as initial conditions.

To discuss power system stability under a large disturbance, the following definitions of attracting set and basin of attraction are required.

Definition 2.4 (Attracting set and attractor [128])**.** *A closed invariant set* $A \subset \mathbb{R}^n$ *is called an attracting set if there is some neighborhood* U *of* A *such that*

$$\forall t \geq 0, \quad \boldsymbol{\phi}(t, U) \subset U, \quad \bigcap_{t>0} \boldsymbol{\phi}(t, U) = A. \tag{2.7}$$

Furthermore, an attracting set A is called an attractor if, for any two open sets U, $V \subset A$,

$$\exists t \in \mathbb{R}, \quad \boldsymbol{\phi}(t, U) \cap V \neq \emptyset. \tag{2.8}$$

Definition 2.5 (Basin of attraction [128])**.** *The domain or basin of attraction of an attracting set A is given by*

$$\bigcup_{t \leq 0} \boldsymbol{\phi}(t, U), \tag{2.9}$$

where U is any open set satisfying Definition 2.4.

For analysis of transient stability of power systems, the so-called *energy function method* [24, 114, 23] provides an analytical criterion[2] for sufficient condition of the basin of attraction of an SEP. An energy function for the system (2.1) is defined as follows:

Definition 2.6. *(Energy function [23]) A smooth proper function $V : X \subset \mathbb{R}^n \to \mathbb{R}$ is called an energy function for the system (2.1) if the following three conditions are satisfied:*

- *The derivative of the energy function $V(\boldsymbol{x})$ along any system trajectory $\boldsymbol{x}(t)$ is non-positive:*

$$\frac{\mathrm{d}V(\boldsymbol{x}(t))}{\mathrm{d}t} = \frac{\partial V(\boldsymbol{x})}{\partial \boldsymbol{x}} \boldsymbol{f}(\boldsymbol{x}(t)) \leq 0. \tag{2.10}$$

- *If $\boldsymbol{x}(t)$ is a nontrivial trajectory (i.e., $\boldsymbol{x}(t)$ is not an equilibrium point), then along the nontrivial trajectory $\boldsymbol{x}(t)$, the set $\{t \in \mathbb{R} \mid \mathrm{d}V(\boldsymbol{x}(t))/\mathrm{d}t = 0\}$ has a measure zero[3] in $\mathbb{R}$*

By using an energy function, a sufficient condition of the domain of attraction is provided as the following open set containing the SEP:

$$\big\{\boldsymbol{x} \in X \mid V(\boldsymbol{x}) < V_{\mathrm{cr}}\big\}, \tag{2.11}$$

where V_{cr} is the value of V at the UEP with the lowest value of V and with greater value at the SEP: see [24, 23] for theoretical foundation of the method.

[2] As well as the analytical criterion, several numerical methods have been established for practical use of the energy function methods [23].

[3] There does not exist a time interval $[t_1, t_2]$ such that $\mathrm{d}V(\boldsymbol{x}(t))/\mathrm{d}t = 0$ for $t \in [t_1, t_2]$ with $t_1 \neq t_2$.

2.2 Dynamical system model

This section derives a dynamical system model of the two-site system for stability analysis. All the variables and parameters are normalized with the per-unit system [77, 114, 84]: see Appendix 2.A in details. The physical meanings of variables and parameters are listed in Appendix 2.B.

2.2.1 Derivation

Here, we derive a dynamical system model by generalizing the classical swing equation model [77, 114, 84] to represent the effect of the heat subsystem. The derivation of the model is based on the following assumptions. The validity of the assumptions is explained in the rest of this section.

(A1) Speed of the synchronous generators are close to the synchronous speed.

(A2) The electromagnetic phenomena in transmission lines and generator windings, which are faster than the electromechanical phenomena of generator rotors, are negligible.

(A3) The thermodynamic phenomena such as transient responses and losses of the heat recovery boilers and heat conduction pipes are negligible.

(A4) Dynamics of the gas turbines are negligible, and the efficiencies of energy conversion from gas to mechanical power and recovered heat are independent of operating condition.

By denoting by δ_i the position of rotor of the generator $\#i$ with respect to a synchronous reference flame, and by ω_i the deviation of rotor speed relative to the synchronous speed, the swing equation for the electric subsystem is given as follows :

$$\frac{\mathrm{d}\delta_1}{\mathrm{d}t} = \omega_1, \tag{2.12a}$$

$$\frac{\mathrm{d}\omega_1}{\mathrm{d}t} = P_{\mathrm{m1}} - D_1\omega_1 - P_{\mathrm{e1}}, \tag{2.12b}$$

$$\frac{\mathrm{d}\delta_2}{\mathrm{d}t} = \omega_2, \tag{2.12c}$$

$$\frac{\mathrm{d}\omega_2}{\mathrm{d}t} = A\{P_{\mathrm{m2}} - D_2\omega_2 - P_{\mathrm{e2}}\}, \tag{2.12d}$$

where the parameter D_i stands for the damping coefficient, and A for the ratio of inertia constants of the two generators. The detailed derivation of the swing equation is based

on Assumption (A1) and is included in Appendix 2.A. While the mechanical input power $P_{\mathrm{m}i}$ is usually considered as a constant parameter in stability studies [84], this term will be modified to represent the effect of the heat subsystem based on Fig. 1.5. The electric output power $P_{\mathrm{e}i}$ represents the interaction between generators and is given by

$$P_{\mathrm{e}i}(\delta_1,\, \delta_2) = \sum_{j\in\{1,2,\infty\}} E_i E_j \{G_{ij}\cos(\delta_i - \delta_j) + B_{ij}\sin(\delta_i - \delta_j)\}, \tag{2.13}$$

where the symbol ∞ represents the infinite bus, and we fix as $\delta_\infty = 0$. The above formulation is based on Assumption (A2)[4] and called as *classical model* [114, 84]. The parameter E_i corresponds to the voltage behind transient reactance, and the transfer admittance $G_{ij} + \mathrm{i}B_{ij}$ is determined by the associated electric network including transient reactances of the generators, transmission lines, and loads, where the symbol i stands for the unit imaginary number.

The mechanical power $P_{\mathrm{m}i}$ in Eq. (2.12) is determined by the characteristics of the gas turbines as shown in Fig. 1.5. The gas turbine at site $\#i$ converts the gas input rate $P_{\mathrm{g}i}$ to both the mechanical power $P_{\mathrm{m}i}$ and the heat flow rate $Q'_{\mathrm{a}i}$. Because its time response is sufficiently fast compared with the electromechanical dynamics of the generators [31], the dynamics of the gas turbine are not considered as in Assumption (A4). Then, the instantaneous conversion of energy at each gas turbine is represented by

$$\begin{bmatrix} P_{\mathrm{m}i} \\ Q'_{\mathrm{a}i} \end{bmatrix} = \begin{bmatrix} \eta_{\mathrm{e}i} \\ \eta_{\mathrm{h}i} \end{bmatrix} P_{\mathrm{g}i}, \tag{2.14}$$

where $\eta_{\mathrm{e}i}$ represents the thermal efficiency of the gas turbine at site $\#i$, and $\eta_{\mathrm{h}i}$ the ratio of heat output rate to gas input rate. The coefficients $\eta_{\mathrm{e}i}$ and $\eta_{\mathrm{h}i}$ correspond to the coupling factor [42] as mentioned in Sec. 1.4 and are assumed to be constant. While, in general, these coefficients depend on operating conditions of the gas turbines [31], the above assumption does not lose generality of the analysis in this chapter.

For the heat subsystem, we do not consider the dynamics and losses of heat transfer through the heat conduction pipe in this chapter. This corresponds to Assumption (A3) and is relevant if the time-scale separation holds for the electric and heat subsystems. By using the following model, the set-points, i.e. the fuel inputs to the CHP plants, are determined to realize a desired heat transfer rate Q'_{n}. In Fig. 1.5, the conservation of

[4]Strictly speaking, as well as Assumption (A2), we need to assume that the transient saliency i.e. the difference between the transient reactances of d and q axes is negligible [77, 84].

energy at each site induces the following equality:

$$Q'_{\mathrm{a}1} = Q'_{\mathrm{L}1} + Q'_{\mathrm{n}}, \quad Q'_{\mathrm{a}2} = Q'_{\mathrm{L}2} - Q'_{\mathrm{n}}. \tag{2.15}$$

Consequently, the dynamics of the two-site electricity and heat supply system are represented by the following nonlinear dynamical system model:

$$\underbrace{\frac{\mathrm{d}}{\mathrm{d}t}\begin{bmatrix}\delta_1\\ \omega_1\\ \delta_2\\ \omega_2\end{bmatrix}}_{\frac{\mathrm{d}\boldsymbol{x}}{\mathrm{d}t}} = \underbrace{\begin{bmatrix}\omega_1\\ \frac{\eta_{\mathrm{e}1}}{\eta_{\mathrm{h}1}}(Q'_{\mathrm{n}} + Q'_{\mathrm{L}1}) - D_1\omega_1 - P_{\mathrm{e}1}(\delta_1,\, \delta_2)\\ \omega_2\\ A\left\{\frac{\eta_{\mathrm{e}2}}{\eta_{\mathrm{h}2}}(-Q'_{\mathrm{n}} + Q'_{\mathrm{L}2}) - D_2\omega_2 - P_{\mathrm{e}2}(\delta_1,\, \delta_2)\right\}\end{bmatrix}}_{\boldsymbol{f}(\boldsymbol{x})}. \tag{2.16}$$

The dynamical model (2.16) contains the parameters Q'_{n} and $Q'_{\mathrm{L}i}$ of the heat subsystem. These parameters represent the effect of ideal operation of the heat subsystem on dynamics of the electric subsystem.

2.2.2 Settings of parameters

In the rest of this chapter, numerical simulations are provided under several settings of the transfer admittances $G_{ij}+\mathrm{i}B_{ij}$ and the damping coefficient D_i. The setting of the other parameters are summarized in Appendix 2.B. Note that the two sites are identical with the setting in Appendix 2.B, and the model (2.16) has a symmetry for the replacement of $(\delta_1,\, \omega_1)$ and $(\delta_2,\, \omega_2)$ if the heat transfer rate Q'_{n} is set to zero. A non-zero value of Q'_{n} parameterizes the difference between the set points of the two sites. The setting of identical sites does not lose generality of the analysis in this chapter.

The values of $G_{ij} + \mathrm{i}B_{ij}$ considered in this chapter are summarized in Tab. 2.1. The setting A in the table was taken from [9, 124]. In the setting, the transfer conductances $G_{1\infty}$, $G_{2\infty}$, and so on are set to be zero. This corresponds to the assumptions that the transmission line is lossless and that there is no consumed electric power in loads. This is commonly assumed in large-scale transmission systems where the conductances are sufficiently small compared to suceptances [84]. Under the setting, the function $P_{\mathrm{e}i}$ in Eq. (2.13) becomes

$$P_{\mathrm{e}i}(\delta_1, \delta_2) = E_i E_\infty B_{i\infty} \sin\delta_i + E_1 E_2 B_{12} \sin(\delta_i - \delta_j). \tag{2.17}$$

Table 2.1: The values of the transfer conductances in the numerical analyses

	$G_{1\infty}+\mathrm{i}B_{1\infty}$	$G_{2\infty}+\mathrm{i}B_{2\infty}$	$G_{12}+\mathrm{i}B_{12}$	G_{11}	G_{22}
Setting A [9, 124]	$0+1.0\mathrm{i}$	$0+1.0\mathrm{i}$	$0+0.5\mathrm{i}$	0	0
Setting B	$-0.1+1.0\mathrm{i}$	$-0.1+1.0\mathrm{i}$	$0.05+0.5\mathrm{i}$	0.05	0.05

On the contrary, the losses in the lines and loads are included in the setting B in order to consider a regional-scale energy system.

For the damping coefficient D_i, the following two settings are considered in this chapter: $D_i = 0.005$ and 0.21. In the classical swing equation, the physical meaning of the damping is subtle because it can represent various effects [114]. Such effects originates from damper windings and standard control systems of generators such as AVR and PSS. Here, we use the setting $D_i = 0.005$ for simulating a situation where no control systems are operating, and $D_i = 0.21$ where the control systems are ideally operated to provide the damping effect.

2.3 Steady operating condition

This section analyzes the steady operating conditions of the electric subsystem affected by the heat subsystem. As mentioned in Sec. 2.1, a steady operating condition is described by a Stable Equilibrium Point (SEP) of the model (2.16). Here, by the linear stability analysis of the model (2.16), we identify a feasible range of steady operating conditions of the two-site system where the two generators are operated with the same frequency as the infinite bus. From the condition $\mathrm{d}\delta_i/\mathrm{d}t = 0$ at an equilibrium point, we have the value of ω_i at any equilibrium point, denoted by ω_i^*, to be zero:

$$\omega_i^* = 0. \tag{2.18}$$

From the condition $\mathrm{d}\omega_i/\mathrm{d}t = 0$, the values of phase angles δ_1^* and δ_2^* satisfy the following equations:

$$\alpha_1 = \sin\delta_1^* + \kappa_1 \sin(\delta_1^* - \delta_2^*) + \lambda_1 \cos\delta_1^* + \mu_1 \cos(\delta_1^* - \delta_2^*), \tag{2.19a}$$

$$\alpha_2 = \sin\delta_2^* + \kappa_2 \sin(\delta_2^* - \delta_1^*) + \lambda_2 \cos\delta_2^* + \mu_2 \cos(\delta_2^* - \delta_1^*), \tag{2.19b}$$

where α_1 and α_2 are defined by

$$\alpha_1 := \frac{\eta_{\mathrm{e}1}(Q'_{\mathrm{L}1} + Q'_{\mathrm{n}}) - \eta_{\mathrm{h}1}E_1^2 G_{11}}{\eta_{\mathrm{h}1}E_1 E_\infty B_{1\infty}}, \qquad \alpha_2 := \frac{\eta_{\mathrm{e}2}(Q'_{\mathrm{L}2} - Q'_{\mathrm{n}}) - \eta_{\mathrm{h}2}E_2^2 G_{22}}{\eta_{\mathrm{h}2}E_2 E_\infty B_{2\infty}}, \tag{2.20}$$

and κ_i, λ_i, and μ_i are given by

$$\kappa_i := \frac{E_1 E_2 B_{12}}{E_i E_\infty B_{i\infty}}, \quad \lambda_i := \frac{G_{i\infty}}{B_{i\infty}}, \quad \mu_i := \frac{E_1 E_2 G_{12}}{E_i E_\infty B_{i\infty}}. \tag{2.21}$$

Thus, the equilibrium points of the model (2.16) are obtained by solving Eq. (2.19). Since Eq. (2.19) retains the formulation of the active power-flow equation [8, 133], the conventional methods of power-flow analysis can be effective utilized. Particularly, in [10, 9], the dependence of existence and stability of equilibrium points on the values of α_1 and α_2 is studied for Eq. (2.19) with $\lambda_i = \mu_i = 0$ as the setting A in Tab. 2.1.

Here, we consider the effect of the parameters $Q'_{\rm n}$, $Q'_{\rm L1}$, and $Q'_{\rm L2}$ of the heat subsystem, which appear in α_1 and α_2 on the left-hand side of Eq. (2.19). First, as $Q'_{\rm n}$ changes, the point (α_1, α_2) moves along the straight line given by

$$e_1\alpha_1 + e_2\alpha_2 = (Q'_{\rm L1} + Q'_{\rm L2}) - e_3, \tag{2.22}$$

where the coefficients e_1, e_2, and e_3 are determined by the parameters of the gas turbine and electric subsystem as follows:

$$\begin{aligned} e_1 &:= \frac{\eta_{\rm h1}}{\eta_{\rm e1}} E_1 E_\infty B_{1\infty}, \quad e_2 := \frac{\eta_{\rm h2}}{\eta_{\rm e2}} E_2 E_\infty B_{2\infty}, \\ e_3 &:= \frac{\eta_{\rm h1}}{\eta_{\rm e1}} E_1^2 G_{11} + \frac{\eta_{\rm h2}}{\eta_{\rm e2}} E_2^2 G_{22}. \end{aligned} \tag{2.23}$$

Equation (2.22) is obtained by eliminating $Q'_{\rm n}$ from Eq. (2.20). Since the line (2.22) is parameterized by $Q'_{\rm L1} + Q'_{\rm L2}$, a steady operating condition is governed by the values of $Q'_{\rm n}$ and $Q'_{\rm sum} := Q'_{\rm L1} + Q'_{\rm L2}$.

Figure 2.1 shows numerical results on the existence of the equilibrium points. For the region R_n ($n = 2, 4, 6$) in the figure, there are n distinct equilibrium points. The *red* line shows Eq. (2.22) with $Q'_{\rm sum} = 1.8$. In the three regions, one of the equilibrium points is asymptotically stable, and the others are unstable. Figure 2.2 shows the steady values of phase angles δ_1^* and δ_2^*. In the figure, the *solid* lines represent the stable equilibrium points, and the *dashed* lines the unstable equilibrium points. The pair of stable and unstable equilibrium points disappears at (a) $Q'_{\rm n} = \pm 0.44$ for the setting A and (b) $Q'_{\rm n} = \pm 0.59$. By analyzing the linearized system of (2.16) around the equilibrium points, the disappearance of equilibrium points is due to the saddle-node bifurcation [128]. This analysis indicates that synchronized operation of the generators is achieved in a finite range of the heat transfer rate $Q'_{\rm n}$: (a) for $Q'_{\rm n} \in [-0.44, 0.44]$ and (b) $Q'_{\rm n} \in [-0.59, 0.59]$.

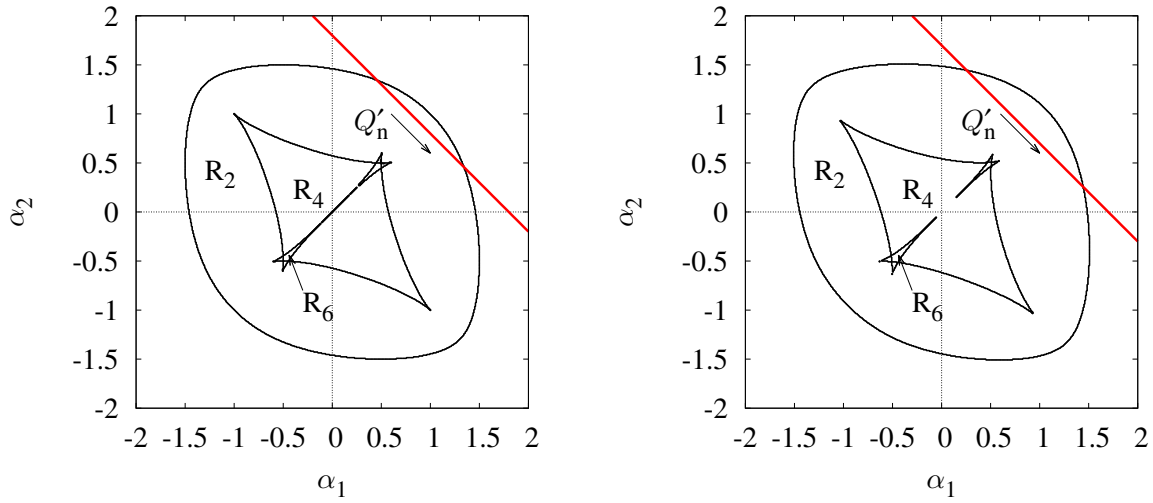

(a) Setting A (lossless)

(b) Setting B (with losses)

Figure 2.1: Numerical result on existence and number of equilibrium points. In the region R_2 (or R_4, R_6), there are two (or four, six) distinct equilibrium points of the dynamical model (2.16). Similar results are obtained for the two settings in Tab. 2.1.

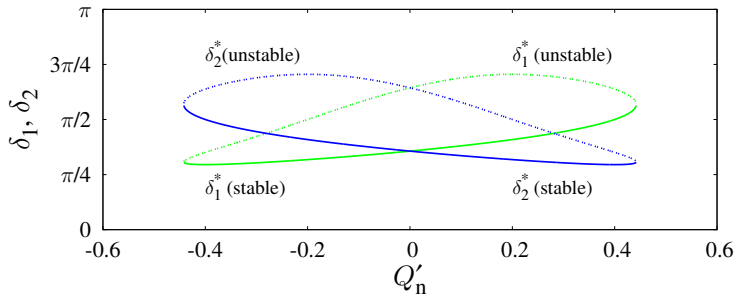

(a) Setting A (lossless)

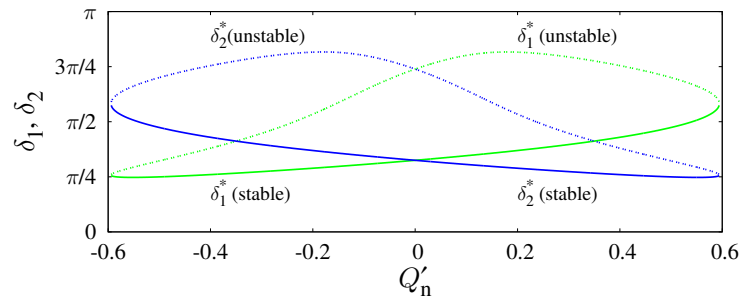

(b) Setting B (with losses)

Figure 2.2: Dependence of the values of phase angles δ_1^* and δ_2^* on the heat transfer rate Q'_n. The *solid* lines represent the stable equilibrium points, and the *dashed* lines the unstable equilibrium points.

In Fig. 2.1 and Fig. 2.2, a similar result is obtained for the setting B. This indicates that the non-zero conductances do not largely affect the analysis under the current settings of parameters.

2.4 Basins of attraction

This section analyzes the basins of attraction of the SEPs representing steady operating conditions under several fixed values of the heat transfer rate Q'_{n}. As well as the SEP, the model (2.16) has several solutions to which nearby solutions converge. Such a solution represents an operating condition where one or both generators are desynchronized from the rest of the system. While such a solution is unrealistic because the modeling assumptions are no longer valid under a desynchronized state[5], their basins involve the basin of the SEP [124, 125, 47]. To investigate these basins, we examine the basins of attraction by systematic and brute-force numerical integrations from a large number of initial conditions in addition to the energy function method presented in Sec. 2.1. This approach is taken in [124, 125, 47] for a double machine-infinite bus system. In [54], a similar method for analyzing basin structure of dynamical systems is developed by using cell state space and mapping on it. While a complete basin portrait of the system requires a full four-dimensional phase space, by following [124, 125, 47], we visualize the basin of attraction by taking the following two-dimensional slice in the entire phase space

$$\{(\delta_1, \delta_2, \omega_1, \omega_2) \in X \mid \omega_1 = 0, \omega_2 = 0\}. \tag{2.24}$$

For the slice (2.24), initial conditions on a grid of 401×401 points were numerically integrated. Each point is colored according to the attractor reached from the corresponding initial condition.

First, we consider an ideal situation, where the transfer conductances are negligible, and the control systems of generators are ideally operated. Thus, the values of $G_{ij} + \mathrm{i}B_{ij}$ are those of the setting A in Tab. 2.1, and $D_i = 0.21$. Figure 2.3 shows the visualization of the basins of attraction under several values of Q'_{n}. Under the current setting of the parameters, the system (2.16) has four attractors. The attractor is the SEP representing the steady operating condition: this is shown by *circle* ($\circ$) in the figure, and its basin is colored in *green*. The second attractor is a periodic orbit, in which generator #1 operates

[5]Furthermore, such a solution never be realized because a desynchronized generator will be tripped out in order not to be destroyed.

at a desynchronized manner with the infinite bus: its basin is colored in *red*. The third one is another periodic orbit, in which generator #2 is desynchronized; its basin is colored in *orange*. In the forth attractor, both generators are desynchronized; its basin is in *yellow*. Figure 2.3 indicates that the basins of attraction of the SEPs become small on the two-dimensional slices as the value of $Q'_{\rm n}$ increases. In addition, the *back closed curve* in each figure represents an analytical estimation of the domain of attraction based on the energy function method given by

$$V(\delta_1,\, \delta_2,\, 0,\, ,0;\, Q'_{\rm n}) = V_{\rm cr}. \tag{2.25}$$

with the following energy function V of the model (2.16):

$$\begin{aligned} V(\delta_1, \delta_2, \omega_1\omega_2; Q'_{\rm n}) = &\sum_{i=1}^{2} \left\{ H_i\omega_i^2 - \frac{\eta_{{\rm e}i}}{\eta_{{\rm h}i}}(\delta_i - \delta_i^*)Q'_{{\rm L}i} - b_i(\cos\delta_i - \cos\delta_i^*) \right\} \\ &- \left\{ \frac{\eta_{\rm e1}}{\eta_{\rm h1}}(\delta_1 - \delta_1^*) - \frac{\eta_{\rm e2}}{\eta_{\rm h2}}(\delta_2 - \delta_2^*) \right\} Q'_{\rm n} \\ &- b_{\rm int}\left\{\cos(\delta_1 - \delta_2) - \cos(\delta_1^* - \delta_2^*)\right\} \end{aligned} \tag{2.26}$$

where δ_1^* and δ_2^* are the values of phase angles at the SEP. The energy function (2.26) is parameterized by the heat transfer rate $Q'_{\rm n}$, and the estimated sets also become small on the slice as the value of $Q'_{\rm n}$ increases. The above results demonstrate that the conventional methods in Sec. 2.1 are applicable for evaluating the static effect of the heat subsystem on the transient stability of the electric subsystem. The *solid* lines in the figure show the stable equilibrium points under various $Q'_{\rm n}$ between 0 and 0.41, and utilized in Sec. 2.5 to discuss dynamic response of the system.

Figures 2.4 and 2.5 show the basins of attraction under different settings of parameters of the electric subsystem. For the both figures, the transfer conductances are taken into account as the setting B in Tab. 2.1. Under the presence of the transfer conductances, it is shown in [22] that there is no analytical energy function, and thus we provide only numerical results on the basins of attraction. While several methods have been established in [17, 23] for extending the energy function approach, we do not discuss them because our main purpose is to show the effectiveness of the conventional methods for evaluating the effect of the heat subsystem and has been verified above. Here we discuss how the basins of attraction are affected by the changes of the parameters. Figure 2.4 shows the result under $D_i = 0.21$ as in Fig. 2.3, and a similar result is obtained: The basins of attraction of the SEPs become small on the two-dimensional slices as $Q'_{\rm n}$ increases. Figure 2.5 shows

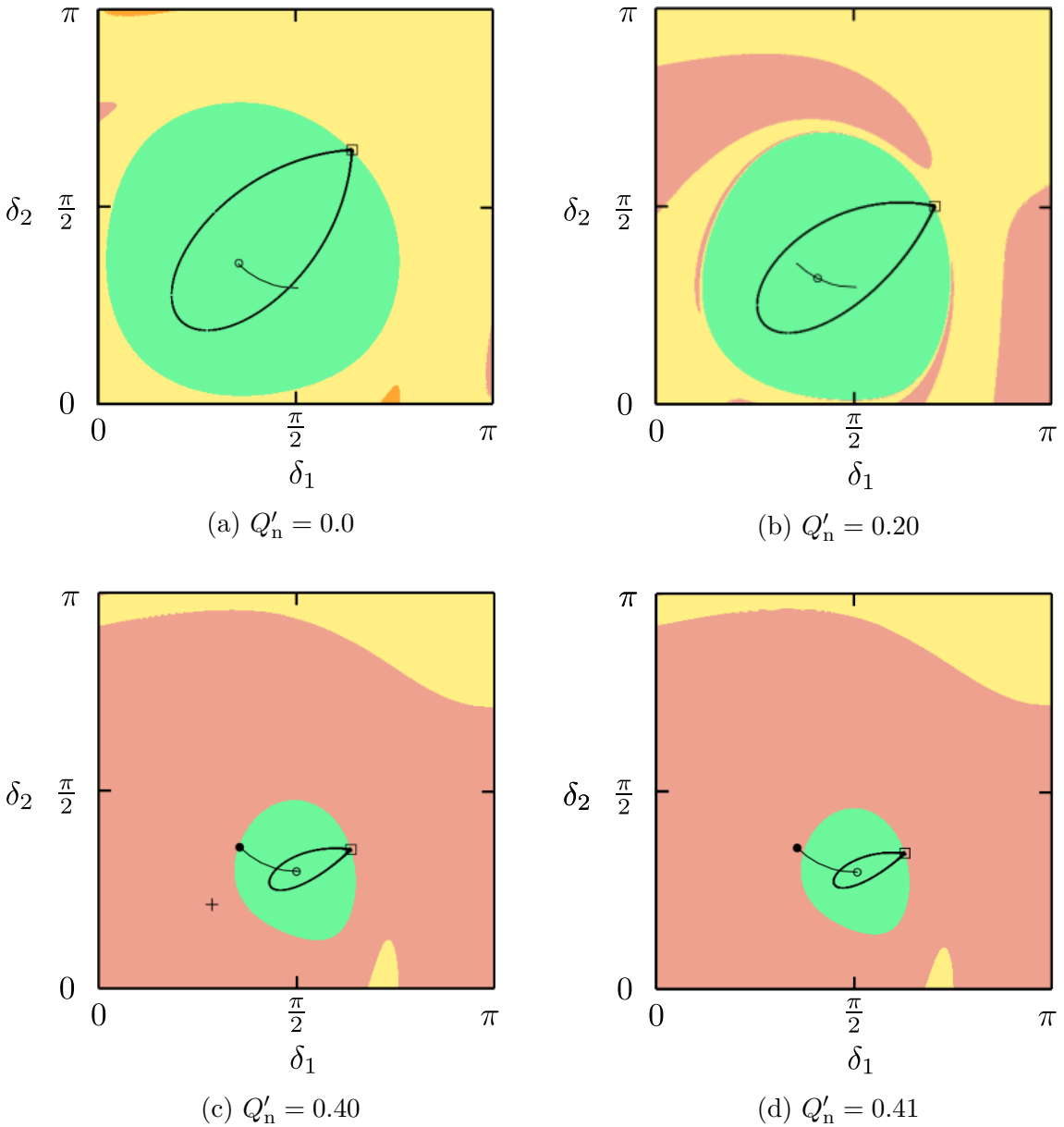

(a) $Q'_{\mathrm{n}} = 0.0$ (b) $Q'_{\mathrm{n}} = 0.20$

(c) $Q'_{\mathrm{n}} = 0.40$ (d) $Q'_{\mathrm{n}} = 0.41$

Figure 2.3: Visualization of basins of attraction. The *circle* (○) shows the stable equilibrium point for each Q'_{n}, and the *square* (□) the unstable equilibrium point. The *back closed curve* represents the analytical estimation of the domain of attraction based on the direct method. The *solid* line shows the equilibrium points under various Q'_{n} between 0 and 0.41.and the dot (●) for $Q'_{\mathrm{n}} = 0$.

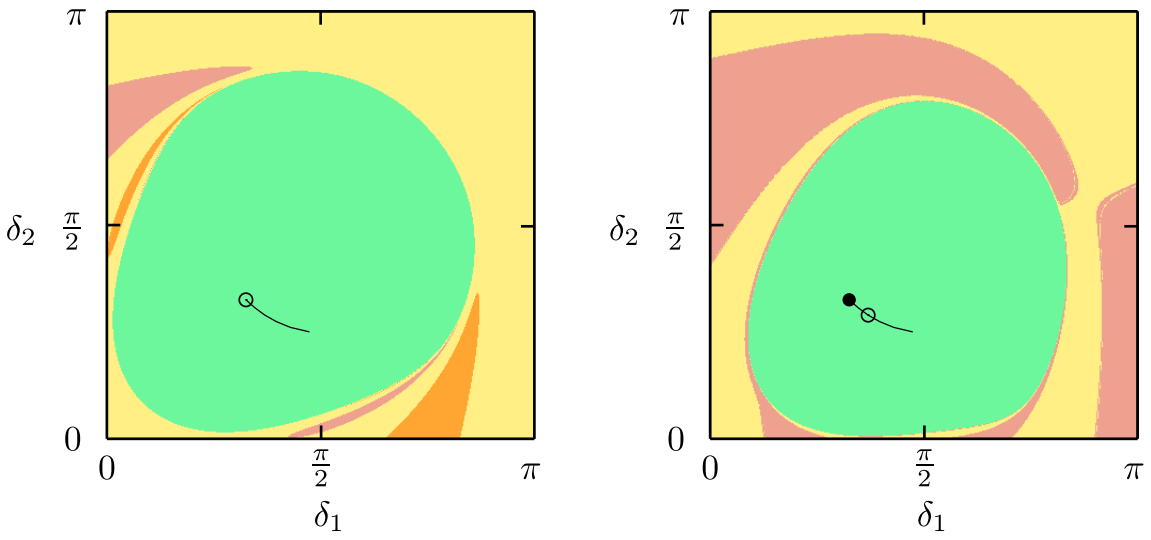

(a) $Q'_{\mathrm{n}} = 0.0$

(b) $Q'_{\mathrm{n}} = 0.2$

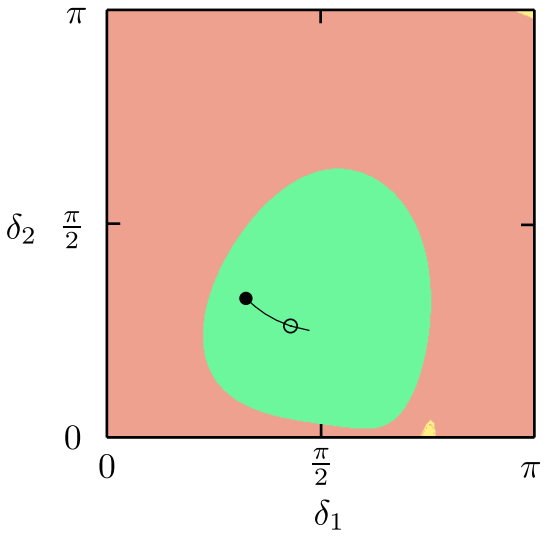

(c) $Q'_{\mathrm{n}} = 0.4$

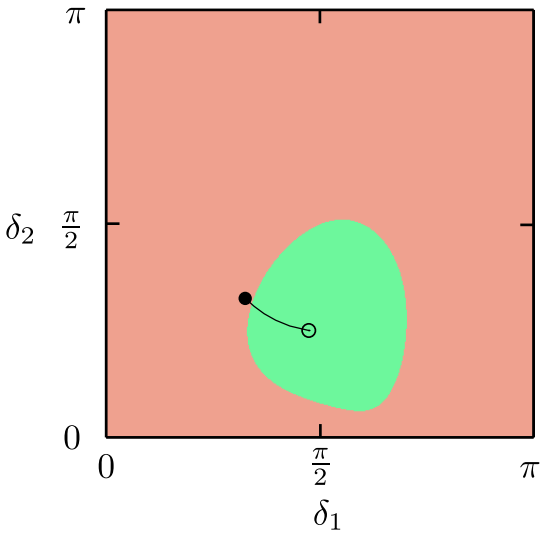

(d) $Q'_{\mathrm{n}} = 0.5$

Figure 2.4: Visualization of basins of attraction under a setting of non-zero transfer conductances shown in Tab. 2.1 and $D = 0.21$. The *solid* line shows the equilibrium points under various Q'_{n} between 0 and 0.5. The *circle* ($\circ$) shows the equilibrium point for each Q'_{n}, and the dot ($\bullet$) for $Q'_{\mathrm{n}} = 0$.

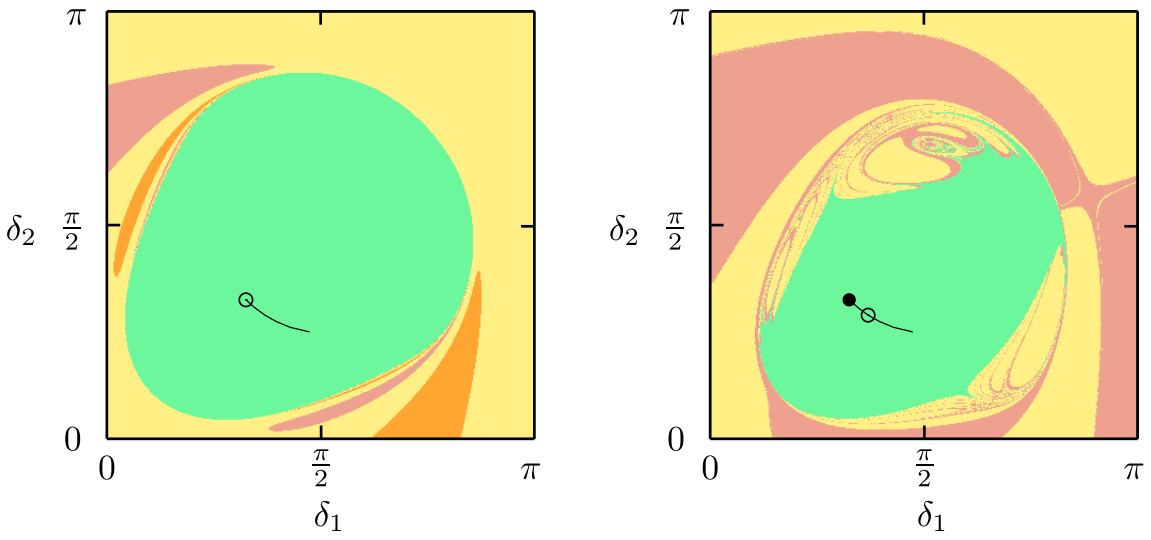

(a) $Q'_{\mathrm{n}} = 0.0$

(b) $Q'_{\mathrm{n}} = 0.2$

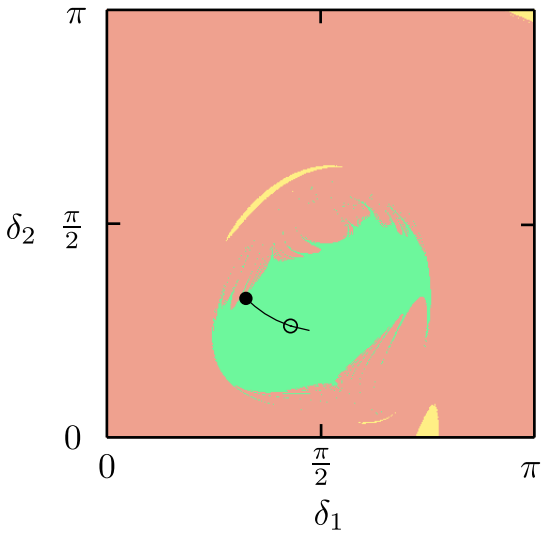

(c) $Q'_{\mathrm{n}} = 0.4$

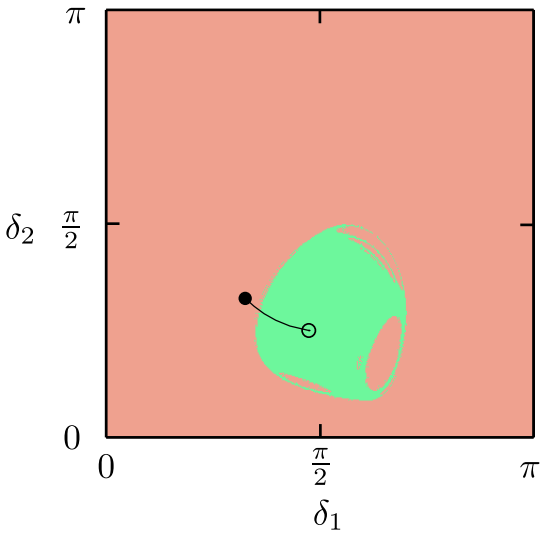

(d) $Q'_{\mathrm{n}} = 0.5$

Figure 2.5: Visualization of basins of attraction under a setting of non-zero transfer conductances shown in Tab. 2.1 and $D = 0.005$. The *solid* line shows the equilibrium points under various Q'_{n} between 0 and 0.5. The *circle* ($\circ$) shows the equilibrium point for each Q'_{n}, and the dot ($\bullet$) for $Q'_{\mathrm{n}} = 0$.

the result under $D_i = 0.05$. In this case, the basin boundaries appear to be complicated, and the slice of basin of attraction is not simply-connected in Fig. 2.5d. This suggests the existence of fractal-like structure in basin boundaries and chaotic transient motions [124, 125, 47]. This indicates that the change of heat transfer rate $Q'_{\rm n}$ possibly induces the complicated transient motions and difficulty in predicting the system's behavior near the boundaries.

2.5 Time-response analysis

As shown in the proceeding sections, the linear and nonlinear stability analyses are effective if the dynamics of the electric and heat subsystems are decoupled. If the scale separation between electric and heat subsystems does not hold, a dynamic change of $Q'_{\rm n}$ should be considered. This section investigates the time responses of the system under a change of the heat transfer rate.

2.5.1 Step-wise change: Ideal operation

The basins of attraction directly illustrates the following two ideal operations of the two-site system. In Fig. 2.3, the *solid* line shows the stable equilibrium points under various $Q'_{\rm n}$ between 0 and 0.41, and the *dot* (•) denotes the equilibrium point under $Q'_{\rm n} = 0$. Since there exists an equilibrium point for each $Q'_{\rm n}$, a quasi-static change of the set-points of the CHP plants enables the change of operating conditions of the generators along the lines in Fig. 2.3. However, a step-wise change of $Q'_{\rm n}$ from 0 to 0.41 desynchronizes the generator #1 because the dot (•) exists outside the domain of attraction of the stable equilibrium point in Fig. 2.3d. Figure 2.6 shows the responses of the system under a step-wise change of the heat transfer rate $Q'_{\rm n}$. In the figure, the system initially has no heat transfer and is at a steady operating condition. In Figs. 2.6a and 2.6b, the heat transfer starts at $t = 10\,{\rm s}$. The value of $Q'_{\rm n}$ is changed as follows:

$$Q'_{\rm n} = \begin{cases} 0 & (t < 10\,{\rm s}), \\ 0.40 \text{ or } 0.41 & (t \geq 10\,{\rm s}). \end{cases} \tag{2.27}$$

The step-wise change of $Q'_{\rm n}$ causes the oscillations of phase angles δ_1 and δ_2. As a result, generator #1 loses the synchronized operation in Fig. 2.6b, while both the generators begin to operate towards a new stable state in Fig. 2.6a. Since the stable equilibrium points exist at both values of $Q'_{\rm n}$, the desynchronization is not due to the local bifurcation

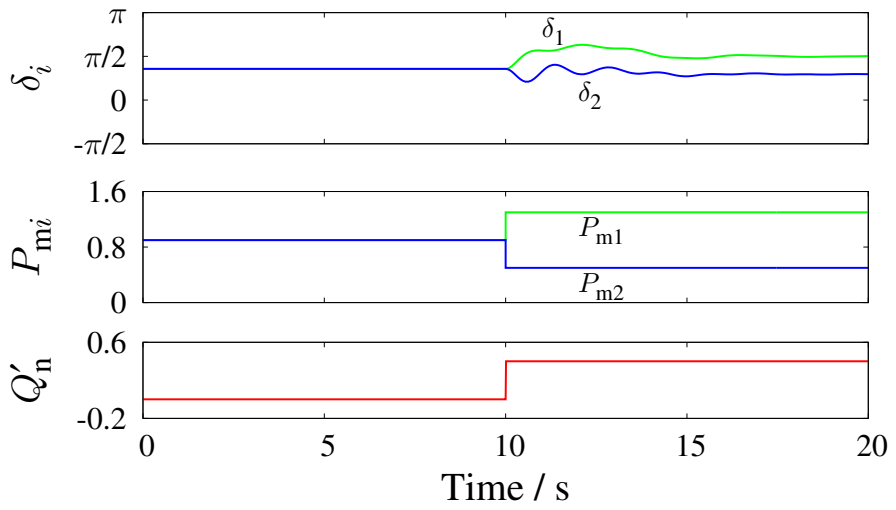

(a) $Q'_{\mathrm{n}} = 0.40$

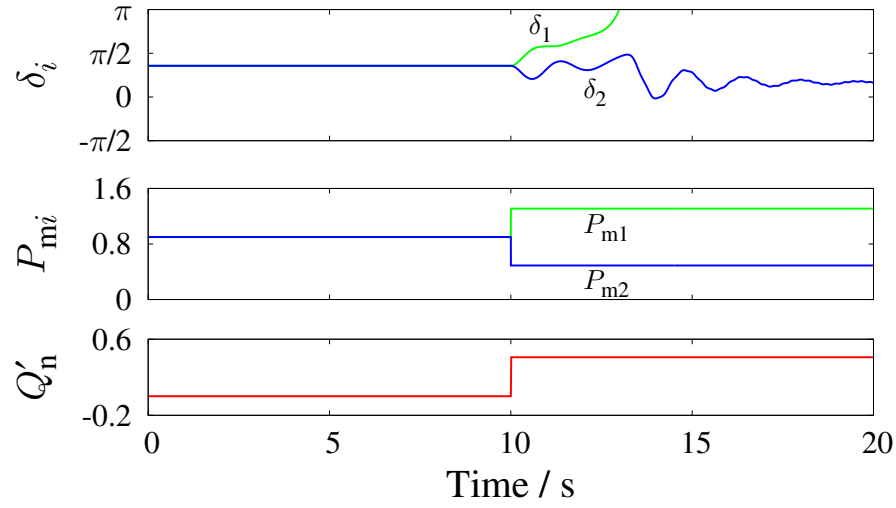

(b) $Q'_{\mathrm{n}} = 0.41$

Figure 2.6: System's responses to step-wise changes of the heat transfer rate Q'_{n}.

of the equilibrium points. This analysis indicates that the boundedness of the domain of attraction possibly induces an instability phenomenon under an abrupt change of the heat transfer rate.

2.5.2 Ramp-wise change: Realistic operation

As a realistic situation, an open-loop control of the heat transfer rate Q'_{n} can be considered as in between the above two ideal situations. Here, based on [111], we consider a ramp-wise change of the set-points of CHP plants from $Q'_{\mathrm{n}} = 0$ to 0.5. The duration

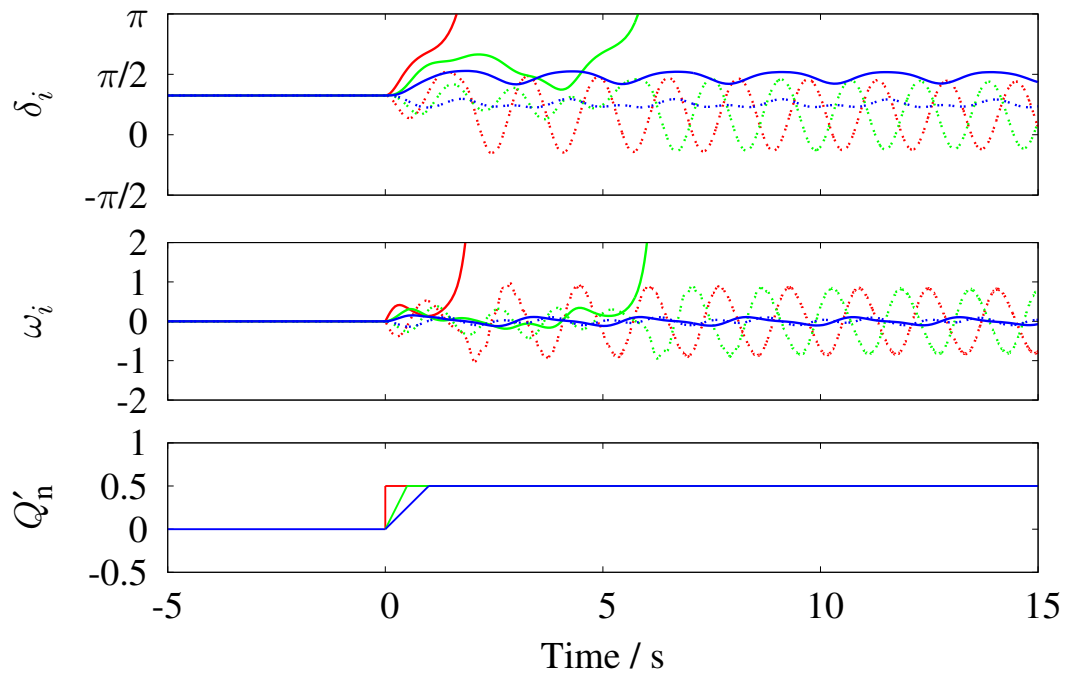

Figure 2.7: System's responses to ramp-wise changes of the heat transfer rate under $T_d = 0$, 0.5, and 1.0 s. The *red* line shows $T_d = 0$, the *green* line $T_d = 0.5$, and the *blue* lien $T_d = 1.0$. The *solid* line shows the response of the generator #1, and the *broken* line the generator #2.

T_d of the change of the set-points is an important parameter: $T_d = 0$ corresponds to the step-wise change, and $T_d = \infty$ the quasi-static change. In an engineering viewpoint, the range of T_d where the instability does not occur is of significant importance. Fig. 2.7 shows the system's responses for $T_d = 0$, 0.5, and 1.0 s. The *red* line shows the case of $T_d = 0$ (step-wise change), and the generator #1 is desynchronized as mentioned above. In the case of $T_d = 1.0$ s (*blue* line), the variables δ_i and ω_i converged to the values of the equilibrium point. In the case of $T_d = 0.5$ s, it is observed that the generator #1 is desynchronized.

2.6 Summary

In this chapter, we reconsidered the effectiveness and limitation of the conventional scale separation of power system dynamics through analyzing the rotor angle stability of the electric subsystem. In the classical swing equation model, the mechanical power

is modeled as an constant parameter. Here we generalized the model by modifying the parameter to represent the effect of the heat subsystem through the CHP plants. It was shown that if the dynamics of the heat subsystem were negligible, conventional methods of stability analysis such as energy function method were applicable to evaluating the current stability problem. If this is not the case, the dynamic interaction between the two subsystems needs to be taken into account. In this direction, we conducted a time-response analysis based on the basins of attraction of stable equilibrium points representing steady operating conditions. The analysis suggests a possibility of instability phenomenon due to dynamic interaction between the two subsystems.

Appendix 2.A Derivation of swing equation

The first appendix derives the swing equation (2.12) in the per-unit system based on [77, 84]. In this appendix, all the variables and parameters are with dimension except for those with superbars ($\bar{\cdot}$) representing per-unit quantities. The derivation starts from the rotor inertia equation describing the effect of unbalance between the electromagnetic torque τ_{e} and the mechanical torque τ_{m} of an individual machine (consisting of a generator and prime mover). The combined inertia of the generator and prime mover is accelerated by the unbalance in the applied torques:

$$J\frac{\mathrm{d}\omega_{\mathrm{m}}}{\mathrm{d}t} = \tau_{\mathrm{m}} - \tau_{\mathrm{e}}, \tag{2.28}$$

where J stands for the total moment of inertia of the turbine and generator rotor, and ω_m for the rotor speed (angular velocity of the rotor shaft). By using the relationships $P_{\mathrm{m}} = \omega_{\mathrm{m}}\tau_{\mathrm{m}}$ and $P_{\mathrm{e}} = \omega_{\mathrm{m}}\tau_{\mathrm{e}}$, Eq. (2.28) becomes

$$J\frac{\mathrm{d}\omega_{\mathrm{m}}}{\mathrm{d}t} = \frac{P_{\mathrm{m}}}{\omega_m} - \frac{P_{\mathrm{e}}}{\omega_{\mathrm{m}}}, \tag{2.29}$$

The above equation can be normalized in terms of the per-unit inertia constant H defined by

$$K := \frac{1}{2}J\omega_{\mathrm{ms}}^2, \quad H := \frac{K}{S_{\mathrm{b}}} = \frac{J\omega_{\mathrm{ms}}^2}{2S_{\mathrm{b}}}, \tag{2.30}$$

where K stands for the kinetic energy at the synchronous speed ω_{ms}, and S_{b} for the rated capacity of the generator. As a result, Eq. (2.29) becomes

$$\frac{2H}{\omega_{\mathrm{ms}}}\frac{\mathrm{d}\omega_{\mathrm{m}}}{\mathrm{d}t} = \frac{\omega_{\mathrm{ms}}}{\omega_m}\left(\frac{P_{\mathrm{m}}}{S_{\mathrm{b}}} - \frac{P_{\mathrm{e}}}{S_{\mathrm{b}}}\right). \tag{2.31}$$

Here, the angular velocity can be expressed in electrical radians rather than in mechanical radian by substituting

$$\omega_{\mathrm{m}} = \frac{\omega_{\mathrm{e}}}{p/2}, \quad \omega_{\mathrm{mr}} = \frac{\omega_{\mathrm{s}}}{p/2}, \tag{2.32}$$

where ω_{e} and ω_{es} stand for the rotor speed and its synchronous speed in electrical radian, and p for the number of poles. Furthermore, by denoting by ω the deviation of rotor speed relative to the synchronous speed, i.e. $\omega := \omega_{\mathrm{e}} - \omega_{\mathrm{es}}$, Eq. (2.31) becomes

$$\frac{2H}{\omega_{\mathrm{es}}}\frac{\mathrm{d}\omega}{\mathrm{d}t} = \frac{1}{1+\omega/\omega_{\mathrm{es}}}\left(\frac{P_{\mathrm{m}}}{S_{\mathrm{b}}} - \frac{P_{\mathrm{e}}}{S_{\mathrm{b}}}\right). \tag{2.33}$$

Under Assumption (A1) implying $\omega/\omega_{\mathrm{es}} \ll 1$, Eq. (2.33) can be approximated by

$$\frac{2H}{\omega_{\mathrm{es}}}\frac{\mathrm{d}\omega}{\mathrm{d}t} \sim \frac{P_{\mathrm{m}}}{P_{\mathrm{b}}} - \frac{P_{\mathrm{e}}}{P_{\mathrm{b}}}. \tag{2.34}$$

Thus, by considering the damping term and denoting by δ the rotor position in electrical radians, we have the swing equation as follows:

$$\frac{\mathrm{d}\delta}{\mathrm{d}\bar{t}} = \bar{\omega}, \tag{2.35a}$$

$$\frac{\mathrm{d}\bar{\omega}}{\mathrm{d}\bar{t}} = \bar{P}_{\mathrm{m}} - \bar{D}\bar{\omega} - \bar{P}_{\mathrm{e}}. \tag{2.35b}$$

where the per-unit quantities are defined by

$$\bar{t} = t\sqrt{\frac{\omega_{\mathrm{es}}}{2H}}, \quad \bar{\omega} = \omega\sqrt{\frac{2H}{\omega_{\mathrm{es}}}}, \quad \bar{P}_{\mathrm{m}} = \frac{P_{\mathrm{m}}}{S_{\mathrm{b}}}, \quad \bar{P}_{\mathrm{e}} = \frac{P_{\mathrm{e}}}{S_{\mathrm{b}}}. \tag{2.36}$$

For the two-site system, the swing equation has the following form:

$$\frac{\mathrm{d}\delta_1}{\mathrm{d}t} = \bar{\omega}_1, \tag{2.37}$$

$$\frac{\mathrm{d}\bar{\omega}_1}{\mathrm{d}t} = \bar{P}_{\mathrm{m}1} - \bar{D}_1\bar{\omega}_1 - \bar{P}_{\mathrm{e}1}, \tag{2.38}$$

$$\frac{\mathrm{d}\delta_2}{\mathrm{d}t} = \bar{\omega}_2, \tag{2.39}$$

$$\frac{\mathrm{d}\bar{\omega}_2}{\mathrm{d}t} = \frac{H_1}{H_2}\{\bar{P}_{\mathrm{m}2} - \bar{D}_2\bar{\omega}_2 - \bar{P}_{\mathrm{e}2}\}, \tag{2.40}$$

where $\bar{\omega}_1$ and $\bar{\omega}_2$ are defined as

$$\bar{t} = t\sqrt{\frac{\omega_{\mathrm{es}}}{2H_1}}, \quad \bar{\omega}_1 = \omega_1\sqrt{\frac{2H_1}{\omega_{\mathrm{es}}}}, \quad \bar{\omega}_2 = \omega_2\sqrt{\frac{2H_1}{\omega_{\mathrm{es}}}}, \quad \bar{P}_{\mathrm{m}i} = \frac{P_{\mathrm{m}i}}{S_{\mathrm{b}}}, \quad \bar{P}_{\mathrm{e}i} = \frac{P_{\mathrm{e}i}}{S_{\mathrm{b}}}. \tag{2.41}$$

Equation (2.12) is obtained by omitting the superbars and defining $A := H_1/H_2$.

Appendix 2.B List of variables and parameters

Table 2.2 lists the meanings and values of parameters. The values of $G_{ij} + \mathrm{i}B_{ij}$ are summarized in Tab. 2.1.

Table 2.2: List of variables and parameters in the model

Physical meaning	Symbol	Value
Synchronous speed	ω_b	$2\pi \cdot 60\,\mathrm{Hz}$
Rated power	P_b	$1.0\,\mathrm{MW}$
Inertia constant	H_i	$10\,\mathrm{s}$
Rotor position relative to synchronous reference flame	δ_i	
Deviation of rotor speed relative to synchronous speed	ω_i	
Mechanical input power to generator	$P_{\mathrm{m}i}$	
Electrical output power from generator	$P_{\mathrm{e}i}$	
Damping coefficient	D_i	0.005 or 0.21
Voltage behind transient reactance	E_i	1.0
Transfer susceptance (#i, ∞)	$B_{i\infty}$	
Transfer conductance (#i, ∞)	$G_{i\infty}$	
Transfer susceptance (#1, #2)	B_{12}	
Transfer conductance (#1, #2)	G_{12}	
Transfer conductance (#i, #i)	G_{ii}	
Heat transfer rate	Q'_n	
Heat load	$Q_{\mathrm{L}i}$	0.9
Coefficient of electricity output	$\eta_{\mathrm{e}i}$	0.40
Coefficient of heat output	$\eta_{\mathrm{h}i}$	0.40

Chapter 3

Multiscale dynamics of the heat subsystem

This chapter focuses on multiple time scale dynamics of the heat subsystem. Chapter 2 revisited the scale separation of power system dynamics and applied the conventional methods of stability analysis by assuming scale separation between electric and heat subsystems. If this is not the case, the interaction between electric and heat subsystems needs to be modeled. In this chapter, we study a problem of mathematical modeling for dynamics occurring in steam supply systems, in which multiple boilers (including a heat recovery boiler within a CHP plant) are connected through a steam pipe network. In such conventional steam-based systems, the primary objective of the CHP operation is to supply a desirable fixed amount of steam [110]. However, in the context of ESI, a rapid operation of the CHP plants can be considered to contribute to the electricity supply by utilizing their ability of rapid electric response [118, 41, 135]. This imposes a problem on mathematical modeling of multiscale dynamics in steam supply systems against a large change of operating condition.

In this chapter, we derive a *lumped-parameter* model that captures the multiscale properties of steam supply. The dynamics of interest are originally described by the model for *fast* steam flows over a pipe network coupled with the model for *slow* internal dynamics of boilers. For a single boiler or single plant, much work has been reported on lumped-parameter modeling [12, 69, 127, 18], whereas for dynamics of steam flows in pipes, partial differential equations or *distributed-parameter* models [101, 4, 81, 126] are normally used. Namely, the lumped-parameter model of boilers is regarded as a slowly time-varying boundary condition of the distributed-parameter model of steam pipes. Although such

models are crucial to plant design, detailed simulation, and commissioning, their simple coupling is too complicated to reveal the system-wide dynamics of interest. In Sec. 3.1, through physically-relevant approximations, we derive a simple lumped-parameter model that captures the multiscale property as well as a graph-theoretic property of the pipe network.

The correctness of the derived model is verified by theoretical and numerical analyses of the model in terms of multiscale property of steam supply. In Sec. 3.2, the theoretical analysis is conducted with dynamical systems and graph theoretic methods [66, 129, 97, 58, 107]. Specifically, the concept of Normally Hyperbolic Invariant Manifold (NHIM) [129, 97, 76] is utilized to discuss structural stability of the derived model. Also, the concept of NHIM characterizes the slow-fast vectorfield near an invariant manifold and becomes dynamical evidence that the derived model preserves the slow-fast dynamics in the original model. We firstly obtain the inner limit of the derived model using the standard regular expansion method [66] and locate a set of non-isolated equilibrium points of the inner-limit model. The set is then proved to form a NHIM under mild technical conditions. In Sec. 3.3, we conduct numerical simulations of the derived model for an example of two-site system under a practical set of parameters. The correctness of the derived model is quantitatively examined by comparison with brute-force simulation of the original model, and the slow-fast dynamics near the NHIM are visualized. The existence of NHIM suggests a separation principle of short-term and long-term operations of steam supply systems, which is analogue to electricity supply operation [84].

3.1 Physical modeling

This section is devoted to derivation of a lumped-parameter model for dynamics of steam supply systems through physically relevant approximations. The modeling procedure is explained in a dimensionless form in order to clearly describe the multiscale property of steam supply. The physical quantities with dimension are denoted by superscript $*$, and the reference quantities for scaling by subscript r. The dimensionless time t is scaled according to the time scale defined by the steam velocity u_{r}^* and the length scale L_{r}^* of the pipes: $t_{\mathrm{r}}^* := L_{\mathrm{r}}^*/u_{\mathrm{r}}^*$. The detailed procedure of scaling and the reference quantities are presented in Appendix 3.A.

3.1.1 Physical processes and modeling assumptions

The basic physical processes of steam supply systems are related to (i) producing, (ii) transporting, and (iii) consuming steam. Figure 3.1 illustrates the three processes for the two-site system. The blocks in the figure represent (a) components of the two-site system and (b) components of a boiler. Each arrow describes the flow of steam, water, or heating gas. For (i), Fig. 3.1b shows the production of steam from combustion gas and water in a boiler. Mixed steam and water are produced in the evaporator due to the boiling of water by high-temperature combustion gas. The mixed steam and water are supplied to the drum and stored at the phase equilibrium condition, while feedwater is supplied to the drum. Thus, the saturated steam in the drum is brought to the outside of boiler. For (ii), the transport of steam to a load in Fig. 3.1a is realized due to the self-pressure of boiler. The transport of steam is also realized by controlling the difference of pressures between the two sites. Finally, for (iii), the transported steam is consumed at each load. The latent heat of the steam is extracted with a heat exchanger, and the resulting condensed water is returned to the boiler.

To understand the system-wide dynamics, the pressure and flow rate of steam are important physical quantities. In order to simply describe essential characteristics of the dynamics, we make the following assumptions:

(A1) Temperatures of drum, evaporator and their wall are equal to temperature of mixed steam and water, i.e. the saturation temperature [12, 69].

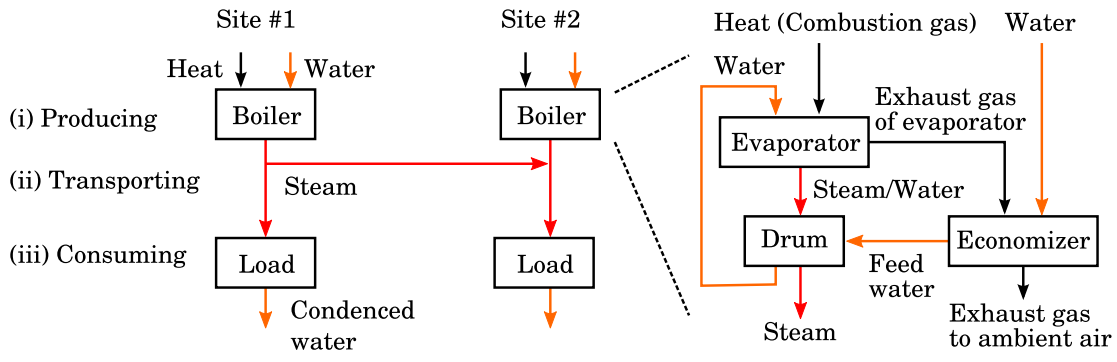

(a) Components of the two-site system (b) Components of a boiler

Figure 3.1: Schematic diagram of the two-site steam supply. Each block in the figure shows (a) components of the two-site system and (b) components of a boiler. *Red*, *orange*, and *black* arrows describe the flow of steam, water, and heating gas, respectively.

(A2) Change of the volumes of steam and water is negligible when the water level of a drum is well regulated [12].

(A3) Feedwater to a drum is at the condition of saturated liquid [69].

(A4) Pressure drop in a pipe is evaluated by the Darcy-Weisbach equation for steady flow [101].

(A5) No dominant effect of compressibility of steam appears on its velocity profile. This is relevant when the steam velocity is sufficiently smaller than the sound speed [78].

(A6) No dominant effect of heat loss appears on the pressure drop and volumetric flow. This is relevant when the mass fraction of vapor in the fluid, i.e. the quality of steam is sufficiently close to one [123, 63].

(A7) Pressure drop in the site's components such as pressure regulators and valves are negligible.

The validity of Assumptions (A1)–(A3) and Assumption (A4) has been tested in [12, 69] and [101, 4], respectively. Thus, we mainly discuss Assumptions (A5)–(A7) in the rest of this chapter.

3.1.2 Derivation of lumped-parameter model

In Secs. 3.1 and 3.2, we will consider a general steam supply system with arbitrary number of sites based on graph theory [58, 107]: see Appendix 3.B for its details. The topology of a steam supply system is described by a directed graph $\mathcal{G} = (\mathcal{V}, \mathcal{L})$, where $\mathcal{V}$ stands for a finite set of vertices representing sites, and $\mathcal{L}$ for a finite set of links representing steam transporting pipes. For a link $l \in \mathcal{L}$, the tail (or head) vertex is denoted by $\partial^+ l$ (or $\partial^- l$). For a vertex $v \in \mathcal{V}$, the set of outgoing (or incoming) links is denoted by $\delta^+ v$ (or $\delta^- v$). Below, the physical variables of boilers and pipes at each vertex and link are denoted by subscripts v and l, respectively. The graph $\mathcal{G}$ is assumed to contain no self-loop and to be connected. The assumption of no self-loop is relevant because a steam transporting pipe normally connects different two sites. Under this assumption, the incidence relation of a graph is completely represented with the incident matrix [58], and hence the matrix will be used in our modeling and analysis. The assumption of

connected graph is intended for simplifying the presentation in this paper and does not lose generality of the modeling and analysis in this chapter.

The dynamical model of a boiler is based on [12, 69]. In the model, V represents volume, ρ density, h specific enthalpy, T temperature, and m' mass flow rate. Furthermore, the three subscripts s, w, and m represent saturated steam, saturated water, and metal, respectively. The total mass of metals of the drum and the evaporator is represented by m_{t}, and the specific heat of the metals by C_{p}. It is stated in [12] that the dynamics of pressure are well captured by global mass and energy balance. This is because the internal energy is rapidly released or absorbed due to the uniform boiling and condensation inside the drum and evaporator. Thus, under Assumptions (A1)–(A3), the dynamics of pressure p_v at vertex $v \in \mathcal{V}$ are formulated as

$$e_v(p_v)\frac{\mathrm{d}p_v}{\mathrm{d}t} = \epsilon_1 \left\{ Q'_v - m'_{\mathrm{s}v} h_{\mathrm{c}}(p_v) \right\}, \tag{3.1}$$

where Q'_v stands for the heat flow rate to the evaporator, and $h_{\mathrm{c}} := h_{\mathrm{s}} - h_{\mathrm{w}}$ corresponds to enthalpy of condensation. The small parameter $\epsilon_1 := d_{\mathrm{r}}^{*2} L_{\mathrm{r}}^* / e_{\mathrm{r}}^*$ determines the slowness of the pressure dynamics (3.1) in terms of the time scale t_{r}^* of steam flow. From [12], the coefficient $e_v(p_v)$ represents the rate of change of internal energy stored in the boiler against a change of pressure, given by

$$\begin{aligned} e_v(p_v) =& h_{\mathrm{c}v} V_{\mathrm{s}v} \frac{\partial \rho_{\mathrm{s}v}}{\partial p_v} + \rho_{\mathrm{s}v} V_{\mathrm{s}v} \frac{\partial h_{\mathrm{s}}}{\partial p_v} + \rho_{\mathrm{w}v} V_{\mathrm{w}v} \frac{\partial h_{\mathrm{w}v}}{\partial p_v} + m_{\mathrm{t}v} C_{\mathrm{p}} \frac{\partial T_{\mathrm{s}v}}{\partial p_v} - V_{\mathrm{s}v} - V_{\mathrm{w}v}. \end{aligned} \tag{3.2}$$

In this paper, as in [12], the thermodynamic properties h_{s}, h_{w}, ρ_{s}, ρ_{w}, and T_{s} are evaluated from the steam table [15] and are represented as functions of pressure p_v, for example, $h_{\mathrm{s}v} = h_{\mathrm{s}}(p_v)$.

The transient steam flow in a pipe is described by the one-dimensional continuity equations of mass, momentum, and energy [101, 4, 81]. For each link $l \in \mathcal{L}$, the mass balance is given by

$$\frac{\partial \rho_l}{\partial t} + \frac{\partial}{\partial x}(\rho_l u_l) = 0, \tag{3.3}$$

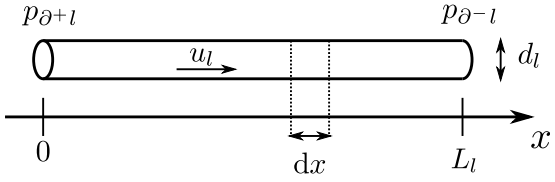

Figure 3.2: Schematic diagram of the steam transporting pipe l.

the momentum balance by

$$\frac{\partial}{\partial t}(\rho_l u_l) + \frac{\partial}{\partial x}(\rho_l u_l^2) + \frac{1}{\epsilon_2}\frac{\partial p_l}{\partial x} + \lambda_l \frac{\rho_l u_l |u_l|}{2d_l} = 0, \tag{3.4}$$

and the energy balance by

$$\frac{\partial}{\partial t}(\rho_l h_l) + \frac{\partial}{\partial x}(\rho_l h_l u_l) = \frac{\partial p_l}{\partial t} + \epsilon_3 Q_{\mathrm{w}l}, \tag{3.5}$$

where u_l stands for the velocity of steam in a pipe l, and x for the displacement variable along the pipe. The parameter λ_l stands for the friction coefficient of the Darcy-Weisbach equation [101, 63, 15] under Assumption (A4). The parameters d_l and $Q_{\mathrm{w}l}$ stand for the diameter of the pipe and the heat flow through walls, respectively. The parameters $\epsilon_2 := \rho^*_{\mathrm{sr}} u^{*2}_{\mathrm{r}}/p^*_{\mathrm{r}}$ and $\epsilon_3 := d^{*2}_{\mathrm{r}} L^*_{\mathrm{r}} Q^*_{\mathrm{wr}}/Q'^*_{\mathrm{r}}$ in Eqs. (3.4) and (3.5) are small, and they reflect Assumptions (A5) and (A6), respectively. Under the two assumptions, the above original equations are simplified through the incompressibility condition $\partial u/\partial x = 0$. It is widely accepted that the low Mach number (described by ϵ_2) implies an incompressible model [78]. Further precise discussions are presented in [93, 108] for Navier-Stokes equations and in [37] for one-dimensional flow equations. The literature [93, 108, 37] shows that the simplification is relevant if both the constants ϵ_2 and ϵ_3 are sufficiently small. Hence, the energy equation (3.5) is decoupled from the other equations, and the dynamics of steam flows are described by the momentum equation (3.4) with the condition $\partial u/\partial x = 0$:

$$\rho_l \frac{\partial u_l}{\partial t} + \frac{1}{\epsilon_2}\frac{\partial p_l}{\partial x} + \frac{\lambda_l \rho_l u_l |u_l|}{2d_l} = 0. \tag{3.6}$$

Therefore, by integrating Eq. (3.6) with respect to x from $x = 0$ to $x = L_l$ (see Fig. 3.2), the following ordinary differential equation is derived:

$$L_l \rho_{\mathrm{av}l} \frac{\mathrm{d}u_l}{\mathrm{d}t} = \frac{p_{\partial^+ l} - p_{\partial^- l}}{\epsilon_2} - \frac{\lambda_l \rho_{\mathrm{av}l} L_l u_l |u_l|}{2d_l}, \tag{3.7}$$

where $\rho_{\mathrm{av}l}$ is given by

$$\rho_{\mathrm{av}l}(t) := \frac{1}{L_l}\int_0^{L_l} \rho_l(x,t)\mathrm{d}x. \tag{3.8}$$

At each site, Eqs. (3.1) and (3.7) are combined via the continuity equations of mass and energy. Under Assumption (A7) we have the following equations [101]: for each $v \in \mathcal{V}$ and all $t \in \mathbb{R}$, the mass balance is given by

$$m'_{\mathrm{s}v}(t) = m'_{\mathrm{L}v}(t) + \sum_{l \in \delta^+ v} \frac{\pi d_l^2}{4}\rho_l(0,t)u_l(t) - \sum_{l \in \delta^- v} \frac{\pi d_l^2}{4}\rho_l(L_l,t)u_l(t), \tag{3.9}$$

and the energy balance by

$$m'_{\mathrm{s}v}(t)h_{\mathrm{s}}(p_v(t)) = m'_{\mathrm{L}v}(t)h_{\mathrm{L}v}(t) + \sum_{l\in\delta^+v}\frac{\pi d_l^2}{4}\rho_l(0,t)u_l(t)h_l(0,t) - \sum_{l\in\delta^-v}\frac{\pi d_l^2}{4}\rho_l(L_l,t)u_l(t)h_l(L_l,t), \tag{3.10}$$

where $m'_{\mathrm{L}v}$ and $h_{\mathrm{L}v}$ stand for the mass flow rate and specific enthalpy consumed by the load at vertex v. They are related to the consumption rate $Q'_{\mathrm{L}v}$ of heat as follows:

$$m'_{\mathrm{L}v}h_{\mathrm{L}v} = Q'_{\mathrm{L}v} + m'_{\mathrm{L}v}h_{\mathrm{w}}(p_v). \tag{3.11}$$

By multiplying both the sides of Eq. (3.9) by $h_{\mathrm{w}}(p_v)$ and using Eq. (3.10), we obtain

$$m'_{\mathrm{s}v}h_{\mathrm{c}}(p_v) = Q'_{\mathrm{L}v} + \sum_{l\in\delta^+v}\frac{\pi d_l^2}{4}\rho_l(0,t)(h_l(0,t)-h_{\mathrm{w}}(p_v))u_l - \sum_{l\in\delta^-v}\frac{\pi d_l^2}{4}\rho_l(L_l,t)(h_l(L_l,t)-h_{\mathrm{w}}(p_v))u_l. \tag{3.12}$$

The above equation is used in Eq. (3.1) and thereby combines the two equations Eq. (3.1) and Eq. (3.7).

Finally, in order to derive a model in a self-consistent manner, it is necessary to determine the thermodynamic quantities in the pipes. While they are calculated in the original model by Eq. (3.3) for mass and Eq. (3.5) for energy, we give their values by functions of pressure p_v based on Assumption (A6) and (A7):

$$\begin{aligned} &h_l(0,t) := h_{\mathrm{s}}(p_{\partial^+l}(t)), \quad h_l(L_l,t) := h_{\mathrm{s}}(p_{\partial^-l}(t)),\\ &\rho_l(0,t) := \rho_{\mathrm{s}}(p_{\partial^+l}(t)), \quad \rho_l(L_l,t) := \rho_{\mathrm{s}}(p_{\partial^-l}(t)),\\ &\rho_{\mathrm{avl}}(t) := \frac{\rho_{\mathrm{s}}(p_{\partial^+l}(t)) + \rho_{\mathrm{s}}(p_{\partial^-l}(t))}{2}. \end{aligned} \tag{3.13}$$

The relevance of these approximations will be discussed in Sec. 3.3.3.

Consequently, the following model is derived for representing the steam supply dynamics: for each $v \in \mathcal{V}$ and $l \in \mathcal{L}$,

$$\frac{\mathrm{d}p_v}{\mathrm{d}t} = \frac{\epsilon}{e_v(p_v)}\left\{Q'_v - Q'_{\mathrm{L}v} - \sum_{l\in\delta^+v}\frac{\pi d_l^2}{4}h_{\mathrm{c}}(p_v)\rho_{\mathrm{s}}(p_v)u_l + \sum_{l\in\delta^-v}\frac{\pi d_l^2}{4}h_{\mathrm{c}}(p_v)\rho_{\mathrm{s}}(p_v)u_l\right\}, \tag{3.14a}$$

$$\frac{\mathrm{d}u_l}{\mathrm{d}t} = \frac{1}{\epsilon}\frac{2(p_{\partial^+l}-p_{\partial^-l})}{L_l\{\rho_{\mathrm{s}}(p_{\partial^+l})+\rho_{\mathrm{s}}(p_{\partial^-l})\}} - \frac{\lambda_l}{2d_l}u_l|u_l|, \tag{3.14b}$$

where ϵ_1 and ϵ_2 were reset as ϵ by choosing the reference quantities as $e_{\mathrm{r}}^* := d_{\mathrm{r}}^{*2} L_{\mathrm{r}}^* / \epsilon_2$. This resetting operation is relevant for a practical setting of parameters shown in Sec. 3.3.

Here, we discuss the multiscale property of the derived model: see Sec. 3.2 for its detailed analysis. The model (3.14) includes a single small parameter ϵ, and the parameters and functions on the right-hand sides are order of 1. From Eq. (3.14a), the pressure p_v changes slowly in time due to the presence of the small parameter. In Eq. (3.14b), the first and second terms on the right-hand side should be order of 1. That is, the pressure difference $p_{\partial^+ l} - p_{\partial^- l}$ should be kept small (order of ϵ). If this is not the case, for example if the pressure difference is $\mathcal{O}(1)$, then the left-hand side of Eq. (3.14b) becomes $\mathcal{O}(1/\epsilon)$, implying the steam velocity u_l becomes large. This indicates the violation of Assumption (A5), and hence the derivation of the lumped-parameter model (3.14) loses its validity. Thus, the smallness of $p_{\partial^+ l} - p_{\partial^- l}$ is necessary and will be assumed in the rest of this paper. Consequently, the short-term dynamics in $t \in [0, T]$ for $T = \mathcal{O}(1)$ are described by the changes of u_l in $\mathcal{O}(1)$ and p_v in $\mathcal{O}(\epsilon)$. On the other hand, the long-term dynamics are related to the change of p_v of $\mathcal{O}(1)$, implying the changes of thermodynamic quantities such as ρ_{s}.

3.2 Theoretical analysis

This section shows that the derived model (3.14) preserves the slow-fast dynamics in the original model. In phase-space geometric concepts, the presence of slow-fast dynamics can be described by the cencept of Normally Hyperbolic Invariant Manifold (NHIM) [129, 97]: slow dynamics along an invariant manifold and fast dynamics transversal to it. In order to theoretically analyze Eq. (3.14), here we simplify the model through the standard regular expansion method [66]. As will be shown later, it corresponds to the inner-limit of the derived model. Thus, we prove the existence of NHIM for the inner-limit model (3.19). This indicates that the slow-fast dynamics are involved in the model (3.14), because a NHIM persists under a perturbation of vectorfield [129, 97]. Indeed, in Sec. 3.3, we will numerically confirm the existence of NHIM for the model (3.14).

3.2.1 Notation

The notation frequently used in this section is summarized below. The symbol T stands for the transpose operation of a vector or matrix. For a matrix A, $\mathrm{Im}(\mathsf{A})$ represents the

image space of linear mapping represented by A, and $\mathrm{Ker}(\mathsf{A})$ the kernel space of the linear mapping A. The symbol $\mathrm{diag}(\boldsymbol{v})$ stands for the diagonal matrix made from a vector $\boldsymbol{v}$. For a vector-valued function $\boldsymbol{f} = (f_1, \ldots, f_m)^\top$, its Jacobian is denoted by $D\boldsymbol{f}$. The constant vector $\mathbf{1}$ stands for all-one vector. For an Euclidean space E, $E^\perp$ stands for the orthogonal space of E.

3.2.2 Derivation of inner-limit model

First, we apply the regular expansion method to the derived model (3.14). The regular expansion starts with assuming a solution of (3.14) in the following form:

$$\begin{aligned} p_v(t,\epsilon) &= p_v^{(0)}(t) + \epsilon p_v^{(1)}(t) + \mathcal{O}(\epsilon^2), \\ u_l(t,\epsilon) &= u_l^{(0)}(t) + \epsilon u_l^{(1)}(t) + \mathcal{O}(\epsilon^2). \end{aligned} \tag{3.15}$$

By substituting them into (3.14) and equating the coefficient of each power of ϵ, a series of differential equations is obtained. From the leading-order terms, we obtain the following conditions: for all $v \in \mathcal{V}$ and $l \in \mathcal{L}$,

$$\frac{\mathrm{d}p_v^{(0)}}{\mathrm{d}t} = 0, \quad p_{\partial^+ l}^{(0)} = p_{\partial^- l}^{(0)}. \tag{3.16}$$

Thus, $p_v^{(0)}$ does not depend on both time and site, and is henceforth denoted by p_0. For the next-order of the series, we obtain the governing equations that contain the graph-theoretic property of the target steam supply system. For the graph $\mathcal{G} = (\mathcal{V}, \mathcal{L})$, by labeling the vertices and links as $\mathcal{V} := \{v_1, \ldots, v_n\}$ and $\mathcal{L} := \{l_1, \ldots, l_m\}$, the first-order term of pressure and the zeroth-order term of volumetric flow of steam are described by

$$\boldsymbol{\psi} := \left[p_1^{(1)}, \ldots, p_n^{(1)}\right]^\top, \quad \boldsymbol{q} := \frac{\pi}{4}\left[d_1^2 u_1^{(0)}, \ldots, d_m^2 u_m^{(0)}\right]^\top. \tag{3.17}$$

The incidence matrix $\mathsf{R} = (R_{ij}) \in \mathbb{R}^{n\times m}$ of the graph is defined by

$$R_{ij} := \begin{cases} 1 & \text{if } v_i = \partial^+ l_j \neq \partial^- l_j, \\ -1 & \text{else if } v_i = \partial^- l_j \neq \partial^+ l_j, \\ 0 & \text{otherwise.} \end{cases} \tag{3.18}$$

With the notation, the dynamics of $(\boldsymbol{\psi}, \boldsymbol{q})$ are described as follows:

$$\begin{bmatrix} \mathsf{G} & 0 \\ 0 & \mathsf{H} \end{bmatrix} \frac{\mathrm{d}}{\mathrm{d}t} \begin{bmatrix} \boldsymbol{\psi} \\ \boldsymbol{q} \end{bmatrix} = \begin{bmatrix} 0 & -\mathsf{R} \\ \mathsf{R}^\top & 0 \end{bmatrix} \begin{bmatrix} \boldsymbol{\psi} \\ \boldsymbol{q} \end{bmatrix} + \begin{bmatrix} \boldsymbol{s} \\ -\boldsymbol{f}(\boldsymbol{q}) \end{bmatrix}, \tag{3.19}$$

with

$$\mathsf{G} := \mathrm{diag}\left(\frac{e_1(p_0)}{h_\mathrm{c}(p_0)\rho_\mathrm{s}(p_0)}, \ldots, \frac{e_n(p_0)}{h_\mathrm{c}(p_0)\rho_\mathrm{s}(p_0)}\right), \tag{3.20}$$

$$\mathsf{H} := \mathrm{diag}\left(\frac{4\rho_\mathrm{s}(p_0)L_1}{\pi d_1^2}, \ldots, \frac{4\rho_\mathrm{s}(p_0)L_m}{\pi d_m^2}\right), \tag{3.21}$$

$$\boldsymbol{s} := \left(\frac{Q'_1 - Q'_{\mathrm{L}1}}{h_\mathrm{c}(p_0)\rho_\mathrm{s}(p_0)}, \ldots, \frac{Q'_n - Q'_{\mathrm{L}n}}{h_\mathrm{c}(p_0)\rho_\mathrm{s}(p_0)}\right)^\top, \tag{3.22}$$

$$\boldsymbol{f}(\boldsymbol{q}) := \left(\frac{8\lambda_1 L_1 \rho_\mathrm{s}(p_0) q_1 |q_1|}{\pi^2 d_1^5}, \ldots, \frac{8\lambda_m L_m \rho_\mathrm{s}(p_0) q_m |q_m|}{\pi^2 d_m^5}\right)^\top. \tag{3.23}$$

Note that (3.19) possibly has a unbounded solution, and thus the expansion (3.15) is not uniformly valid for all time $t \in \mathbb{R}$. Namely, there exists a finite T such that the expansion is valid at all $t \in [0, T]$, and thus the limitation $\epsilon \to 0$ implies the inner limit [66]. In this sense, we call (3.19) as the *inner-limit model* of the lumped-parameter model (3.14).

3.2.3 Characterization of invariant manifold

In this subsection, we locate the invariant manifold in the inner-limit model (3.19) using graph theory: see Appendix 3.B for its summary. As will be shown below, the manifold is located as a set of non-isolated equilibrium points. An equilibrium point $(\boldsymbol{\psi}^*, \boldsymbol{q}^*)$ of Eq. (3.19) satisfies the following condition: for given $\boldsymbol{s}$, R, and $\boldsymbol{f}$,

$$\mathsf{R}\boldsymbol{q}^* = \boldsymbol{s}, \tag{3.24a}$$

$$\mathsf{R}^\top \boldsymbol{\psi}^* = \boldsymbol{f}(\boldsymbol{q}^*). \tag{3.24b}$$

The above conditions can be regarded as the combination of two linear equations defined by R and $\mathsf{R}^\top$. Thus, they are analyzed using the image and kernel spaces of R and $\mathsf{R}^\top$. First, Eq. (3.24a) has a solution if $\boldsymbol{s}$ belongs to the image of R:

$$\boldsymbol{s} \in \mathrm{Im}(\mathsf{R}) = (\mathrm{Ker}(\mathsf{R}^\top))^\perp. \tag{3.25}$$

Since Eq. (3.25) implies that $\boldsymbol{s}$ is orthogonal to $\mathbf{1}$ (see (3.58) in Appendix 3.B), the sum of all the elements $s_1 + \cdots + s_n$ should be zero. By the definition in Eq. (3.22), this condition is equivalent to

$$Q'_1 + \cdots + Q'_n = Q'_{\mathrm{L}1} + \cdots + Q'_{\mathrm{L}n}. \tag{3.26}$$

This clearly indicates that the sum of all generation and consumption of steam at vertices is zero. Even if the above condition does not hold, the following analysis in this section is

still applicable by introducing a new state variable $(\boldsymbol{\psi}', \boldsymbol{q})$ with the following time-varying transformation:

$$\boldsymbol{\psi}' = \boldsymbol{\psi} - \left(\frac{s_1 + \cdots + s_n}{G_{11} + \cdots + G_{nn}} t \right) \mathbf{1}. \tag{3.27}$$

Thus, under the condition (3.25), the set of all solutions of Eq. (3.24a), denoted by $Q^*(\boldsymbol{s})$, is described as follows:

$$Q^*(\boldsymbol{s}) = \left\{ \boldsymbol{q_0} + \boldsymbol{q} \;\middle|\; \boldsymbol{q} \in \mathrm{Ker}(\mathsf{R}) \right\}, \tag{3.28}$$

where $\boldsymbol{q_0}$ stands for one of the solutions of (3.24a). Second, (3.24b) has a solution if $\boldsymbol{f}(\boldsymbol{q})$ belongs to the image of $\mathsf{R}^\top$:

$$\boldsymbol{f}(\boldsymbol{q}) \in \mathrm{Im}(\mathsf{R}^\top). \tag{3.29}$$

This implies that $\boldsymbol{f}(\boldsymbol{q})$ belongs to the subspace of cutsets, which is known as the Kirchhoff's law for tensions [58]. Under the condition (3.29) and for $\boldsymbol{q}^* \in Q^*(\boldsymbol{s})$, the set $\Psi^*(\boldsymbol{q}^*)$ of all solutions of (3.24b) is described as follows:

$$\Psi^*(\boldsymbol{q}^*) = \left\{ \boldsymbol{\psi_0} + \boldsymbol{\psi} \;\middle|\; \boldsymbol{\psi} \in \mathrm{Ker}(\mathsf{R}^\top) = c\,\mathbf{1}\ , c \in \mathbb{R} \right\}. \tag{3.30}$$

where $\boldsymbol{\psi_0}$ stands for one of the solutions of (3.24b). Consequently, under the two conditions

$$\boldsymbol{s} \in (\mathrm{Ker}(\mathsf{R}^\top))^\perp \quad \text{and} \quad \mathrm{Im}(\mathsf{R}^\top) \cap \boldsymbol{f}(Q^*(\boldsymbol{s})) \neq \emptyset, \tag{3.31}$$

the set of equilibrium points $(\boldsymbol{\psi}^*, \boldsymbol{q}^*)$ is described as follows:

$$\left\{ (\boldsymbol{\psi}^*, \boldsymbol{q}^*) \in \mathbb{R}^{n+m} \;\middle|\; \boldsymbol{\psi}^* = \boldsymbol{\psi}_0 + c\,\mathbf{1},\ c \in \mathbb{R},\ \boldsymbol{q}^* \in \boldsymbol{f}^{-1}(\mathrm{Im}(\mathsf{R}^\top)) \cap Q^*(\boldsymbol{s}) \right\}, \tag{3.32}$$

where $\boldsymbol{f}^{-1}(\mathrm{Im}(\mathsf{R}^\top) \cap \boldsymbol{f}(Q^*(\boldsymbol{s})) = \boldsymbol{f}^{-1}(\mathrm{Im}(\mathsf{R}^\top)) \cap Q^*(\boldsymbol{s})$ holds because $\boldsymbol{f}$ is bijective from the definition in Eq. (3.23). This fact also indicates the uniqueness of $\boldsymbol{q}^*$ if it exists [58]. As a result, the set Eq. (3.32) of equilibrium points becomes a one-dimensional curve (line) in the state space of the inner-limit model (3.19). This curve forms an invariant manifold consisting of all the non-isolated equilibrium points, which we will denote by $\mathcal{I}$.

In order to discuss the technological implication in Sec. 3.3, the dynamics of the model (3.14) near $\mathcal{I}$ are described below. Since the invariant manifold herein is one-dimensional, the slow dynamics will be characterized by one-dimensional reduced system on it. A perturbation to solutions of Eq. (3.19) along $\mathcal{I}$ represents the uniform change of the pressures, and thus the slow dynamics correspond to the responses of pressure level of the entire system. On the other hand, the dynamics transverse to $\mathcal{I}$ represent the change of steam velocities and pressure fluctuations near the manifold, and the fast dynamics correspond to the transport of steam between the different sites.

3.2.4 Proof of normal hyperbolicity of the invariant manifold

In this subsection, we prove that the located invariant manifold $\mathcal{I}$ in Eq. (3.32) is normally hyperbolic under certain conditions. An invariant manifold is called normally hyperbolic [52, 129] if the expansion or contraction rate of vectors transverse to the manifold dominates that of vectors tangent to the manifold: see Appendix 3.C for its details. For the present discussion, since $\mathcal{I}$ consists of non-isolated equilibrium points, it is characterized by eigenvalues associated with the linearization of the model (3.19) at each equilibrium point. By substituting $\boldsymbol{\psi} = \boldsymbol{\psi}^* + \boldsymbol{\Delta\psi}$ and $\boldsymbol{q} = \boldsymbol{q}^* + \boldsymbol{\Delta q}$ into Eq. (3.19), the linearized system around $(\boldsymbol{\psi}^*, \boldsymbol{q}^*)$ is obtained as follows:

$$\frac{\mathrm{d}}{\mathrm{d}t}\begin{bmatrix}\boldsymbol{\Delta\psi}\\ \boldsymbol{\Delta q}\end{bmatrix} = \mathsf{A}\begin{bmatrix}\boldsymbol{\Delta\psi}\\ \boldsymbol{\Delta q}\end{bmatrix}, \tag{3.33}$$

with

$$\mathsf{A} := \begin{bmatrix}0 & -\mathsf{G}^{-1}\mathsf{R}\\ \mathsf{H}^{-1}\,\mathsf{R}^\top & -\mathsf{H}^{-1}D\boldsymbol{f}(\boldsymbol{q}^*)\end{bmatrix}. \tag{3.34}$$

In below, we will show that the center subspace of the linearized system (3.34) is one-dimensional and is tangent to $\mathcal{I}$. To do this, we analyze the eigenvector associated with zero eigenvalue under the following two assumptions. The first one is that the matrix $D\boldsymbol{f}(\boldsymbol{q}^*)$ is non-singular. This is relevant if $q_i^* \neq 0$ for all $i = 1, \ldots, m$. Under the assumption, the eigenvector $(\boldsymbol{\Delta\psi_0}, \boldsymbol{\Delta q_0})$ associated with zero eigenvalue satisfies the following equations:

$$\mathsf{G}^{-1}\mathsf{R}\boldsymbol{\Delta q_0} = \mathbf{0}, \tag{3.35a}$$

$$\boldsymbol{\Delta q_0} = D\boldsymbol{f}(\boldsymbol{q}^*)^{-1}\,\mathsf{R}^\top\boldsymbol{\Delta\psi_0}. \tag{3.35b}$$

The second assumption states non-existence of pure imaginary eigenvalues of A. As stated in [16], non-singularity of $D\boldsymbol{f}(\boldsymbol{q}^*)$ is closely related to the non-oscillating condition, that is, non-existence of pure imaginary eigenvalues. However, in this paper, we will simply make both the assumptions. Under the two assumptions, one can verify that the center subspace is spanned by eigenvector associated to zero eigenvalue and is tangent to $\mathcal{I}$. By substituting Eq. (3.35b) into Eq. (3.35a), the following condition holds for $\boldsymbol{\Delta\psi_0}$:

$$\mathsf{R}\Sigma\mathsf{R}^\top\boldsymbol{\Delta\psi_0} = \mathbf{0}, \quad \Sigma := D\boldsymbol{f}(\boldsymbol{q}^*)^{-1}. \tag{3.36}$$

Since Σ is diagonal by definition, $\mathsf{R}\Sigma\mathsf{R}^\top$ corresponds to the so-called Kirchhoff matrix [107]. From the assumption of connected graph, the kernel of $\mathsf{R}\Sigma\mathsf{R}^\top$ is represented by

$$\{c\mathbf{1} \in \mathbb{R}^n \mid c \in \mathbb{R}\}. \tag{3.37}$$

From Eq. (3.35b), $\boldsymbol{\Delta q_0} = \mathbf{0}$ holds because this space is also the kernel of $\mathsf{R}^\top$, that is, $\mathsf{R}^\top \boldsymbol{\Delta \psi_0} = \mathbf{0}$. Note that, by discussion similar to above, one can verify that there is no generalized eigenvector associated with zero eigenvalue other than $(\boldsymbol{\Delta \psi_0}, \boldsymbol{\Delta q_0})$. Thus, the center subspace of the linearized system (3.34) is explicitly represented as follows:

$$\Big\{(\boldsymbol{\Delta \psi}, \mathbf{0}) \in \mathbb{R}^{n+m} | \boldsymbol{\Delta \psi} = c\,\mathbf{1},\ c \in \mathbb{R}\Big\}. \tag{3.38}$$

This clearly indicates that the center subspace is one-dimensional and is tangent to the invariant manifold $\mathcal{I}$. From the definition, if the two assumptions—non-singularity of $D\boldsymbol{f}(\boldsymbol{q}^*)$ and non-existence of pure imaginary eigenvalues of A—are satisfied, then $\mathcal{I}$ is normally hyperbolic. The proof is thus completed.

3.3 Numerical simulations for two-site system

This section demonstrates the slow-fast dynamics near the NHIM and verifies the correctness of the derived model (3.14) by numerical simulations for the two-site system.

$$\frac{\mathrm{d}p_1}{\mathrm{d}t} = \frac{\epsilon}{e_1(p_1)} \left\{ Q_1' - Q_{\mathrm{L}1}' - \frac{\pi d^2}{4} h_{\mathrm{c}}(p_1)\rho_{\mathrm{s}}(p_1) u \right\}, \tag{3.39}$$

$$\frac{\mathrm{d}p_2}{\mathrm{d}t} = \frac{\epsilon}{e_2(p_2)} \left\{ Q_2' - Q_{\mathrm{L}2}' + \frac{\pi d^2}{4} h_{\mathrm{c}}(p_2)\rho_{\mathrm{s}}(p_2) u \right\}, \tag{3.40}$$

$$\frac{\mathrm{d}u}{\mathrm{d}t} = \frac{1}{\epsilon} \frac{2(p_1 - p_2)}{L_l\{\rho_{\mathrm{s}}(p_1) + \rho_{\mathrm{s}}(p_2)\}} - \frac{\lambda_l}{2d} u|u|, \tag{3.41}$$

For the two-site system, the dimension of the derived model is three, and hence it is possible to perfectly visualize the state space of the model including a NHIM and to apply phase-space geometric concepts [129] to it.

In [12] transient responses of a single boiler are examined experimentally as well as numerically under a setting of fuel profiles for a real plant. Following this, in this paper we provide responses of physical quantities under a step change and periodic change of the heat flow rates Q_i' to boilers. Although the abrupt change of Q_i' may not be possible in realistic operation, it provides basic information on the multiscale dynamics. The values of parameters used for the current simulations are shown Appendix 3.E and based on district heating systems [18, 63]. As in [127], the thermodynamic properties are calculated by using Xsteam package [53]. Numerical values of $e_i(p_i)$ and $h_{\mathrm{c}}(p_i)\rho_{\mathrm{s}}(p_i)$ in (3.14) are shown in Fig. 3.3 for a practical range of pressure [18]: $0.1\,\mathrm{MPa} \le p_i \le 2\,\mathrm{MPa}$.

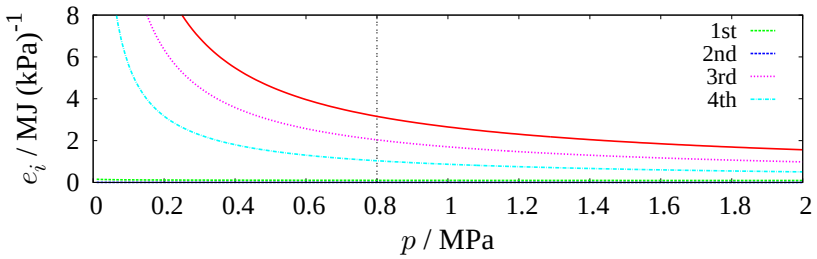

(a) $e_i(p_i)$ (*solid* line) and the values of terms on the right-hand side of Eq. (3.2)

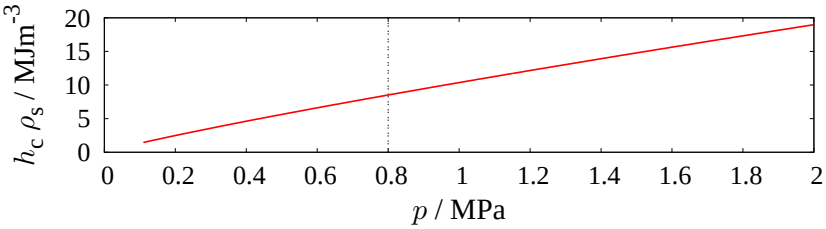

(b) $h_c(p_i)\,\rho_s(p_i)$

Figure 3.3: Numerical values of (a) e_i and (b) $h_c\rho_s$

3.3.1 Time-response analysis

First, we simulate the short-term dynamics related to transport of steam between the two sites. Time-responses of physical quantities are provided under the following step change:

$$(Q'_1, Q'_2) = \begin{cases} (5\,\mathrm{MJ/s}, 5\,\mathrm{MJ/s}), & t < 10\,\mathrm{s} \\ (6\,\mathrm{MJ/s}, 4\,\mathrm{MJ/s}), & t \geq 10\,\mathrm{s} \end{cases} \tag{3.42}$$

This implies an abrupt change of operating conditions of the boilers, and thereby 1 MJ/s surplus (or deficit) of heat is caused in site #1 (or site #2). Note that in both cases the condition (3.26) is satisfied. Figure 3.4 shows step responses of the state variables (p_1, p_2, u) of (3.14) and heat output rates Q'_{oi} from the boilers. The system is initially at a steady operating condition with no transport of steam between the sites, and then Q'_i changes at $t = 10\,\mathrm{s}$. The pressures p_1 and p_2 and velocity u move to a new operating condition after transients in a few tens of seconds. At the new operating condition, the values of $p_1 - p_2$ and u become positive. This clearly shows that the positive pressure drop $p_1 - p_2$ induces the transport of steam from site #1 to site #2. The heat output rates Q'_{o1} and Q'_{o2} change symmetrically, and thus the surplus and deficit of heat at the two sites are compensated by the transport of steam.

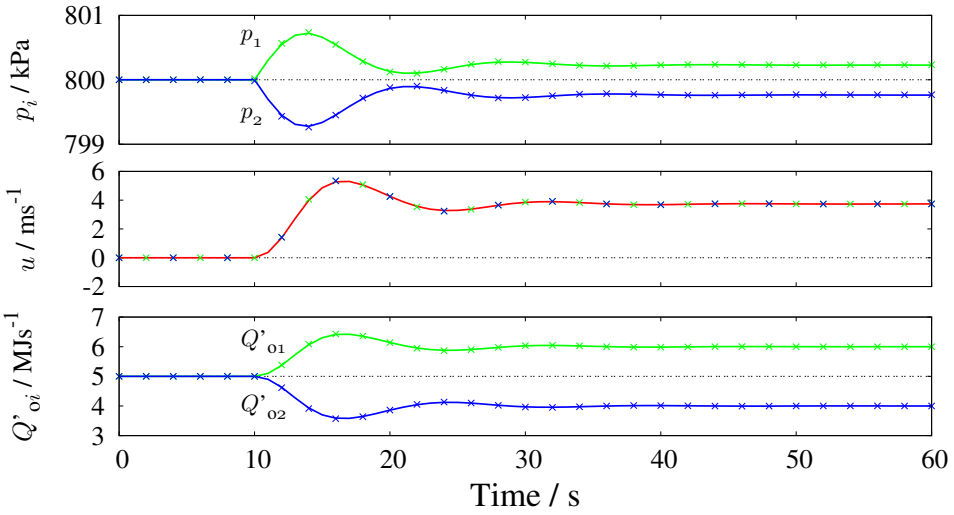

Figure 3.4: Responses of state variables (p_1, p_2, u) and heat output rates $Q'_{oi} := m'_{si}h_c(p_i)$ from the boilers. The *solid* lines show the responses of Eq. (3.14), and the *points* ($\times$) show the sample plot of responses of Eq. (3.19). They are initiated by a step change of the parameters from $(Q'_1, Q'_2) = (5\,\mathrm{MJ/s}, 5\,\mathrm{MJ/s})$ to $(Q'_1, Q'_2) = (6\,\mathrm{MJ/s}, 4\,\mathrm{MJ/s})$.

3.3.2 Phase-space analysis

Second, we analyze the dynamics described by the model (3.14) from the viewpoint of phase space. Especially, the long-term dynamics described by (3.14) are considered in this subsection. The model (3.14) for the two-site system has the three independent variables. Based on the analysis in Sec. 3.2.3, we introduce the following variable transformation:

$$\begin{bmatrix} (p_1+p_2)/2 \\ p_1-p_2 \\ u \end{bmatrix} = \begin{bmatrix} 1/2 & 1/2 & 0 \\ 1 & -1 & 0 \\ 0 & 0 & 1 \end{bmatrix} \begin{bmatrix} p_1 \\ p_2 \\ u \end{bmatrix}. \tag{3.43}$$

Figure 3.5 shows trajectories of the model (3.14) under the parameter setting as $(Q'_1, Q'_2) = (6\,\mathrm{MJ/s}, 4\,\mathrm{MJ/s})$. The *red* trajectory corresponds to the time response presented in Fig. 3.4 with subsequent long-term response from $t = 0\,\mathrm{s}$ to $10,000\,\mathrm{s}$. This trajectory shows typical *slow-fast* dynamics as mentioned in Sec. 3.2. The mean pressure value $(p_1 + p_2)/2$ does not change dominantly while the pressure difference $p_1 - p_2$ and the velocity u exhibit fast oscillations shown in Fig. 3.4. After the fast oscillation is settled, the mean pressure $(p_1 + p_2)/2$ begins to decrease slowly. The *blue* trajectory in the figure shows a one-dimensional invariant manifold located with direct numerical integration of (3.14). It is confirmed that the trajectories converge to the located invariant manifold while exhibiting the slow and fast dynamics as mentioned above. This result becomes a

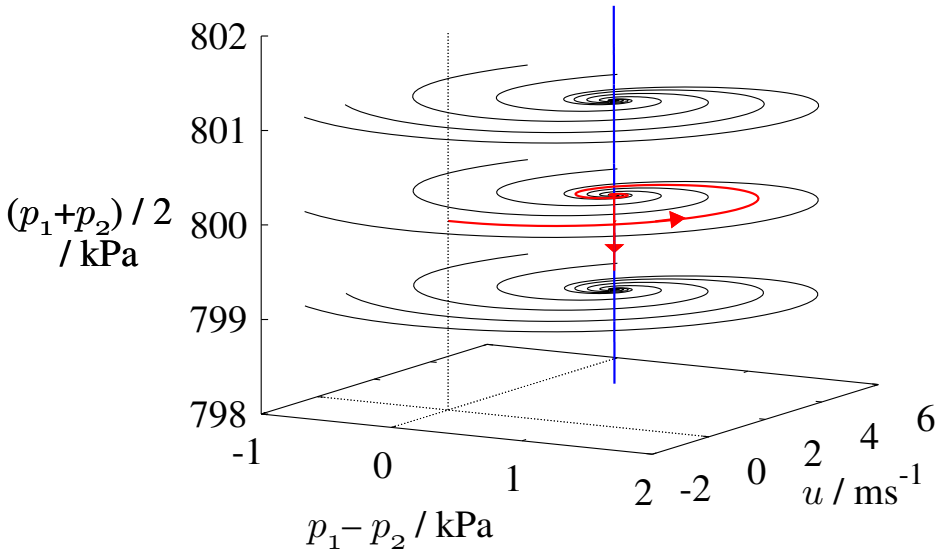

Figure 3.5: Trajectories of the derived model (3.14) with $(Q'_1, Q'_2) = (6\,\mathrm{MJ/s}, 4\,\mathrm{MJ/s})$. The *red* trajectory corresponds to the time response presented in Fig. 3.4 with subsequent long-term response. The *blue* trajectory shows a invariant manifold located with direct numerical integration of (3.14).

numerical evidence that the located invariant manifold possesses the normal hyperbolicity.

Also, we analyze the long-term dynamics related to the boilers' operation to offer several technological implications of the phase space analysis. Here, we consider the following periodic change of Q'_1: for $n = 1, 2, \ldots,$

$$Q'_1 = \begin{cases} 7\,\mathrm{MJ/s}, & 600(n-1)\,\mathrm{s} \le t < 600n - 300\,\mathrm{s}, \\ 5\,\mathrm{MJ/s}, & 600n - 300\,\mathrm{s} \le t < 600n\,\mathrm{s}, \end{cases} \tag{3.44}$$

and $Q'_2 = 4\,\mathrm{MJ/s}$. This periodic change is intended to the novel electricity-oriented operation of CHP plants, and the similar profiles of the fuel flow rate are shown in [12] as experiment data of a real plant. Under the above setting, the condition (3.26) is not satisfied. Figure 3.6 shows (a) the time responses of the state variables and (b) the corresponding trajectory in the phase space. The appearing short-term and long-term dynamics are characterized by the NHIM. For the short-term regime, the fast motion towards to the NHIM guarantees that the pressure and velocity oscillation are settled after a change of operating condition. This ensures that the amount of transport of steam

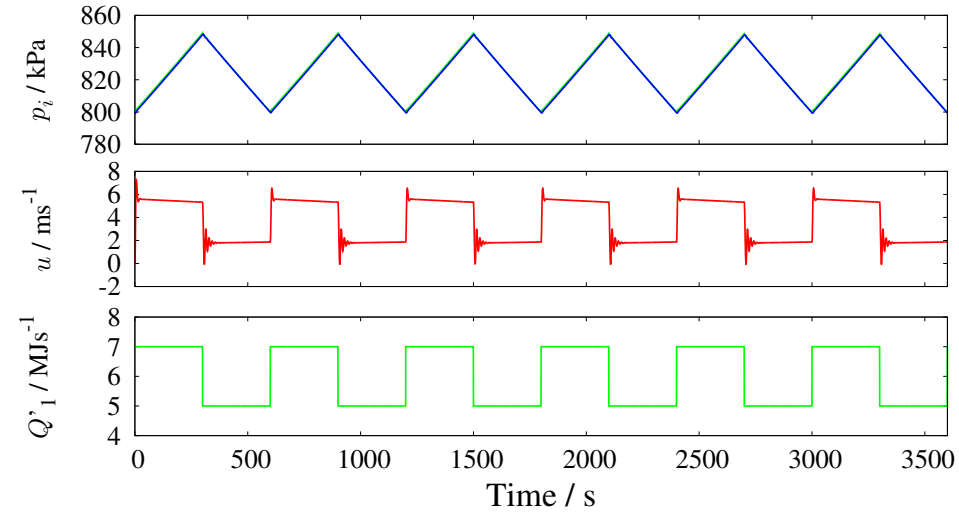

(a) Time responses

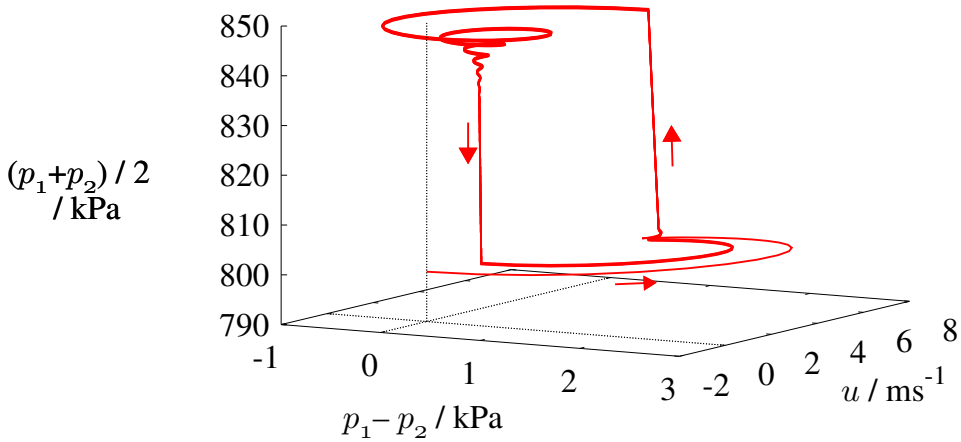

(b) Trajectory in the phase space

Figure 3.6: Long-term dynamics for the periodic change of the parameter Q'_1. Numerical simulation of (a) time responses of the state variables and (b) trajectory in the phase space are shown.

between the two sites becomes bounded in the short-term regime. On the other hand, for the long-term regime, the mean pressure value changes due to the slow motion along the NHIM. Thus, the success of the novel electricity-oriented operation can be clarified as the existence of NHIM near which the separation of fast and slow motions holds.

It should be here noted that this type of slow-fast separation plays an important role in power system operation [84]. Conventionally, the frequency dynamics in power systems

can be classified into three stages with different time-scales and are regulated separately with different mechanisms [84]. In this sense, we here identified a similar time-scale separation in the steam supply system, which has not been reported yet in literature. The time-scale separation enables independent operations of transport of steam between the sites in *short-term* regime and *long-term* supply-demand balancing of steam in order to maintain the pressure level in the system. The finding of the time-scale separation is thus expected to become a dynamical principle for operational design of steam supply.

3.3.3 Comparison with the original model

Lastly, in order to verify the correctness of the derived model (3.14), we present a comparison with the brute-force simulation of the original model represented by equations (3.1) to (3.5) and Eq. (3.12). The equations were implemented using the COMSOL Multiphysics® Software [30]: see Appendix 3.D for details. From the procedure of lumped-parameter modeling, the approximations necessary for deriving (3.14) are the incompressibility condition and the evaluation of thermodynamic quantities in Eq. (3.13). Since the relevance of these approximations is related to the parameter $\epsilon_3 := d_{\mathrm{r}}^2 L_{\mathrm{r}} Q_{\mathrm{wr}} / Q'_{\mathrm{r}}$,

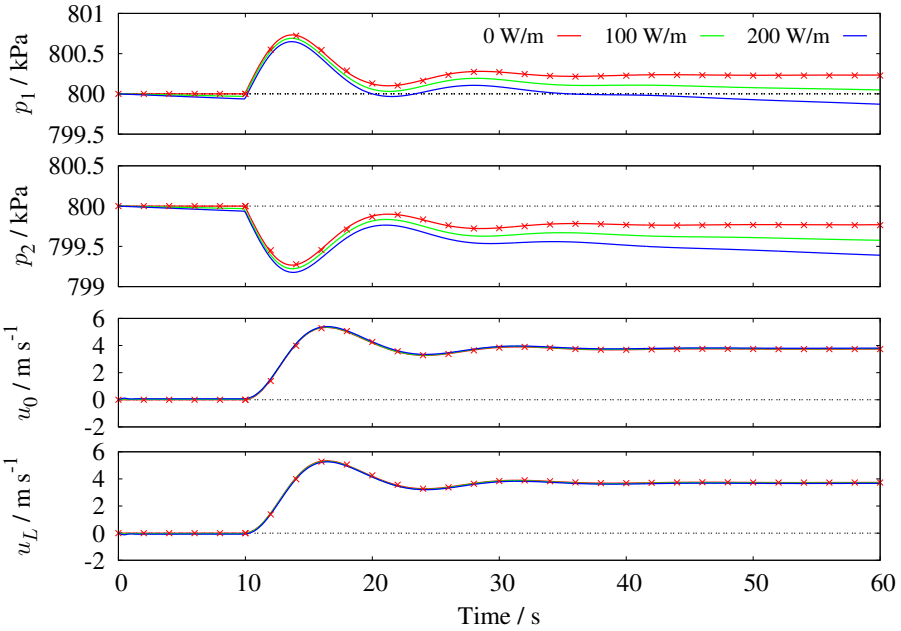

Figure 3.7: Responses of p_1, p_2, $u_0 := u(t,0)$, and $u_L := u(t,L)$ by the original coupled equations. The points ($\times$) show the sequence of time responses of the derived lumped-parameter model (3.14).

we present in Fig. 3.7 the simulation results for various setting of the heat loss, represented by Q_{w} in Eq. (3.5). The lines in the figure show the results of brute-force simulation of the original model with $-Q_{\mathrm{w}} \cdot \pi d^2/4 = 0\,\mathrm{W/m}$, $100\,\mathrm{W/m}$, and $200\,\mathrm{W/m}$, respectively. The sequence of *points*, denoted by $\times$, represents a sample plot of time responses of (3.14) presented in Fig. 3.4. The simulation result clearly shows that the lumped-parameter model (3.14) well approximates the dynamics of the original model when the heat loss is sufficiently small, i.e. when the steam pipes are well insulated.

For the cases with large heat loss, while the pressures p_1 and p_2 in the original model slowly decrease, the responses of u_0 and u_L are well captured by the derived model (3.14). Also, the responses of pressures and velocities in $[10\,\mathrm{s}, 20\,\mathrm{s}]$ are correctly produced by the derived model. The result shows that the derived model describes the transport of steam in the shot-term regime even if the heat loss becomes large. This model is thus useful for designing the coordinated operation of heat and electricity supply because the typical time scale of the swing dynamics in power systems is also in the same time regime [84].

3.4 Summary

This chapter studied a problem on mathematical modeling for multiscale dynamics in steam supply systems. The dynamics of interest were originally described by a distributed-parameter model for fast steam flows over a pipe network coupled with a lumped-parameter model for slow internal dynamics of boilers. Through physically relevant approximations, we newly derived a lumped-parameter model that captured stability and multiscale properties of the dynamics. In order to describe the slowfast dynamics, we used the notion of Normally Hyperbolic Invariant Manifold (NHIM). By theoretically analyzing the inner limit of the derived model, we located a set of nonisolated equilibrium points that formed an NHIM. Also, the numerical simulations under practical settings of parameters demonstrated the slow-fast dynamics near the NHIM. The existence of the NHIM clearly shows the so-called separation principle for operational design of steam supply, which is analog to power system operation.

Appendix 3.A Derivation of dimensionless equations

This first appendix derives the dimensionless equations from Eq. (3.1) to (3.5). The physical quantities with dimension are denoted by superscript $*$, and the reference quan-

tities by subscript r: A physical quantity z^* is associated by $z^* = z_{\mathrm{r}}^* z$ to a dimensionless quantity z. Similarly, a function f^* is related by $f_{\mathrm{r}}^* f(z^*/z_{\mathrm{r}}^*) = f^*(z^*)$ to a dimensionless function f. The reference quantities are related by the following equations:

$$\begin{aligned} &x_{\mathrm{r}}^* = L_{\mathrm{r}}^*, \quad t_{\mathrm{r}}^* = \frac{L_{\mathrm{r}}^*}{u_{\mathrm{r}}^*}, \quad \rho_{\mathrm{r}}^* = \rho_{\mathrm{sr}}^*, \quad h_{\mathrm{r}}^* = h_{\mathrm{sr}}^* = h_{\mathrm{wr}}^* = \frac{p_{\mathrm{r}}^*}{\rho_{\mathrm{r}}^*}, \\ &d_{\mathrm{r}}^* = \lambda_{\mathrm{r}} L_{\mathrm{r}}^*, \quad m_{\mathrm{r}}'^* = \rho_{\mathrm{r}}^* d_{\mathrm{r}}^{*2} u_{\mathrm{r}}^*, \quad Q_{\mathrm{r}}'^* = Q_{\mathrm{Lr}}'^* = h_{\mathrm{r}}^* \rho_{\mathrm{r}}^* d_{\mathrm{r}}^{*2} u_{\mathrm{r}}^*. \end{aligned} \tag{3.45}$$

It is well-known in [12, 69] that the dynamic behavior of boiler's pressure is well captured by global mass and energy balances. The global mass balance is given by

$$\frac{\mathrm{d}}{\mathrm{d}t^*}(\rho_{\mathrm{s}}^* V_{\mathrm{s}}^* + \rho_{\mathrm{w}}^* V_{\mathrm{w}}^*) = m_{\mathrm{f}}'^* - m_{\mathrm{s}}'^*, \tag{3.46}$$

and the global mass balance by

$$\frac{\mathrm{d}}{\mathrm{d}t^*}\{(\rho_{\mathrm{s}}^* h_{\mathrm{s}v}^* - p^*)V_{\mathrm{s}}^* + (\rho_{\mathrm{w}}^* h_{\mathrm{w}}^* - p^*)V_{\mathrm{w}}^* + m_{\mathrm{t}}^* C_{\mathrm{p}}^* T_{\mathrm{m}}^*\} = Q'^* + m_{\mathrm{f}}'^* h_{\mathrm{f}}'^* - m_{\mathrm{s}}'^* h_{\mathrm{s}}'^*, \tag{3.47}$$

where the term $h^* - p^*/\rho^*$ corresponds to internal energy. Under Assumption (A2), by multiplying (3.46) by h_{w}^* and subtracting the result from (3.47) we have

$$e^* \frac{\mathrm{d}p^*}{\mathrm{d}t^*} = Q'^* - m_{\mathrm{f}}'^*(h_{\mathrm{w}}^* - h_{\mathrm{f}}^*) - m_{\mathrm{s}}'^*(h_{\mathrm{s}}^* - h_{\mathrm{w}}^*), \tag{3.48}$$

with

$$e^* = (h_{\mathrm{s}}^* - h_{\mathrm{w}}^*)V_{\mathrm{s}}^* \frac{\partial \rho_{\mathrm{s}}^*}{\partial p^*} + \rho_{\mathrm{s}}^* V_{\mathrm{s}}^* \frac{\partial h_{\mathrm{s}}^*}{\partial p^*} + \rho_{\mathrm{w}}^* V_{\mathrm{w}}^* \frac{\partial h_{\mathrm{w}}^*}{\partial p^*} + m_{\mathrm{t}}^* C_{\mathrm{p}}^* \frac{\partial T_{\mathrm{m}}^*}{\partial p^*} - V_{\mathrm{s}}^* - V_{\mathrm{w}}^*. \tag{3.49}$$

In addition, Assumption (A1) implies $T_{\mathrm{m}}^* = T_{\mathrm{s}}^*$, and Assumption (A3) does $h_{\mathrm{f}}^* = h_{\mathrm{w}}^*$ in (3.48) and (3.49). As a result, by using the relation (3.45), the pressure dynamics of boiler are formulated as follows:

$$e(p)\frac{\mathrm{d}p}{\mathrm{d}t} = \frac{d_{\mathrm{r}}^{*2} L_{\mathrm{r}}^*}{e_{\mathrm{r}}^*}\left\{Q' - m_{\mathrm{s}}' h_{\mathrm{c}}(p)\right\}, \tag{3.50}$$

Thus, Eq. (3.1) is derived by defining the small parameter $\epsilon_1 := d_{\mathrm{r}}^{*2} L_{\mathrm{r}}^*/e_{\mathrm{r}}^*$.

The continuity equations of mass, momentum, and energy with dimension are given as follows [101, 4, 81]:

$$\frac{\partial \rho^*}{\partial t^*} + \frac{\partial}{\partial x^*}(\rho^* u^*) = 0, \tag{3.51}$$

$$\frac{\partial}{\partial t^*}(\rho^* u^*) + \frac{\partial}{\partial x^*}(\rho^* u^{*2}) + \frac{\partial p^*}{\partial x^*} + F_{\mathrm{w}}^* = 0, \tag{3.52}$$

$$\frac{\partial}{\partial t^*}\left\{\rho^*\left(h^* - \frac{p^*}{\rho^*}\right)\right\} + \frac{\partial}{\partial x^*}(\rho^* u^* h^*) + Q_{\mathrm{l}}^* = 0, \tag{3.53}$$

where $F_{\rm w}$ stands for the shear force acting on a steam element and is approximated by the Darcy-Weisbach equation [101, 15, 63] as follows:

$$F_{\rm w}^* := \lambda \frac{\rho^* u^* |u^*|}{2d^*}, \tag{3.54}$$

The coefficient λ depends on the Reynolds number Re, pipe diameter d, and roughness of the inner surface of the pipe and therefore varies according to the steam velocity u. In the case of laminar flow under a low Reynolds number, the value of λ is derived in [15] theoretically as $\lambda = 64/Re$. On the other hand, in the case of turbulent flow under high Reynolds numbers, λ is approximated by a constant that is determined by d and the roughness [63, 15]. In this paper, the friction coefficient λ is considered as a constant because the steam flow used in standard steam supply is turbulent [63, 15]. By using the relation (3.45), the above equations become

$$\frac{\partial \rho}{\partial t} + \frac{\partial}{\partial x}(\rho u) = 0, \tag{3.55}$$

$$\frac{\partial}{\partial t}(\rho u) + \frac{\partial}{\partial x}(\rho u^2) + \frac{p_{\rm r}^*}{\rho_{\rm r}^* u_{\rm r}^{*2}} \frac{\partial p}{\partial x} + \lambda \frac{\rho_l u |u|}{2d} = 0, \tag{3.56}$$

$$\frac{\partial}{\partial t}(\rho h) + \frac{\partial}{\partial x}(\rho h u) = \frac{\partial p}{\partial t} + \frac{d_{\rm r}^{*2} L_{\rm r}^* Q_{\rm wr}^*}{Q_{\rm r}'^*} Q_{\rm w}. \tag{3.57}$$

Thus, (3.3) to (3.5) are derived by defining the parameters $\epsilon_2 := \rho_{\rm sr}^* u_{\rm r}^{*2}/p_{\rm r}^*$ and $\epsilon_3 := d_{\rm r}^{*2} L_{\rm r}^* Q_{\rm wr}^*/Q_{\rm r}'^*$.

Appendix 3.B Summarized graph theory

The second appendix provides a brief review of graph theory [58] for the analysis in Secs. 3.2.3 and 3.2.4. Along the notation in Sec. 3.2.1, consider a directed graph $\mathcal{G}$ with n vertices and m links. Assume $\mathcal{G}$ is connected and is represented by the incidence matrix R. The matrix R (or $\mathsf{R}^\top$) is regarded as a linear map $\mathsf{R} : \mathbb{R}^m \to \mathbb{R}^n$ (or $\mathsf{R}^\top : \mathbb{R}^n \to \mathbb{R}^m$), and its image and kernel are related to the graph's topology. $\mathrm{Ker}(\mathsf{R})$ and $\mathrm{Im}(\mathsf{R}^\top)$ are subspaces of $\mathbb{R}^m$, and their dimensions coincide with the number of independent loops and cutsets, respectively. Since $\mathcal{G}$ is connected, we have $\mathrm{dimKer}(\mathsf{R}) = m - n + 1$ and $\mathrm{dimIm}(\mathsf{R}^\top) = n - 1$ (see [58]). Also, $\mathrm{Ker}(\mathsf{R}^\top)$ is a subspace of $\mathbb{R}^n$ given as

$$\mathrm{Ker}(\mathsf{R}^\top) = \{c\mathbf{1} \in \mathbb{R}^n \mid c \in \mathbb{R}\}. \tag{3.58}$$

This result is derived from $\dim\mathrm{Im}(\mathsf{R}^\top) = n-1$ and the fact that every link connects exactly two vertices. Finally, $\mathrm{Im}(\mathsf{R})$ is a subspace of $\mathbb{R}^n$ orthogonal to $\mathrm{Ker}(\mathsf{R}^\top)$, and its dimension is equal to $n-1$.

Appendix 3.C Concept of normal hyperbolicity

This appendix reviews the concept of Normally Hyperbolic Invariant Manifold (NHIM) based on [52, 38, 129, 76]. The definition of NHIM is based on the so-called generalized Lyapunov-type numbers, which can be evaluated by eigenvalues of the associated linearized system in the case of an equilibrium point. Here, we first introduce the general case, and then provide a transition to fast-slow systems.

For the flow $\boldsymbol{\phi}_t$ of an autonomous dynamical system, consider a compact, connected, and invariant manifold M of class C^r for some $r \leq 1$. Suppose there exists a continuous splitting

$$\mathrm{T}\mathbb{R}^n|_M = \mathcal{N}^{\mathrm{u}} \oplus \mathrm{T}M \oplus \mathcal{N}^{\mathrm{s}}, \tag{3.59}$$

where $\oplus$ stands for the Whitey sum, $\mathrm{T}M$ for the tangent bundle, and $\mathcal{N} := \mathcal{N}^{\mathrm{u}} \oplus \mathcal{N}^{\mathrm{s}}$ for the normal bundle. Assume that the subbundles $\mathrm{T}M \oplus \mathcal{N}^{\mathrm{u}}$ and $\mathrm{T}M \oplus \mathcal{N}^{\mathrm{s}}$ are invariant under $\mathrm{D}\boldsymbol{\phi}_t$. Then, for a point $p \in M$, we consider the following nonzero vectors:

$$\boldsymbol{u}_0 \in \mathcal{N}^{\mathrm{u}}_p, \quad \boldsymbol{v}_0 \in \mathrm{T}M_p, \quad \boldsymbol{w}_0 \in \mathcal{N}^{\mathrm{s}}_p, \tag{3.60}$$

and the images of the linearized flow:

$$\boldsymbol{u}_{-t} = \Pi^{\mathrm{u}}\mathrm{D}\boldsymbol{\phi}(p)\boldsymbol{u}_0, \quad \boldsymbol{v}_{-t} = \mathrm{D}\boldsymbol{\phi}(p)\boldsymbol{v}_0, \quad \boldsymbol{w}_{-t} = \Pi^{\mathrm{s}}\mathrm{D}\boldsymbol{\phi}(p)\boldsymbol{w}_0, \tag{3.61}$$

where Π^{u} and Π^{s} are the projection operators $\Pi^{\mathrm{u}} : \mathrm{T}\mathbb{R}^n|_M \to \mathcal{N}^{\mathrm{u}}$ and $\Pi^{\mathrm{s}} : \mathrm{T}\mathbb{R}^n|_M \to \mathcal{N}^{\mathrm{s}}$, respectively. Then, the generalized Lyapunov-type numbers are defined as follows:

Definition 3.1 (generalized Lyapunov-type number [129, 76])**.** *The generalized Lyapunov-type numbers are defined by*[1]

$$\nu^{\mathrm{u}}(p) := \inf\left\{a : \frac{||\boldsymbol{u}_{-t}||}{a^t} \to 0 \quad \text{as} \quad t \to \infty, \quad \forall \boldsymbol{u}_0 \in \mathcal{N}^{\mathrm{u}}_p\right\}, \tag{3.62}$$

$$\nu^{\mathrm{s}}(p) := \inf\left\{a : \frac{1}{||\boldsymbol{w}_{-t}||a^t} \to 0 \quad \text{as} \quad t \to \infty, \quad \forall \boldsymbol{w}_0 \in \mathcal{N}^{\mathrm{s}}_p\right\}, \tag{3.63}$$

[1] In [129], they are defined by using the expressions $(||\boldsymbol{u}_{-t}||/||\boldsymbol{u}_0||)/a^t$ and $(||\boldsymbol{w}_0||/||\boldsymbol{w}_{-t}||)/a^t$. In this case, for $a = 1$, $||\boldsymbol{u}_{-t}||/||\boldsymbol{u}_0|| \to 0$ implies expansion of a vector, and $||\boldsymbol{w}_0||/||\boldsymbol{w}_{-t}|| \to 0$ contraction.

and if $\nu^{\mathrm{u}}(p) < 1$ *and* $\nu^{\mathrm{s}}(p) < 1$,

$$\sigma^{\mathrm{u}} := \inf\left\{b : ||\boldsymbol{v}_{-t}||\,||\boldsymbol{u}_{-t}||^b \to 0 \quad \text{as} \quad t \to \infty, \quad \forall \boldsymbol{u}_0 \in \mathcal{N}_p^{\mathrm{u}},\ \boldsymbol{v}_0 \in \mathrm{T}M_p\right\}, \tag{3.64}$$

$$\sigma^{\mathrm{s}} := \inf\left\{b : \frac{||\boldsymbol{v}_{-t}||}{||\boldsymbol{w}_{-t}||^b} \to 0 \quad \text{as} \quad t \to \infty, \quad \forall \boldsymbol{w}_0 \in \mathcal{N}_p^{\mathrm{s}},\ \boldsymbol{v}_0 \in \mathrm{T}M_p\right\}. \tag{3.65}$$

Then, the concept of normal hyperbolicity is defined as follows:

Definition 3.2 (normal hyperbolicity [129, 76])**.** *Let* M *be a compact connected invariant manifold in* $\mathbb{R}^n$*. A splitting* $\mathrm{T}\mathbb{R}^n|_M = \mathcal{N}^{\mathrm{u}} \oplus \mathrm{TM} \oplus \mathcal{N}^{\mathrm{s}}$ *is called normally hyperbolic*[2] *if* $\nu^{\mathrm{u}} < 1$, $\nu^{\mathrm{s}} < 1$, $\sigma^{\mathrm{s}} < 1$, *and* $\sigma^{\mathrm{s}} < 1$ *for all* $p \in M$*. If an invariant manifold* M *admits a normally hyperbolic splitting, then it is called a normally hyperbolic invariant manifold.*

Thus, an invariant manifold is normally hyperbolic if the linearized flow in the normal direction dominates the linearized flow in the tangential direction. An important implication of the normal hyperbolicity is the following perturbation theorem:

Theorem 3.3 (Fenichel [38, 129, 76])**.** *Let* $\boldsymbol{f}$ *be a* C^r *vector field on* $\mathbb{R}^n$ *with* $r \leq 1$*. Let* M *be a compact, connected* C^r*-manifold properly embedded in* $\mathbb{R}^n$*. Suppose that* M *is invariant and normally hyperbolic under the flow of* $\boldsymbol{f}$*. Given any* C^r *vector field* f^{pert} *sufficiently* C^1*-close to* $\boldsymbol{f}$*, there exists a* C^r*- manifold* M^{pert} *that is invariant under the flow of* $\boldsymbol{f}^{\mathrm{pert}}$ *and diffeomorphic to* M*.*

Next, we review the fact that the above discussion can be applied to fast-slow systems [39, 76]. Consider the general formulation of an $(m,\, n)$-fast-slow system

$$\epsilon\frac{\mathrm{d}\boldsymbol{x}}{\mathrm{d}\tau} = \boldsymbol{f}(\boldsymbol{x}, \boldsymbol{y}, \epsilon), \tag{3.66a}$$

$$\frac{\mathrm{d}\boldsymbol{y}}{\mathrm{d}\tau} = \boldsymbol{g}(\boldsymbol{x}, \boldsymbol{y}, \epsilon), \tag{3.66b}$$

where $(\boldsymbol{x},\, \boldsymbol{y}) \in \mathbb{R}^m \times \mathbb{R}^n$ and $0 < \epsilon \ll 1$ is a small parameter representing the ratio of time scales. The functions $\boldsymbol{f} : \mathbb{R}^m \times \mathbb{R}^n \times \mathbb{R} \to \mathbb{R}^m$ and $\boldsymbol{g} : \mathbb{R}^m \times \mathbb{R}^n \times \mathbb{R} \to \mathbb{R}^n$ are assumed to be sufficiently smooth. Here, the slow subsystem is defined by considering $\epsilon \to 0$ in Eq. (3.66):

$$0 = \boldsymbol{f}(\boldsymbol{x}, \boldsymbol{y}, 0), \tag{3.67a}$$

$$\frac{\mathrm{d}\boldsymbol{y}}{\mathrm{d}t} = \epsilon\boldsymbol{g}(\boldsymbol{x}, \boldsymbol{y}, 0), \tag{3.67b}$$

[2] A splitting with $\sigma^{\mathrm{u}} < 1/r$ and $\sigma^{\mathrm{s}} < 1/r$ is called r-normally hyperbolic [52], and r stands for a degree of scale separation.

The critical manifold is defined as follows:

$$C_0 = \{(\boldsymbol{x},\, \boldsymbol{y}) \in \mathbb{R}^{m+n} \mid \boldsymbol{f}(\boldsymbol{x},\, \boldsymbol{y},\, 0) = 0\} \tag{3.68}$$

Definition 3.4 (normal hyperbolicity for fast-slow systems [39, 76])**.** *A subset $S \subset C_0$ is called* normally hyperbolic *if the $m \times n$ matrix $(\mathrm{D}_x \boldsymbol{f})(p,\, 0)$ of the first partial derivatives with respect to the fast variables has no eigenvalues with zero real part for all $p \in S$.*

On the fast time scale $t = \tau/\epsilon$, the system (3.66) is rewritten as

$$\frac{\mathrm{d}\boldsymbol{x}}{\mathrm{d}t} = \boldsymbol{f}(\boldsymbol{x}, \boldsymbol{y}, \epsilon), \tag{3.69a}$$

$$\frac{\mathrm{d}\boldsymbol{y}}{\mathrm{d}t} = \epsilon \boldsymbol{g}(\boldsymbol{x}, \boldsymbol{y}, \epsilon), \tag{3.69b}$$

On this time scale, a subset $S \subset C_0$ is normally hyperbolic if and only if for each $p = (\boldsymbol{x}^*,\, \boldsymbol{y}^*) \in S$, we have that $\boldsymbol{x}^*$ is a hyperbolic equilibrium point of

$$\frac{\mathrm{d}\boldsymbol{x}}{\mathrm{d}t} = \boldsymbol{f}(\boldsymbol{x}, \boldsymbol{y}^*, 0). \tag{3.70}$$

If a subset $S \subset C_0$ is a compact and normally hyperbolic subset of S, then there exists a manifold S_ϵ, which is called the slow manifold, invariant under Eq. (3.66).

Finally, we mention that the lumped-parameter model (3.14) possesses a NHIM in both meanings of Definitions 3.2 and 3.4. The discussion in this chapter has mainly focused on Definition 3.2, and a set of equilibrium points is identified. When there exists no equilibrium point, the time-varying coordinate transformation (3.27) enables the same analysis. For Definition 3.4, the model can be rewritten in the form of Eq. (3.66) by using a coordinate transformation as in (3.43) and a suitable rescaling of the variables.

Appendix 3.D Simulation of the original model

Here, we describe the simulation of the original model utilized in Sec. 3.3.3. As mentioned in Sec. 3.3.3, the purpose of the simulation is to evaluate the effect of heat loss from the pipes. For this purpose, a brute-force simulation is conducted to obtain the short-term response of the model described by Eqs. (3.1) to (3.5) and Eq. (3.12). These equations can be implemented by using COMSOL Multiphysics® Software [30], which is a general-purpose software based on finite element method. In particular, Pipe Flow

Module® is utilized for simulating the fluid flow described by Eqs. (3.3) and (3.4) to determine velocity u_l and pressure p_l. To determine enthalpy h_l, the energy continuity equation (3.5) is implemented by using a PDE Interface. The time-varying boundary conditions are imposed by Eqs. (3.1) and (3.2) and implemented by an ODEs and DAEs Interface. Finally, density ρ_l is given by a function of p_l and h_l. Following [81], in this dissertation, the function $\rho_l(p_l, h_l)$ is obtained by the first order approximation at the condition $(p_l,\, h_l) = (800\,\mathrm{kPa},\, 2768\,\mathrm{kJ/kg})$.

Appendix 3.E List of variables and parameters

Table 3.1: List of variables and parameters in the derived model (3.14). The values used for numerical simulations in Sec. 3.3 are also presented.

Meaning	Symbol	(Nominal) Value	Scaled value
Pressure of steam	p	$800\,\mathrm{kPa}$	1.0 (base)
Density of saturated steam	ρ_s	$4.16\,\mathrm{kg/m^3}$	1.0 (base)
Density of saturated water	ρ_w	$897\,\mathrm{kg/m^3}$	
Specific enthalpy of saturated steam	h_s	$2768\,\mathrm{kJ/kg}$	14.3
Specific enthalpy of saturated water	h_w	$721\,\mathrm{kJ/kg}$	3.74
Specific enthalpy of the feed water	h_f		
Mass flow rate of saturated steam from drum	m'_s		
Mass flow rate of feed water to drum	m'_f		
Coefficient of pressure variation given in (3.2)	e	$3073\,\mathrm{J/Pa}$	1.8
Temperature of saturated steam	T_s	$443\,\mathrm{K}$	
Total mass of evaporator and drum of a boiler	m_t	$50,000\,\mathrm{kg}$	
Specific heat of the metal of boiler	C_p	$0.4\,\mathrm{kJ/(K\cdot kg)}$	
Total volume of steam	V_s	$10.0\,\mathrm{m^3}$	
Total volume of water	V_w	$10.0\,\mathrm{m^3}$	
Velocity of steam in the pipe	u	$30\,\mathrm{m/s}$	1.0 (base)
Length of the steam pipe	L	$200\,\mathrm{m}$	1.0 (base)
Diameter of the steam pipe	d	$0.2\,\mathrm{m}$	1.0 (base)
Friction coefficient of the steam pipe	λ	0.016	16
Input rate of heat of a boiler	Q'		
Consumption rate of heat at a load	Q'_L	$5.0\,\mathrm{MJ/s}$	5.2

Chapter 4

Control of energy balance

This and next chapters address problems of controller synthesis to achieve the coordinated operation of CHP plants described in Sec. 1.4. For electricity supply, a CHP plant is expected to contribute to ancillary services [70, 109] of power systems. This is achieved by regulating the electric power flow interchanged with the infinite bus. In addition, in terms of heat supply, the following two control objectives are considered. One is to maintain the steady energy balance of demand and supply characterized by Eq. (1.5). The other is to regulate the heat transfer rate between the two sites for achieving transient energy supply driven by market or energy-efficiency policies. In this chapter, we focus on the former objective, and the latter will be considered in Chapter 5.

Since the above control objectives require a large change of operating conditions of CHP plants, our aim is to synthesize a nonlinear control system that is applicable to a wide range of operating conditions. With this aim, we perform structural analysis of the state-space model of the two-site system based on geometric nonlinear control theory [59, 113, 68]. The analysis is conducted by the method of *input-output linearization*. The method is different from Jacobian linearization of a nonlinear system used in Sec. 2.3 and is a process of making the input-output response exactly linear by deriving a suitable coordinate transformation. The coordinate transformation provides the so-called *normal form* and *zero dynamics* representing inherent structure of the system. In this and next chapters, we will show that the existence of NHIM in Chapter 3 plays an essential role in the structural analysis for controller synthesis.

In this chapter, we address a basic stabilization problem[1] of the two-site system to

[1]The stabilization problem can be considered as the fist step to a more sophisticated design such as output tracking control [33, 113] and robust and adaptive control [115, 68]. The relationship between each control problem and the associated operation of CHP plants is discussed in subsequent paragraphs.

maintain the steady energy balance. Specifically, we synthesize a state-feedback controller that determines the signals of fuel inputs to the CHP plants to render an equilibrium point of a state-space model of the two-site system asymptotically (exponentially) stable. As illustrated in Chapters 2 and 3, the energy imbalance causes not only short-term dynamics of generators in the electric subsystem but also long-term dynamics of boilers in the heat subsystem. Based on this observation of the multiscale dynamics, we choose the outputs of the state-space model as the electric power flow to the infinite bus and the averaged pressure level, which parameterizes the slow dynamics along the NHIM. It is then shown that the state-space model becomes *minimum phase*[2] under a certain condition. We show that the condition can be simplified due to the existence of the NHIM. Furthermore, since the system becomes minimum phase, a standard stabilizing controller is directly obtained with the input-output linearization. We derive a state-feedback controller through pole placement of the linearized system.

With the derived controller, as will be shown in Sec. 4.4, the equilibrium point to be stabilized depends on the references of the chosen outputs. Thus, the stabilizing controller achieves asymptotic tracking of the electric power flow to a time-invariant reference. This implies that the controller enables the ancillary services with a constant or slowly varying reference. Simultaneously, to maintain the steady energy balance in terms of heat supply, the controller regulates the heat transfer rate so as to satisfy Eq. (1.5). The equilibrium point representing this steady operating condition persists under a small disturbance in terms of model parameters as well as initial conditions because the closed-loop system has an exponentially stable equilibrium point: see Sec. 2.1.

When a time-varying reference or a large disturbance in terms of model parameters is taken into consideration, more sophisticated control methods come into play. For example, this is important when we consider the task of compensating variable outputs of renewable energy sources on the time scale of seconds or tens of seconds [135]. If such renewable energy sources exist inside the region, the task can be formulated by considering uncertainty in consumption of electric loads in the model. This is dealt with by *robust and adaptive control* [115, 68] under uncertainty in model parameters[3]. Similarly, for compensating renewable energy sources outside the region, *output tracking* [33, 113] of a desired reference becomes significant. In this direction, *output regulation problem* [59, 55]

[2]That is, the zero dynamics of the system with the chosen output has an asymptotically stable equilibrium point [113]: see Definition 4.3.

[3]Moreover, this problem is important due to model uncertainty inherent in mathematical modeling.

has been extensively studied, where a feedback controller is pursued to achieve asymptotic tracking of a class of exosystem-generated references and disturbance rejection for a class of disturbances in an uncertain system while maintaining closed-loop stability. The stabilization problem studied in this chapter becomes a basis for considering these control problems.

4.1 Concepts of normal form and zero dynamics

This section briefly reviews geometric nonlinear control theory [59, 113, 68]. In particular, we introduce the concepts of *normal form* and *zero dynamics* that are derived through the method of input-output linearization. For this goal, we consider the following class of affine nonlinear control system of the form[4]

$$\dot{\boldsymbol{x}} = \boldsymbol{f}(\boldsymbol{x}) + \boldsymbol{g}_1(\boldsymbol{x})u_1 + \cdots + \boldsymbol{g}_p(\boldsymbol{x})u_p, \tag{4.1a}$$

$$\boldsymbol{y} = \boldsymbol{h}(\boldsymbol{x}) := \left[h_1(\boldsymbol{x}),\, \ldots,\, h_p(\boldsymbol{x})\right]^\top, \tag{4.1b}$$

where $\boldsymbol{x} \in X \subset \mathbb{R}^n$, $\boldsymbol{u} := [u_1, \ldots, u_p]^\top \in \mathbb{R}^p$, and $\boldsymbol{y} \in \mathbb{R}^p$, where X stands for the state space of the system. The symbol $\dot{\boldsymbol{x}}$ stands for the time derivative of $\boldsymbol{x}$. The vector fields $\boldsymbol{f}$, $\boldsymbol{g}_1, \ldots, \boldsymbol{g}_p$ and the function $\boldsymbol{h}(\boldsymbol{x})$ are assumed to be sufficiently smooth. To investigate the input-output response, the procedure of input-output linearization starts from differentiating $\boldsymbol{y}$ with respect to time: for the i-th element of $\boldsymbol{y}$ ($i = 1, \ldots, p$),

$$\dot{y}_i = \frac{\partial h_i(\boldsymbol{x})}{\partial \boldsymbol{x}}\dot{\boldsymbol{x}} = \frac{\partial h_i(\boldsymbol{x})}{\partial \boldsymbol{x}}\boldsymbol{f}(\boldsymbol{x}) + \frac{\partial h_i(\boldsymbol{x})}{\partial \boldsymbol{x}}\boldsymbol{g}_1(\boldsymbol{x})u_1 + \cdots + \frac{\partial h_i(\boldsymbol{x})}{\partial \boldsymbol{x}}\boldsymbol{g}_p(\boldsymbol{x})u_p. \tag{4.2}$$

By using the notation of Lie derivative (see Appendix 4.A for details), Eq. (4.2) becomes

$$\dot{y}_i = L_f h_i(\boldsymbol{x}) + (L_{g_1} h_i(\boldsymbol{x}))u_1 + \cdots + (L_{g_p} h_i(\boldsymbol{x}))u_p, \tag{4.3}$$

where $L_\alpha \beta(\boldsymbol{x})$ stands for the Lie derivative of a function $\beta(\boldsymbol{x})$ with respect to a vector field $\boldsymbol{\alpha}$. Note that the Lie derivative $L_\alpha \beta(\boldsymbol{x})$ is a function on the state space X. If

[4] The term "affine" indicates that the system is linear in terms of the input [113]. Furthermore, we consider a square system [113], i.e. a system with as many inputs as outputs, because the two-site system is modeled by a double input and double output system in Sec. 4.2. The concepts introduced in this section can be extended for a m-tuple input p-tuple output system with $m > p$ [55]. Also, a general nonlinear system of the form

$$\dot{\boldsymbol{x}} = \boldsymbol{f}(\boldsymbol{x}, \boldsymbol{u}), \quad \boldsymbol{y} = \boldsymbol{h}(\boldsymbol{x})$$

can be rewritten as an affine nonlinear system by considering the augmented system defined by a new state variable $\bar{\boldsymbol{x}} = (\boldsymbol{x}, \boldsymbol{u})^\top$ and input $\boldsymbol{v}$ satisfying $\dot{\boldsymbol{u}} = \boldsymbol{v}$.

$L_{g_j} h_i(\boldsymbol{x}) \equiv 0$ for all $j = 1, \ldots, p$, then the inputs do not appear in the above equation. Define r_i to be the smallest integer such that at least one of the inputs appears in $y_i^{(r_i)}$,

$$y_i^{(r_i)} = L_f^{r_i} h_i(\boldsymbol{x}) + (L_{g_1} L_f^{r_i - 1} h_i(\boldsymbol{x}))u_1 + \cdots + (L_{g_p} L_f^{r_i - 1} h_i(\boldsymbol{x}))u_p, \tag{4.4}$$

where $y_i^{(r_i)}$ stands for the r_i-th derivative of y_i, and $L_{g_j} L_f^{r_i - 1} h_i \neq 0$ for at least one of $j = 1, \ldots, p$. Then, we obtain the following definition of relative degree that provides structural information regarding the input-output relation of the system (4.1).

Definition 4.1 (Relative degree [59, 113])**.** *For each $i = 1, \ldots, p$, the i-th element y_i of the output of the system (4.1) is said to have a relative degree r_i at a point $\boldsymbol{x}_0$ if (i) for all $k < r_i - 1$ and for all $\boldsymbol{x}$ in an open neighborhood of $\boldsymbol{x}_0$,*

$$L_g L_f^k h_i(\boldsymbol{x}) := \left[L_{g_1} L_f^k h_i(\boldsymbol{x}),\ L_{g_2} L_f^k h_i(\boldsymbol{x}), \ldots,\ L_{g_p} L_f^k h_i(\boldsymbol{x}) \right] = \mathbf{0}^\top, \tag{4.5}$$

where $\mathbf{0}$ stands for the all-zero vector, and (ii)

$$L_g L_f^{r_i - 1} h_i(\boldsymbol{x}_0) \neq \mathbf{0}^\top. \tag{4.6}$$

Furthermore, the system (4.1) is said to be have a vector relative degree $\{r_1, r_2, \ldots, r_p\}$ at $\boldsymbol{x}_0$ if (i) for all $i = 1, \ldots, p$, the i-th element $h_i(x)$ has a relative degree r_i at $\boldsymbol{x}_0$, and (ii) the state-dependent matrix $\mathsf{A}(\boldsymbol{x})$ given by

$$\mathsf{A}(\boldsymbol{x}) := \begin{bmatrix} L_g L_f^{r_1 - 1} h_1(\boldsymbol{x}) \\ L_g L_f^{r_2 - 1} h_2(\boldsymbol{x}) \\ \vdots \\ L_g L_f^{r_p - 1} h_p(\boldsymbol{x}) \end{bmatrix} \tag{4.7}$$

is nonsingular at $\boldsymbol{x}_0$.

If the system (4.1) has a well defined vector relative degree, then it is rewritten as

$$\begin{bmatrix} y_1^{(r_1)} \\ \vdots \\ y_n^{(r_p)} \end{bmatrix} = \begin{bmatrix} L_f^{r_1} h_1(\boldsymbol{x}) \\ \vdots \\ L_f^{r_p} h_p(\boldsymbol{x}) \end{bmatrix} + \mathsf{A}(\boldsymbol{x}) \begin{bmatrix} u_1 \\ \vdots \\ u_p \end{bmatrix}. \tag{4.8}$$

Since the matrix $\mathsf{A}(\boldsymbol{x})$ is non-singular, the following state-feedback control law can be defined with a new input $\boldsymbol{v} := [v_1, \ldots, v_p]^\top$:

$$\boldsymbol{u} = -\mathsf{A}^{-1}(\boldsymbol{x}) \begin{bmatrix} L_f^{r_1} h_1(\boldsymbol{x}) \\ \vdots \\ L_f^{r_p} h_p(\boldsymbol{x}) \end{bmatrix} + \mathsf{A}^{-1}(\boldsymbol{x}) \boldsymbol{v}. \tag{4.9}$$

Under the control law (4.9), the closed-loop system is given by

$$\begin{bmatrix} y_1^{(r_1)} \\ \vdots \\ y_n^{(r_p)} \end{bmatrix} = \begin{bmatrix} v_1 \\ \vdots \\ v_p \end{bmatrix}. \tag{4.10}$$

Thus, the control law (4.9) achieves the input-output linearization of the system (4.1). Furthermore, the above procedure provides a normal form as follows. In order to do this, we define new coordinates given by

$$\xi_1^1 = h_1(\boldsymbol{x}), \quad \xi_1^2 = L_f h_1(\boldsymbol{x}), \quad \ldots, \quad \xi_1^{r_1} = L_f^{r_1-1} h_1(\boldsymbol{x}), \tag{4.11a}$$

$$\xi_2^1 = h_2(\boldsymbol{x}), \quad \xi_2^2 = L_f h_2(\boldsymbol{x}), \quad \ldots, \quad \xi_2^{r_2} = L_f^{r_2-1} h_2(\boldsymbol{x}), \tag{4.11b}$$

$$\vdots$$

$$\xi_p^1 = h_p(\boldsymbol{x}), \quad \xi_p^2 = L_f h_p(\boldsymbol{x}), \quad \ldots, \quad \xi_p^{r_p} = L_f^{r_p-1} h_p(\boldsymbol{x}). \tag{4.11c}$$

If $r := r_1 + \cdots + r_p$ is equal to n, these coordinates provide a candidate of coordinate transformation $T : \mathbb{R}^n \to \mathbb{R}^n$ defined by $\boldsymbol{\xi} = \boldsymbol{T}(\boldsymbol{x})$, where $\boldsymbol{\xi} := [\boldsymbol{\xi}_1^\top, \ldots, \boldsymbol{\xi}_p^\top]^\top$ and $\boldsymbol{\xi}_i := [\xi_i^1, \ldots, \xi_i^{r_i}]^\top$. Here, in order for $\boldsymbol{\xi} = \boldsymbol{T}(\boldsymbol{x})$ to be a coordinate transformation, the mapping $\boldsymbol{T}$ needs to be a diffeomorphism[5]. If the Jacobian matrix $\mathrm{D}\boldsymbol{T}(\boldsymbol{x})$ is nonsingular at a point $\boldsymbol{x}_0$, then from the inverse function theorem [1], there exists an open neighborhood U such that T restricted to U is a diffeomorphism on U. For this, the following theorem states that Eq. (4.11) provides a coordinate transformation.

Theorem 4.2 ([59, 113])**.** *Suppose that the system (4.1) has a vector relative degree* $\{r_1, \ldots, r_p\}$ *at* $\boldsymbol{x}_0$*. Then, for all* $0 \le j \le r_i - 1$ *and* $1 \le i \le p$*, the derivatives* $\mathrm{d}L_f^j h_i(\boldsymbol{x})$ *are linearly independent on a neighborhood* U *of* $\boldsymbol{x}_0$*.*

If $r = r_1 + \cdots + r_p$ is less than n, then there exist $n - r$ scalar functions $\Phi_{r+1}, \ldots, \Phi_n$ such that

$$\boldsymbol{\Phi}(\boldsymbol{x}) := [\boldsymbol{T}(\boldsymbol{x})^\top, \Phi_{r+1}(\boldsymbol{x}), \ldots, \Phi_n(\boldsymbol{x})]^\top \tag{4.12}$$

is a diffeomorphism on a open neighborhood of $\boldsymbol{x}_0$. By considering the coordinate transformation $(\boldsymbol{\xi}, \boldsymbol{\eta}) = \boldsymbol{\Phi}(\boldsymbol{x})$, the system (4.1) is converted into the following *normal form*:

[5]That is, the map $\boldsymbol{T}$ is invertible, and $\boldsymbol{T}$ and the inverse $\boldsymbol{T}^{-1}$ are continuously differentiable: see [1]

$$\dot{\xi}_1^1 = \xi_1^2, \tag{4.13a}$$
$$\vdots$$
$$\dot{\xi}_1^{r_1-1} = \xi_1^{r_1} \tag{4.13b}$$
$$\dot{\xi}_1^{r_1} = b_1(\boldsymbol{\xi}, \boldsymbol{\eta}) + \sum_{j=1}^{p} a_1^j(\boldsymbol{\xi}, \boldsymbol{\eta}) u_j, \tag{4.13c}$$
$$\vdots$$
$$\dot{\xi}_p^1 = \xi_p^2, \tag{4.13d}$$
$$\vdots$$
$$\dot{\xi}_p^{r_p-1} = \xi_p^{r_p} \tag{4.13e}$$
$$\dot{\xi}_p^{r_p} = b_p(\boldsymbol{\xi}, \boldsymbol{\eta}) + \sum_{j=1}^{p} a_j^p(\boldsymbol{\xi}, , \boldsymbol{\eta}) u_j, \tag{4.13f}$$
$$\dot{\boldsymbol{\eta}} = \boldsymbol{q}(\boldsymbol{\xi}, \boldsymbol{\eta}) + \mathsf{P}(\boldsymbol{\xi}, \boldsymbol{\eta})\boldsymbol{u}, \tag{4.13g}$$

where the functions b_i, a_i^1, …, a_i^p (for $i = 1, \ldots, p$), $\boldsymbol{q} = (q_1, \ldots q_{n-r})^\top$, and $\mathsf{P} = (P_{ij})$ (for $i = 1, \ldots, n-r$ and $j = 1, \ldots, p$) are given by

$$b_i(\boldsymbol{\xi}, \boldsymbol{\eta}) = L_f^{r_i} h_i(\boldsymbol{\Phi}^{-1}(\boldsymbol{\xi}, \boldsymbol{\eta})), \tag{4.14a}$$
$$a_j^i(\boldsymbol{\xi}, \boldsymbol{\eta}) = L_{g_j} L_f^{r_i - 1} h_i(\boldsymbol{\Phi}^{-1}(\boldsymbol{\xi}, \boldsymbol{\eta})), \tag{4.14b}$$
$$q_i(\boldsymbol{\xi}, \boldsymbol{\eta}) = L_f \eta_i(\boldsymbol{\Phi}^{-1}(\boldsymbol{\xi}, \boldsymbol{\eta})), \tag{4.14c}$$
$$P_{ij}(\boldsymbol{\xi}, \boldsymbol{\eta}) = L_{g_j} \eta_i(\boldsymbol{\Phi}^{-1}(\boldsymbol{\xi}, \boldsymbol{\eta})). \tag{4.14d}$$

Since the input-output linearizing control law (4.9) renders the $\boldsymbol{\eta}$ variables unobservable, the dynamics described by Eq. (4.13g) are referred to as *internal dynamics*. Particularly, the internal dynamics with constraint $\boldsymbol{y}(t) \equiv 0$ are referred to as *zero dynamics* and given by

$$\dot{\boldsymbol{\eta}} = \boldsymbol{q}(0, \boldsymbol{\eta}) - \mathsf{P}(0, \boldsymbol{\xi})\mathsf{A}^{-1}(\boldsymbol{\Phi}^{-1}(0, \boldsymbol{\eta}))\boldsymbol{b}(0, \boldsymbol{\eta}). \tag{4.15}$$

Then, the concept of minimum phase system is defined as follows:

Definition 4.3 (Minimum phase [59, 113])**.** *The system (4.1) is said to be minimum phase at $\boldsymbol{x}_0$ if (i) $\boldsymbol{\eta}_0 := [\Phi_{n-r}(\boldsymbol{x}_0), \ldots, \Phi_n(\boldsymbol{x}_0)]^\top$ is an equilibrium point of Eq. (4.15) and (ii) the equilibrium point $\boldsymbol{\eta}_0$ is asymptotically stable.*

4.2 Nonlinear state-space model

This section derives a nonlinear state-space model of the two-site system to which the method of input-output linearization is applied in Sec. 4.3. The model represents dynamics of the gas turbines as well as the electric and heat subsystems. By defining the state variable of the gas turbines as $\boldsymbol{x}_{\mathrm{g}}$, of the electric subsystem as $\boldsymbol{x}_{\mathrm{e}}$, and of the heat subsystem as $\boldsymbol{x}_{\mathrm{h}}$, the resultant state equation is given as follows:

$$\underbrace{\begin{bmatrix}\dot{\boldsymbol{x}}_{\mathrm{g}}\\ \dot{\boldsymbol{x}}_{\mathrm{e}}\\ \dot{\boldsymbol{x}}_{\mathrm{h}}\end{bmatrix}}_{\dot{\boldsymbol{x}}} = \underbrace{\begin{bmatrix}\boldsymbol{f}_{\mathrm{g}}(\boldsymbol{x}_{\mathrm{g}})\\ \boldsymbol{f}_{\mathrm{e}}(\boldsymbol{x}_{\mathrm{g}},\boldsymbol{x}_{\mathrm{e}})\\ \boldsymbol{f}_{\mathrm{h}}(\boldsymbol{x}_{\mathrm{g}},\boldsymbol{x}_{\mathrm{h}})\end{bmatrix}}_{\boldsymbol{f}(\boldsymbol{x})} + \underbrace{\begin{bmatrix}\boldsymbol{g}_{\mathrm{g1}}(\boldsymbol{x}_{\mathrm{g}})\\ 0\\ 0\end{bmatrix}}_{\boldsymbol{g}_1(\boldsymbol{x})} u_1 + \underbrace{\begin{bmatrix}\boldsymbol{g}_{\mathrm{g2}}(\boldsymbol{x}_{\mathrm{g}})\\ 0\\ 0\end{bmatrix}}_{\boldsymbol{g}_2(\boldsymbol{x})} u_2, \tag{4.16a}$$

$$\boldsymbol{y} = \begin{bmatrix}y_1 & y_2\end{bmatrix}^\top = \underbrace{\begin{bmatrix}h_{\mathrm{e}}(\boldsymbol{x}) & h_{\mathrm{h}}(\boldsymbol{x})\end{bmatrix}^\top}_{\boldsymbol{h}(\boldsymbol{x})}, \tag{4.16b}$$

where the vector fields $\boldsymbol{f}_{\mathrm{g}}$, $\boldsymbol{f}_{\mathrm{e}}$, $\boldsymbol{f}_{\mathrm{h}}$, $\boldsymbol{g}_{\mathrm{g1}}$, and $\boldsymbol{g}_{\mathrm{g2}}$ represent dynamic characteristics of the model and are given in the rest of this section. The functions h_{e} and h_{h} are the outputs of the electric and heat subsystems, respectively, and are determined later. All the variables and parameters are dimensionless as shown in Chapters 2 and 3, while the dimensionless time t is scaled by 1 s, and additional time constants are introduced in the model. The physical meanings of the variables and parameters are listed in Sec. 4.C.

The dynamics of the gas turbines are described by a simplified form of the model in [111, 31, 64]. The state variable is given by

$$\boldsymbol{x}_{\mathrm{g}} = \begin{bmatrix}x_{\mathrm{g1}} & x_{\mathrm{g2}} & \dots & x_{\mathrm{g6}}\end{bmatrix}^\top := \begin{bmatrix}v_{\mathrm{p1}} & w_{\mathrm{f1}} & w_{\mathrm{t1}} & v_{\mathrm{p2}} & w_{\mathrm{f2}} & w_{\mathrm{t2}}\end{bmatrix}^\top, \tag{4.17}$$

where, for $i = 1, 2$, the variable $v_{\mathrm{p}i}$ stands for the position of the fuel valve, and $w_{\mathrm{f}i}$ and $w_{\mathrm{t}i}$ for the fuel flow rates at the combustor and at the turbine. They are dimensionless variables scaled by their designed values and are in the range of $[0, 1]$. The dynamics of the gas turbine are represented by the following equations:

$$\underbrace{\begin{bmatrix}\dot{v}_{\mathrm{p1}}\\ \dot{w}_{\mathrm{f1}}\\ \dot{w}_{\mathrm{t1}}\\ \dot{v}_{\mathrm{p2}}\\ \dot{w}_{\mathrm{f2}}\\ \dot{w}_{\mathrm{t2}}\end{bmatrix}}_{\dot{\boldsymbol{x}}_{\mathrm{g}}} = \underbrace{\begin{bmatrix}(-v_{\mathrm{p1}} + W_{\mathrm{o1}})/T_{\mathrm{v1}}\\ (-w_{\mathrm{f1}} + v_{\mathrm{p1}})/T_{\mathrm{f2}}\\ (-w_{\mathrm{t1}} + w_{\mathrm{f1}})/T_{\mathrm{CD1}}\\ (-v_{\mathrm{p2}} + W_{\mathrm{o2}})/T_{\mathrm{v2}}\\ (-w_{\mathrm{f}i} + v_{\mathrm{p2}})/T_{\mathrm{f2}}\\ (-w_{\mathrm{t2}} + w_{\mathrm{f2}})/T_{\mathrm{CD2}}\end{bmatrix}}_{\boldsymbol{f}_{\mathrm{g}}(\boldsymbol{x}_{\mathrm{g}})} + \underbrace{\begin{bmatrix}(1 - W_{\mathrm{o1}})/T_{\mathrm{v1}}\\ 0\\ 0\\ 0\\ 0\\ 0\end{bmatrix}}_{\boldsymbol{g}_{\mathrm{g1}}(\boldsymbol{x}_{\mathrm{g}})} u_1 + \underbrace{\begin{bmatrix}0\\ 0\\ 0\\ (1 - W_{\mathrm{o2}})/T_{\mathrm{v}s2}\\ 0\\ 0\end{bmatrix}}_{\boldsymbol{g}_{\mathrm{g2}}(\boldsymbol{x}_{\mathrm{g}})} u_2, \tag{4.18}$$

where the time constants $T_{\mathrm{v}i}$, $T_{\mathrm{f}i}$, and $T_{\mathrm{CD}i}$ are of the valve positioning system, of the down stream piping and fuel gas distribution, and of the compressor discharge, respectively. The parameter $W_{\mathrm{o}i}$ stands for the lower limit of the fuel valve. As a result of the fuel combustion, as shown in Fig. 1.5, the mechanical power $P_{\mathrm{m}i}$ and the heat flow rate $Q'_{\mathrm{a}i}$ are supplied to the generators and the heat recovery boilers. In the model, they are given as follows[6]:

$$P_{\mathrm{m}i} = K_{\mathrm{e}i}\left(w_{\mathrm{t}i} - W_{\mathrm{o}i}\right)/(1 - W_{\mathrm{o}i}), \tag{4.19a}$$

$$Q'_{\mathrm{a}i} = K_{\mathrm{h}i}(w_{\mathrm{f}i} + \beta_i)/(1 + \beta_i), \tag{4.19b}$$

where $K_{\mathrm{e}i}$ and $K_{\mathrm{h}i}$ stand for the rated outputs of mechanical power and heat flow rate. The parameter $K_{\mathrm{h}i}\beta_i/(1 + \beta_i)$ represents the heat output with no fuel input.

The model of the electric subsystem is basically the same as that in Chapter 2. The state variable is given by

$$\boldsymbol{x}_{\mathrm{e}} = \begin{bmatrix} x_{\mathrm{e}1} & x_{\mathrm{e}2} & x_{\mathrm{e}3} & x_{\mathrm{e}4} \end{bmatrix}^\top := \begin{bmatrix} \delta_1 & \omega_1 & \delta_2 & \omega_2 \end{bmatrix}^\top, \tag{4.20}$$

where the physical meanings of the variables and parameters are listed in Appendix 2.B. The dynamics are represented as follows:

$$\underbrace{\begin{bmatrix} \dot{\delta}_1 \\ \dot{\omega}_1 \\ \dot{\delta}_2 \\ \dot{\omega}_2 \end{bmatrix}}_{\dot{\boldsymbol{x}}_{\mathrm{e}}} = \underbrace{\begin{bmatrix} \omega_1/T_{\mathrm{e}1} \\ \{P_{\mathrm{m}1}(\boldsymbol{x}_{\mathrm{g}}) - D_1\omega_1 - P_{\mathrm{e}1}(\delta_1,\, \delta_2)\}/T_{\mathrm{e}1} \\ \omega_2/T_{\mathrm{e}2} \\ \{P_{\mathrm{m}2}(\boldsymbol{x}_{\mathrm{g}}) - D_2\omega_2 - P_{\mathrm{e}2}(\delta_1,\, \delta_2)\}/T_{\mathrm{e}2} \end{bmatrix}}_{\boldsymbol{f}_{\mathrm{e}}(\boldsymbol{x}_{\mathrm{g}},\, \boldsymbol{x}_{\mathrm{e}})} \tag{4.21}$$

where $T_{\mathrm{e}i}$ is the time constant of swing dynamics of each generator, and given by $T_{\mathrm{e}i} = \sqrt{2H_i/\omega_{\mathrm{s}}}$. The parameter H_i stands for the per-unit inertia constant, and ω_{s} for synchronous speed. The electric power $P_{\mathrm{e}i}(\delta_1,\, \delta_2)$ is given by

$$P_{\mathrm{e}i}(\delta_1, \delta_2) = \sum_{j \in \{1,2,\infty\}} P_{ij}(\delta_1, \delta_2) \tag{4.22}$$

with the symbol ∞ representing the infinite bus, and $P_{ij}(\delta_1, \delta_2)$ given by

$$P_{ij}(\delta_1, \delta_2) = E_i E_j \{G_{ij}\cos(\delta_i - \delta_j) + B_{ij}\sin(\delta_i - \delta_j)\}. \tag{4.23}$$

[6] As pointed out in [31], the causality of these values does not necessarily follow their relation to the process physics. In the model (4.19), the heat flow rate $Q'_{\mathrm{a}i}$ is absorbed by the heat recovery boiler before the process of compressor discharging. This is because the time constant of the discharging is negligible compared to those of boilers [31]. Here, we follow [111, 31, 64] and utilize the above model.

The electric power $P_{\mathrm{e}\infty}$ to the infinite bus is described by

$$P_{\mathrm{e}\infty}(\delta_1, \delta_2) := -P_{\infty 1}(0, \delta_1) - P_{\infty 2}(0, \delta_2). \tag{4.24}$$

For the heat subsystem, the inner-limit model derived in Sec. 3.2 is utilized. The state variable is given by

$$\boldsymbol{x}_{\mathrm{h}} = \begin{bmatrix} x_{\mathrm{h}1} & x_{\mathrm{h}2} & x_{\mathrm{h}3} \end{bmatrix}^\top := \begin{bmatrix} p_1 & p_2 & w \end{bmatrix}^\top, \tag{4.25}$$

where p_i stands for the deviation of boiler pressure relative to the nominal value, and $w(> 0)$ for the velocity of steam inside the pipe. The variables w and p are scaled by $w_{\mathrm{r}} := Q'_{\mathrm{r}}/d^2 h_{\mathrm{r}} \rho_{\mathrm{r}}$ and $p_{\mathrm{r}} := \rho_{\mathrm{r}} w_{\mathrm{r}}^2$, where Q'_{r}, h_{r}, and ρ_{r} are rated values of the heat flow rate, enthalpy, and density, respectively. The dynamics of heat sub-system are represented by the following equations:

$$\underbrace{\begin{bmatrix} \dot{p}_1 \\ \dot{p}_2 \\ \dot{w} \end{bmatrix}}_{\dot{\boldsymbol{x}}_{\mathrm{h}}} = \underbrace{\begin{bmatrix} \{Q'_{\mathrm{a}1}(w_{\mathrm{f}i}) - Q'_{\mathrm{L}1} - Q'_{12}(w)\}/T_{\mathrm{h}1} \\ \{Q'_{\mathrm{a}2}(w_{\mathrm{f}i}) - Q'_{\mathrm{L}2} - Q'_{21}(w)\}/T_{\mathrm{h}2} \\ \{(p_1 - p_2)/\rho_{\mathrm{s}} - \lambda L w^2/(2d)\}/T_{\mathrm{h}3} \end{bmatrix}}_{\boldsymbol{f}_{\mathrm{h}}(\boldsymbol{x}_{\mathrm{g}},\, \boldsymbol{x}_{\mathrm{h}})} \tag{4.26}$$

where the functions $Q'_{12}(w)$ and $Q'_{21}(w)$ stand for the heat flow rates through the pipe and given as follows:

$$Q'_{12}(w) = -Q'_{21}(w) = \frac{\pi}{4} h_{\mathrm{c}} \rho_{\mathrm{s}} w, \tag{4.27}$$

where h_{c} stands for the enthalpy of condensation. The time constants $T_{\mathrm{h}i}$ of boilers for $i = 1, 2$ are given by $T_{\mathrm{h}i} := Q'_{\mathrm{r}} e_i / d^4 h_{\mathrm{r}}^2 \rho_{\mathrm{r}}$, where e_i stands for the rate of change of internal energy stored in the boilers. The time constant $T_{\mathrm{h}3}$ of responses of steam flows in the pipe is given as $T_{\mathrm{h}3} := d^2 L h_{\mathrm{r}} \rho_{\mathrm{r}} / Q'_{\mathrm{r}}$.

Finally, we mention several features of the derived model (4.16). The state space X of the model is given by

$$X := \left\{ \boldsymbol{x} \in \mathbb{R}^{13} \mid 0 \le x_{\mathrm{g}i} \le 1,\ i = 1, \ldots, 6,\ \ x_{\mathrm{h}3} > 0 \right\}. \tag{4.28}$$

While we do not explicitly consider the conditions in (4.28) in the structural analysis in Sec. 4.3 and controller synthesis in Sec. 4.4, it is confirmed by the numerical simulations in Sec. 4.5 that the trajectories of the closed-loop system remain within X in order to show that the synthesized controller is feasible. In terms of an equilibrium point of the model,

note that the equilibrium point $\boldsymbol{x}^*$ to be stabilized is considered under a nominal input $\boldsymbol{u}^*$, i.e. $\boldsymbol{f}(\boldsymbol{x}^*) + \boldsymbol{g}(\boldsymbol{x}^*)\boldsymbol{u}^* = 0$. Although it is possible to derive a coordinate transformation such that the desired equilibrium point $\boldsymbol{x}^*$ satisfies $\boldsymbol{f}(\boldsymbol{x}^*) = 0$, we do not utilized such a coordinate transformation because the location of the desired equilibrium point depends on the references of outputs.

4.3 Structural analysis

This section performs a structural analysis of the model (4.16) based on the method of input-output linearization. For the purpose of synthesizing stabilization control, the following two outputs are considered:

$$y_1 = h_{\mathrm{e}}(\boldsymbol{x}) := P_{\mathrm{e}\infty}(x_{\mathrm{e}1},\, x_{\mathrm{e}3}), \tag{4.29a}$$

$$y_2 = h_{\mathrm{h}}(\boldsymbol{x}) := \frac{T_{\mathrm{h}1}x_{\mathrm{h}1} + T_{\mathrm{h}2}x_{\mathrm{h}2}}{T_{\mathrm{h}1} + T_{\mathrm{h}2}}. \tag{4.29b}$$

where y_1 stands for the electric power to the infinite bus, and y_2 for the averaged pressure of the two boilers. For the above choice of the outputs, we derive the normal form of the model (4.16) in Sec. 4.3.1. The internal dynamics are then analyzed in Sec. 4.3.2 to clarify the minimum phase property of the model and to facilitate the controller synthesis in Sec. 4.4 and Chapter 5.

4.3.1 Derivation of normal form

To derive the normal form of the model (4.16), the following lemma summarizes the result of the input-output linearization of the model. The Lie derivatives required for the analysis are obtained with symbolic computation by using Mathematica® [132].

Lemma 4.4. *Consider the model (4.16) with the outputs in Eq. (4.29). Then, there exists an open subset D of the state space X such that the system has vector relative degree $\{5, 3\}$ at $\boldsymbol{x} \in D$, and the coordinate transformation defined by*

$$\boldsymbol{\Phi} : \boldsymbol{x} \mapsto (\boldsymbol{\xi}_{\mathrm{e}}^{\top},\ \boldsymbol{\xi}_{\mathrm{h}}^{\top},\ \boldsymbol{\eta}^{\top})^{\top}, \tag{4.30}$$

is a diffeomorphism on D, where $\boldsymbol{\xi}_{\mathrm{e}}$, $\boldsymbol{\xi}_{\mathrm{h}}$, and $\boldsymbol{\eta}$ are given by[7]

$$\boldsymbol{\xi}_{\mathrm{e}} := \begin{bmatrix} h_{\mathrm{e}}(\boldsymbol{x}) & L_f h_{\mathrm{e}}(\boldsymbol{x}) & L_f^2 h_{\mathrm{e}}(\boldsymbol{x}) & L_f^3 h_{\mathrm{e}}(\boldsymbol{x}) & L_f^4 h_{\mathrm{e}}(\boldsymbol{x}) \end{bmatrix}^\top, \tag{4.31}$$

$$\boldsymbol{\xi}_{\mathrm{h}} := \begin{bmatrix} h_{\mathrm{h}}(\boldsymbol{x}) & L_f h_{\mathrm{h}}(\boldsymbol{x}) & L_f^2 h_{\mathrm{h}}(\boldsymbol{x}) \end{bmatrix}^\top. \tag{4.32}$$

$$\boldsymbol{\eta} := \begin{bmatrix} x_{\mathrm{g3}} & x_{\mathrm{e1}} & x_{\mathrm{e2}} & x_{\mathrm{h1}} - x_{\mathrm{h2}} & x_{\mathrm{h3}} \end{bmatrix}^\top = \begin{bmatrix} w_{\mathrm{t1}} & \delta_1 & \omega_1 & p_1 - p_2 & w \end{bmatrix}^\top. \tag{4.33}$$

Proof. The proof follows from direct application of the method of input-output linearization. For the chosen outputs, the decoupling matrix $\mathsf{A}(\boldsymbol{x})$ is obtained by differentiating the outputs y_1 and y_2 in 5 and 3 times, respectively:

$$\mathsf{A}(\boldsymbol{x}) := \begin{bmatrix} L_{g_1} L_f^4 h_{\mathrm{e}}(\boldsymbol{x}) & L_{g_2} L_f^4 h_{\mathrm{e}}(\boldsymbol{x}) \\ L_{g_1} L_f^2 h_{\mathrm{h}}(\boldsymbol{x}) & L_{g_2} L_f^2 h_{\mathrm{h}}(\boldsymbol{x}) \end{bmatrix}, \tag{4.34}$$

It can be verified that $\mathsf{A}(\boldsymbol{x})$ depends only on $\boldsymbol{x}_{\mathrm{e}}$, and its determinant is given by

$$\det \mathsf{A}(\boldsymbol{x}) = -A_1 \frac{\mathrm{d}P_{\infty 1}}{\mathrm{d}x_{\mathrm{e1}}}(x_{\mathrm{e1}}) + A_2 \frac{\mathrm{d}P_{\infty 2}}{\mathrm{d}x_{e3}}(x_{\mathrm{e3}}), \tag{4.35}$$

where A_1 and A_2 are positive constants determined by the parameters of the model, and the functions $P_{\infty 1}$ and $P_{\infty 2}$ are given by Eq. (4.23). Thus, there exists an open set $D_1 \subset X$ such that $\det \mathsf{A}(\boldsymbol{x}) \neq 0$ for $\boldsymbol{x} \in D_1$, and the model has vector relative degree $\{5, 3\}$ at $\boldsymbol{x} \in D_1$. Then, for the following coordinate transformation

$$\boldsymbol{\Phi} : \boldsymbol{x} \mapsto (\boldsymbol{\xi}_{\mathrm{e}},\ \boldsymbol{\xi}_{\mathrm{h}},\ \boldsymbol{\eta}) \tag{4.36}$$

with the variables $\boldsymbol{\xi}_{\mathrm{e}}$ $\boldsymbol{\xi}_{\mathrm{h}}$, and $\boldsymbol{\eta}$ chosen as in Eqs. (4.31)–(4.33), the determinant $\det \mathrm{D}\boldsymbol{\Phi}(\boldsymbol{x})$ of the Jacobian matrix $\mathrm{D}\Phi(\boldsymbol{x})$ is given by

$$\begin{aligned} \det \mathrm{D}\boldsymbol{\Phi}(\boldsymbol{x}) =& F_0 \left\{ \frac{\mathrm{d}P_{\infty 2}}{\mathrm{d}x_{\mathrm{e3}}}(x_{\mathrm{e3}}) \right\}^3 \cdot \left\{ F_1 \frac{\mathrm{d}P_{\infty 1}}{\mathrm{d}x_{\mathrm{e1}}}(x_{\mathrm{e1}}) - F_2 \frac{\mathrm{d}P_{\infty 2}}{\mathrm{d}x_{\mathrm{e3}}}(x_{\mathrm{e3}}) \right\} \\ & \cdot \left\{ F_3 \frac{\mathrm{d}P_{\infty 1}}{\mathrm{d}x_{\mathrm{e1}}}(x_{\mathrm{e1}}) - F_4 \frac{\mathrm{d}P_{\infty 2}}{\mathrm{d}x_{\mathrm{e3}}}(x_{\mathrm{e3}}) \right\}, \end{aligned} \tag{4.37}$$

where $F_0, \ldots, F_4$ are positive constants determined by the parameters of the model. Thus, there exists an open set $D_2 \subset X$ such that $\det \mathrm{D}\boldsymbol{\Phi}(\boldsymbol{x}) \neq 0$ at $x \in D_2$. The proof is completed by choosing $D := D_1 \cap D_2$. □

[7] The choice of the variable $\boldsymbol{\eta}$ is not unique. For the motivation of the choice of Eq. (4.33), see Appendix 4.B.

As a result, for the outputs in Eq. (4.29), the model (4.16) has the following normal form on the open subset D stated in Lemma 4.4:

$$\dot{\xi}_{\mathrm{e}1} = \xi_{\mathrm{e}2}, \tag{4.38a}$$

$$\vdots$$

$$\dot{\xi}_{\mathrm{e}4} = \xi_{\mathrm{e}5}, \tag{4.38b}$$

$$\dot{\xi}_{\mathrm{e}5} = b_1(\boldsymbol{\xi}_{\mathrm{e}}, \boldsymbol{\xi}_{\mathrm{h}}, \boldsymbol{\eta}) + \sum_{j=1}^{2} a_1^j(\boldsymbol{\xi}_e, \boldsymbol{\xi}_{\mathrm{h}}, \boldsymbol{\eta})u_j \tag{4.38c}$$

$$\dot{\xi}_{\mathrm{h}1} = \xi_{\mathrm{h}2}, \tag{4.38d}$$

$$\dot{\xi}_{\mathrm{h}2} = \xi_{\mathrm{h}3}, \tag{4.38e}$$

$$\dot{\xi}_{\mathrm{h}3} = a_2(\boldsymbol{\xi}_{\mathrm{e}}, \boldsymbol{\xi}_{\mathrm{h}}, \boldsymbol{\eta}) + \sum_{j=1}^{2} a_2^j(\boldsymbol{\xi}_{\mathrm{e}}, \boldsymbol{\xi}_{\mathrm{h}}, \boldsymbol{\eta})u_j \tag{4.38f}$$

$$\dot{\boldsymbol{\eta}} = \boldsymbol{q}(\boldsymbol{\xi}_{\mathrm{e}}, \boldsymbol{\xi}_{\mathrm{h}}, \boldsymbol{\eta}), \tag{4.38g}$$

where the functions $a_1^1, \ldots, a_2^2$, b_1, and b_2 are given as in Eq. (4.14), and $\boldsymbol{q}$ as

$$\boldsymbol{q}(\boldsymbol{\xi}_{\mathrm{e}}, \boldsymbol{\xi}_{\mathrm{h}}, \boldsymbol{\eta}) := \bar{\boldsymbol{q}}(\Phi^{-1}(\boldsymbol{\xi}_{\mathrm{e}}, \boldsymbol{\xi}_{\mathrm{h}}, \boldsymbol{\eta})) \tag{4.39}$$

with

$$\bar{\boldsymbol{q}}(\cdot) = \begin{bmatrix} f_{\mathrm{g}3}(\cdot) & f_{\mathrm{e}1}(\cdot) & f_{\mathrm{e}2}(\cdot) & f_{\mathrm{h}1}(\cdot) - f_{\mathrm{h}2}(\cdot) & f_{\mathrm{h}3}(\cdot) \end{bmatrix}^\top. \tag{4.40}$$

4.3.2 Analysis of internal dynamics

Here, we investigate the internal dynamics with respect to the outputs in Eq. (4.29) in order to characterize the minimum phase property of the model. As introduced in Sec. 4.1, the property is determined by the zero dynamics, which are derived by considering the internal dynamics with the output kept to zero for all time. For the two site system, it is rather meaningful to keep the outputs to nonzero values Y_1^{ref} and Y_2^{ref}. Strictly speaking, this corresponds to modifying the outputs to the set-point error given by

$$\boldsymbol{e}_{\mathrm{s}} := \begin{bmatrix} y_1 - Y_1^{\mathrm{ref}} & y_2 - Y_2^{\mathrm{ref}} \end{bmatrix}^\top. \tag{4.41}$$

Thus, the minimum phase property depends on the set point of the outputs. The following lemma states that the property does not affected by the set point Y_2^{ref}.

Lemma 4.5. *The internal dynamics (4.38g) are independent of the variable* $\xi_{\mathrm{h}1}$.

Proof. The function $\boldsymbol{q}(\boldsymbol{\xi}_\mathrm{e}, \boldsymbol{\xi}_\mathrm{h}, \boldsymbol{\eta})$, which describes the internal dynamics, is given by $\bar{\boldsymbol{q}}(\boldsymbol{x})$ in Eq. (4.40) through the coordinate transformation $\boldsymbol{\Phi}$. Thus, it needs to be clarified how the state variables $\boldsymbol{x}_\mathrm{g}$, $\boldsymbol{x}_\mathrm{e}$, and $\boldsymbol{x}_\mathrm{h}$ depend on the variables $\boldsymbol{\xi}_\mathrm{e}$, $\boldsymbol{\xi}_\mathrm{h}$, and $\boldsymbol{\eta}$. Particularly, if the variables appearing in $\bar{\boldsymbol{q}}$ do not depend on $\xi_{\mathrm{h}1}$, the proof is completed. For this purpose, we firstly discuss how the variables $\boldsymbol{\xi}_\mathrm{e}$ and $\boldsymbol{\xi}_\mathrm{h}$ depend on $\boldsymbol{x}$. Figure 4.1 shows the interconnections of the state variables of the model (4.16). Note that the variables of the heat subsystem are changed according to the following coordinate transformation $\boldsymbol{\Phi}_\mathrm{h}(\boldsymbol{x}_\mathrm{h})$ given by

$$\boldsymbol{\Phi}_\mathrm{h}(\boldsymbol{x}_\mathrm{h}) := \begin{bmatrix} 1 & -1 & 0 \\ 0 & 0 & 1 \\ T_{\mathrm{h}1}/(T_{\mathrm{h}1}+T_{\mathrm{h}2}) & T_{\mathrm{h}2}/(T_{\mathrm{h}1}+T_{\mathrm{h}2}) & 0 \end{bmatrix} \begin{bmatrix} x_{\mathrm{h}1} \\ x_{\mathrm{h}2} \\ x_{\mathrm{h}3} \end{bmatrix} = \begin{bmatrix} \eta_4 \\ \eta_5 \\ \xi_{\mathrm{h}1} \end{bmatrix}. \tag{4.42}$$

This transformation corresponds to the transformation (3.43) in Chapter 3. The first two variables of $\Phi_\mathrm{h}(\boldsymbol{x}_\mathrm{h})$ describe the dynamics transversal to the NHIM, and the last variable does the dynamics along the NHIM. From Fig. 4.1, it follows that the variable $\boldsymbol{\xi}_\mathrm{e}$ depends only on $\boldsymbol{x}_\mathrm{e}$ and $\boldsymbol{x}_\mathrm{g}$. It is also verified that $\boldsymbol{\xi}_\mathrm{h}$ depends only on $(T_{\mathrm{h}1}x_{\mathrm{h}1}+T_{\mathrm{h}2}x_{\mathrm{h}2})/(T_{\mathrm{h}1}+T_{\mathrm{h}2})$ and $\boldsymbol{x}_\mathrm{g}$. Especially, the variables $\xi_{\mathrm{h}2}$ and $\xi_{\mathrm{h}3}$ depend only on $\boldsymbol{x}_\mathrm{g}$. Thus, we can define the following 10-dimensional coordinate transformation $\boldsymbol{\Phi}_\mathrm{ge}$:

$$\boldsymbol{\Phi}_\mathrm{ge} := (\boldsymbol{x}_\mathrm{g}, \boldsymbol{x}_\mathrm{e}) \mapsto (\boldsymbol{\xi}_\mathrm{e}, [\xi_{\mathrm{h}2}, \xi_{\mathrm{h}3}]^\top, [\eta_1, \eta_2, \eta_3]^\top). \tag{4.43}$$

Here, the dependence of $\boldsymbol{x}_\mathrm{g}$, $\boldsymbol{x}_\mathrm{e}$, and $\boldsymbol{x}_\mathrm{h}$ on $\boldsymbol{\xi}_\mathrm{e}$, $\boldsymbol{\xi}_\mathrm{h}$, and $\boldsymbol{\eta}$ are given by the inverses of $\boldsymbol{\Phi}_\mathrm{h}$ and $\boldsymbol{\Phi}_\mathrm{ge}$ if they exist. By defining a coordinate transformation $\bar{\boldsymbol{\Phi}} : \boldsymbol{x} \mapsto (\boldsymbol{\Phi}_\mathrm{eg}(\boldsymbol{x}_\mathrm{g}, \boldsymbol{x}_\mathrm{e}), \boldsymbol{\Phi}_\mathrm{h}(\boldsymbol{x}_\mathrm{h}))$,

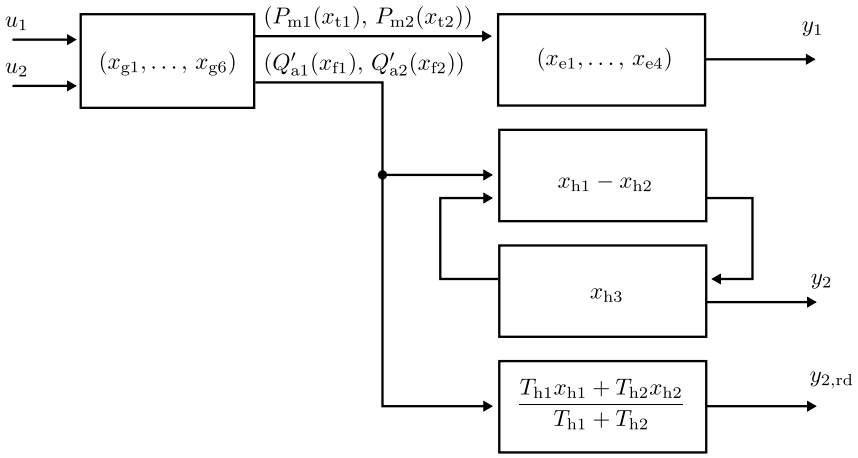

Figure 4.1: Graphical representation of the interconnection of the state variables

which is equivalent to $\boldsymbol{\Phi}$, the following equation holds:

$$\mathrm{detD}\bar{\boldsymbol{\Phi}} = \mathrm{detD}\boldsymbol{\Phi}_{\mathrm{ge}} \cdot \mathrm{detD}\boldsymbol{\Phi} s_{\mathrm{h}}. \tag{4.44}$$

Since $\mathrm{detD}\bar{\boldsymbol{\Phi}} \neq 0$ holds on the subset D stated in Lemma 4.4, the coordinate transformation Φ_{ge} is one-to-one on the subset D. Thus, the variables $\boldsymbol{x}_{\mathrm{e}}$ and $\boldsymbol{x}_{\mathrm{g}}$ are independent of ξ_{h1}. Since the function $\bar{\boldsymbol{q}}(\boldsymbol{x})$ depends only on $\boldsymbol{x}_{\mathrm{g}}$, $\boldsymbol{x}_{\mathrm{e}}$, $x_{\mathrm{h1}} - x_{\mathrm{h2}} = \eta_4$, and $x_{\mathrm{h3}} = \eta_5$, the function $\boldsymbol{q}$ is independent of ξ_{h1}. □

Thus, the minimum phase property for given references Y_1^{ref} and Y_2^{ref} is characterized by the following theorem:

Theorem 4.6. *Consider the system (4.16) with the outputs in Eq. (4.29), and suppose that there exists an equilibrium point $\boldsymbol{x}^*$ of (4.16) satisfying $\boldsymbol{e}_{\mathrm{s}} = 0$ for given references Y_1^{ref} and Y_2^{ref}. Then, the system is minimum phase at $\boldsymbol{x}^*$ if (i) $\boldsymbol{x}^*$ exists in the open set D stated by Lemma 4.4, and (ii) the eigenvalues of the matrix Q given by*

$$\mathsf{Q} := \frac{\partial \boldsymbol{q}}{\partial \boldsymbol{\eta}}([Y_1^{\mathrm{ref}}, 0, \ldots, 0]^\top, [0, 0, 0]^\top, \boldsymbol{\eta}^*), \tag{4.45}$$

have negative real parts.

Proof. The proof follows from the definition of minimum phase system, Lemmas 4.4 and 4.5. □

4.4 Controller synthesis

This section synthesizes a controller that renders an equilibrium point of the state-space model (4.16) asymptotically (exponentially) stable. As mentioned in the beginning of this chapter, the position of the equilibrium point to be stabilized depends on the references of the outputs. Thus, it is required to synthesize a nonlinear feedback controller that is applicable to a wide range of operating conditions. However, as mentioned in [115, 68], the whole design of a nonlinear feedback controller can not be accomplished by one design tool[8]. Here, since our main objective is to demonstrate the effectiveness of the structural analysis in Sec. 4.3, we synthesize a standard stabilizing controller [113, 68] by pole placement through input-output linearization. For given references

$$y_1^{\mathrm{ref}}(t) = P_{\mathrm{e}\infty}^{\mathrm{ref}}, \quad y_2^{\mathrm{ref}}(t) = p^{\mathrm{ref}}, \tag{4.46}$$

[8]For more nonlinear design tools, see [115, 59, 113, 68, 55].

the controller is given as follows:

$$\begin{bmatrix} u_1 \\ u_2 \end{bmatrix} = \mathsf{A}^{-1}(\boldsymbol{x}) \begin{bmatrix} -L_f^5 h_1(\boldsymbol{x}) - \sum_{j=1}^{5} \alpha_{\mathrm{e}j} \tilde{\xi}_{\mathrm{e}i}(t) \\ -L_f^3 h_2(\boldsymbol{x}) - \sum_{j=1}^{3} \alpha_{\mathrm{h}j} \tilde{\xi}_{\mathrm{h}i}(t) \end{bmatrix}, \tag{4.47}$$

where $\tilde{\boldsymbol{\xi}}_{\mathrm{e}} := [\tilde{\xi}_{\mathrm{e}1}, \ldots, \tilde{\xi}_{\mathrm{e}5}]^\top$ and $\tilde{\boldsymbol{\xi}}_{\mathrm{h}} := [\tilde{\xi}_{\mathrm{h}1}, \tilde{\xi}_{\mathrm{h}2}, \tilde{\xi}_{\mathrm{h}3}]^\top$ depend on the references $P_{\mathrm{e}\infty}^{\mathrm{ref}}$ and p^{ref} and are given by

$$\tilde{\boldsymbol{\xi}}_{\mathrm{e}} := \left[\ \xi_{\mathrm{e}1} - P_{\mathrm{e}\infty}^{\mathrm{ref}},\ \xi_{\mathrm{e}2}, \xi_{\mathrm{e}3}, \xi_{\mathrm{e}4}, \xi_{\mathrm{e}5}\ \right]^\top, \tag{4.48a}$$

$$\tilde{\boldsymbol{\xi}}_{\mathrm{h}} := \left[\ \xi_{\mathrm{h}1} - p^{\mathrm{ref}},\ \xi_{\mathrm{h}2},\ \xi_{\mathrm{h}3}\ \right]^\top. \tag{4.48b}$$

With the control law (4.47), the poles of the linearized system is placed at the zeros of the polynomials $s^5 + \alpha_{\mathrm{e}5}s^4 + \cdots + \alpha_{\mathrm{e}1}$ and $s^3 + \alpha_{\mathrm{h}3}s^2 + \alpha_{\mathrm{h}2}s + \alpha_{\mathrm{h}1}$. The stability of the closed-loop system is given by the following theorem.

Theorem 4.7. *Consider the model (4.16) with the feedback control law (4.47). Suppose that for given $P_{\mathrm{e}\infty}^{\mathrm{ref}}$, there exist $\boldsymbol{\eta}^{\mathrm{ref}}$ satisfying the following equation:*

$$\boldsymbol{q}([P_{\mathrm{e}\infty}^{\mathrm{ref}}, 0, \ldots 0]^\top,\ [0,0,0]^\top, \boldsymbol{\eta}^{\mathrm{ref}}) = 0. \tag{4.49}$$

Further suppose the point $(\boldsymbol{\xi}_{\mathrm{e}},\ \boldsymbol{\xi}_{\mathrm{h}},\ \boldsymbol{\eta}) = ([P_{\mathrm{e}\infty}^{\mathrm{ref}}, 0, \ldots 0]^\top,\ [0,0,0]^\top, \boldsymbol{\eta}^{\mathrm{ref}})$ exists in the open subset D stated in Lemma 4.4. Then, there exists a trajectory of the closed-loop system given by

$$(\boldsymbol{\xi}_{\mathrm{e}}(t),\ \boldsymbol{\xi}_{\mathrm{h}}(t),\ \boldsymbol{\eta}(t)) = ([P_{\mathrm{e}\infty}^{\mathrm{ref}}, 0, \ldots 0],\ [p^{\mathrm{ref}},\ 0,\ 0],\ \boldsymbol{\eta}^{\mathrm{ref}}). \tag{4.50}$$

In addition to the existence, the trajectory is asymptotically stable if the polynomials $s^5 + \alpha_{\mathrm{e}5}s^4 + \cdots + \alpha_{\mathrm{e}1}$ and $s^3 + \alpha_{\mathrm{h}3}s^2 + \alpha_{\mathrm{h}2}s + \alpha_{\mathrm{h}1}$ are Hurwitz, and all of the eigenvalues of the matrix Q defined as

$$\mathsf{Q} := \frac{\partial \boldsymbol{q}}{\partial \boldsymbol{\eta}}(([P_{\mathrm{e}\infty}^{\mathrm{ref}}, 0, \ldots 0]^\top,\ [0,0,0]^\top, \boldsymbol{\eta}^{\mathrm{ref}})) \tag{4.51}$$

has negative real parts.

Proof. By consider the system in the normal form (4.38) with the control law (4.47), the closed-loop system has the following form:

$$\dot{\tilde{\boldsymbol{\xi}}}_{\mathrm{e}} = \mathsf{A}_{\mathrm{e}}\tilde{\boldsymbol{\xi}}_{\mathrm{e}}, \tag{4.52a}$$

$$\dot{\tilde{\boldsymbol{\xi}}}_{\mathrm{h}} = \mathsf{A}_{\mathrm{h}}\tilde{\boldsymbol{\xi}}_{\mathrm{h}}, \tag{4.52b}$$

$$\dot{\boldsymbol{\eta}} = \boldsymbol{q}(\tilde{\boldsymbol{\xi}}_{\mathrm{e}} + [P_{\mathrm{e}\infty}^{\mathrm{ref}},\ 0, \ldots,\ 0]^\top,\ \tilde{\boldsymbol{\xi}}_{\mathrm{h}} + [p^{\mathrm{ref}},\ 0,\ 0]^\top,\ \boldsymbol{\eta}), \tag{4.52c}$$

with

$$\mathsf{A}_{\mathrm{e}} := \begin{bmatrix} 0 & 1 & 0 & 0 & 0 \\ 0 & 0 & 1 & 0 & 0 \\ 0 & 0 & 0 & 1 & 0 \\ 0 & 0 & 0 & 0 & 1 \\ -\alpha_{\mathrm{e}1} & -\alpha_{\mathrm{e}2} & -\alpha_{\mathrm{e}3} & -\alpha_{\mathrm{e}4} & -\alpha_{\mathrm{e}5} \end{bmatrix}, \tag{4.53a}$$

$$\mathsf{A}_{\mathrm{h}} := \begin{bmatrix} 0 & 1 & 0 \\ 0 & 0 & 1 \\ -\alpha_{\mathrm{h}1} & -\alpha_{\mathrm{h}2} & -\alpha_{\mathrm{h}3} \end{bmatrix}. \tag{4.53b}$$

Thus, $(\tilde{\boldsymbol{\xi}}_{\mathrm{e}}(t),\, \tilde{\boldsymbol{\xi}}_{\mathrm{h}}(t),\, \boldsymbol{\eta}(t)) = (0,\, 0,\, \boldsymbol{\eta}^{\mathrm{ref}})$ is an equilibrium point of the closed-loop system. From Lemma 4.5, the stability of the equilibrium is determined by the eigenvalues of the following matrix

$$\begin{bmatrix} \mathsf{A}_{\mathrm{e}} & 0 & 0 \\ 0 & \mathsf{A}_{\mathrm{h}} & 0 \\ * & * & \mathsf{Q} \end{bmatrix} \tag{4.54}$$

By assumption, the eigenvalues of Q have negative real parts, and the eigenvalues of A_{e} and A_{h} are the zeros of the Hurwitz polynomials. The proof is thus completed. □

4.5 Numerical simulation

This section demonstrates the effectiveness of the control law (4.47) under a practical setting of parameters. The values of parameters are listed in Appendix 4.C. We first verify the assumptions of Theorem 4.7, which depend on the value of the reference $P^{\mathrm{ref}}_{\mathrm{e}\infty}$. Note that they are independent of p^{ref} due to Lemma 4.5. In terms of the existence of the trajectory given by Eq. (4.50), the open set D stated in Lemma 4.4 can be considered by Fig. 4.2. The figure shows the singularity conditions of $\mathsf{A}(\boldsymbol{x})$ and $\mathrm{D}\boldsymbol{\Phi}(\boldsymbol{x})$. The *solid* lines show the condition $\det\mathsf{A}(\boldsymbol{x}) = 0$ and the *broken* lines $\det\mathrm{D}\Phi(\boldsymbol{x}) = 0$. Since the conditions depend only on $x_{\mathrm{e}1}$ and $x_{\mathrm{e}3}$, by defining a set D_{e} as the inside of these lines containing $(x_{\mathrm{e}1},\, x_{\mathrm{e}3}) = (0,\, 0)$, the set D is given as follows:

$$D = \left\{ \left[\boldsymbol{x}_{\mathrm{g}}^{\top},\, \boldsymbol{x}_{\mathrm{e}}^{\top},\, \boldsymbol{x}_{\mathrm{h}}^{\top}\right]^{\top} \in X \mid (x_{\mathrm{e}1}, x_{\mathrm{e}3}) \in D_{\mathrm{e}} \right\}. \tag{4.55}$$

In Fig. 4.2, the points (×) show the values of $x_{\mathrm{e}1}$ and $x_{\mathrm{e}3}$ under various settings of $P^{\mathrm{ref}}_{\mathrm{e}\infty}$. It is confirmed that the trajectory given by Eq. (4.50) exists in the open set D when $P^{\mathrm{ref}}_{\mathrm{e}\infty} \in [0.6,\, 1.32]$. Then, the stability of the trajectory is determined by the matrix Q

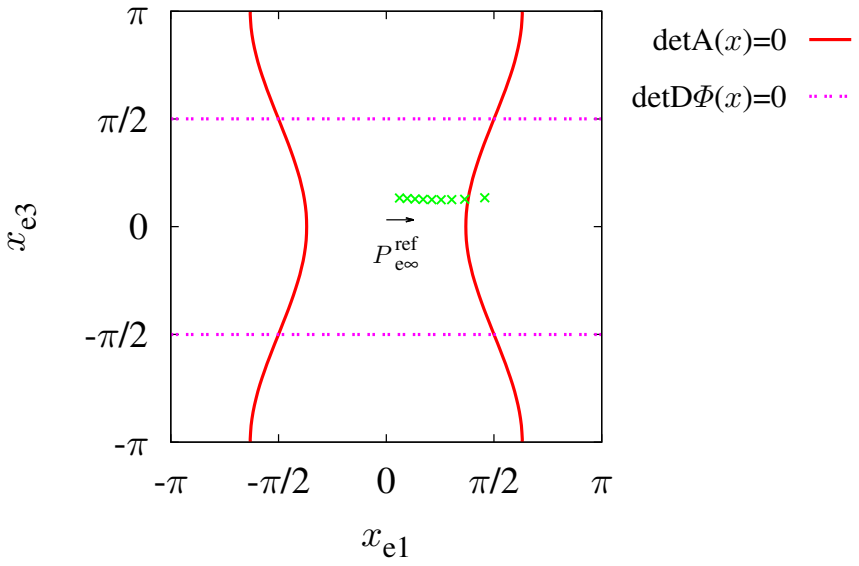

Figure 4.2: Singularity condition of $\mathsf{A}(\boldsymbol{x})$ and $\mathrm{D}\boldsymbol{\Phi}(\boldsymbol{x})$. The inside of the lines containing $(x_{e1}, x_{e3}) = (0, 0)$ can be chosen as the subset D in Lemma 4.4.

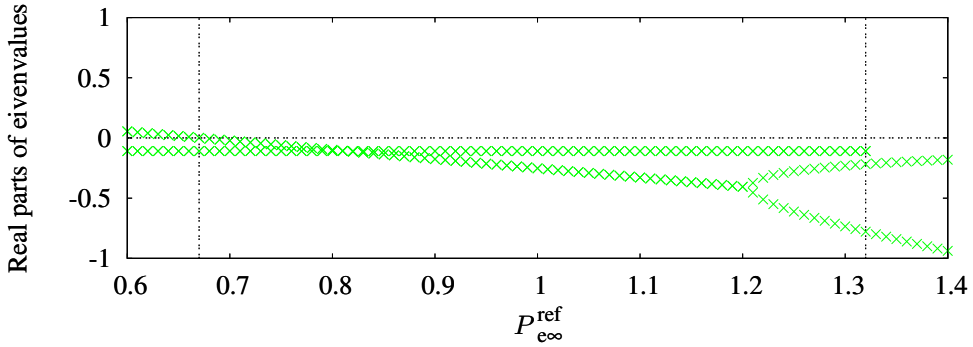

Figure 4.3: Real parts of eigenvalues of Q for various $P^{\mathrm{ref}}_{e\infty}$

in Eq. (4.51). It is confirmed that the matrix Q has two pairs of complex conjugate eigenvalues and one real eigenvalue for $P^{\mathrm{ref}}_{e\infty} > 1.2$. Figure 4.3 shows the real parts of the two sets of eigenvalues, and the real eigenvalue exists around -10. For $P^{\mathrm{ref}}_{e\infty} < 0.67$, a set of eigenvalues has positive real parts. Thus, the model (4.16) is a minimum phase system under $P^{\mathrm{ref}}_{e\infty} \in [0.67, 1.32]$.

Figure 4.4 shows the responses of the outputs y_1, y_2 and inputs u_1, u_2 of the closed-loop system. In the figure, the *solid* lines show the responses under $(P^{\mathrm{ref}}_{e\infty}, p^{\mathrm{ref}}) = (1.0, 0)$, and the *broken* lines under $(P^{\mathrm{ref}}_{e\infty}, p^{\mathrm{ref}}) = (1.0, 0.1)$. For both cases, the initial condition

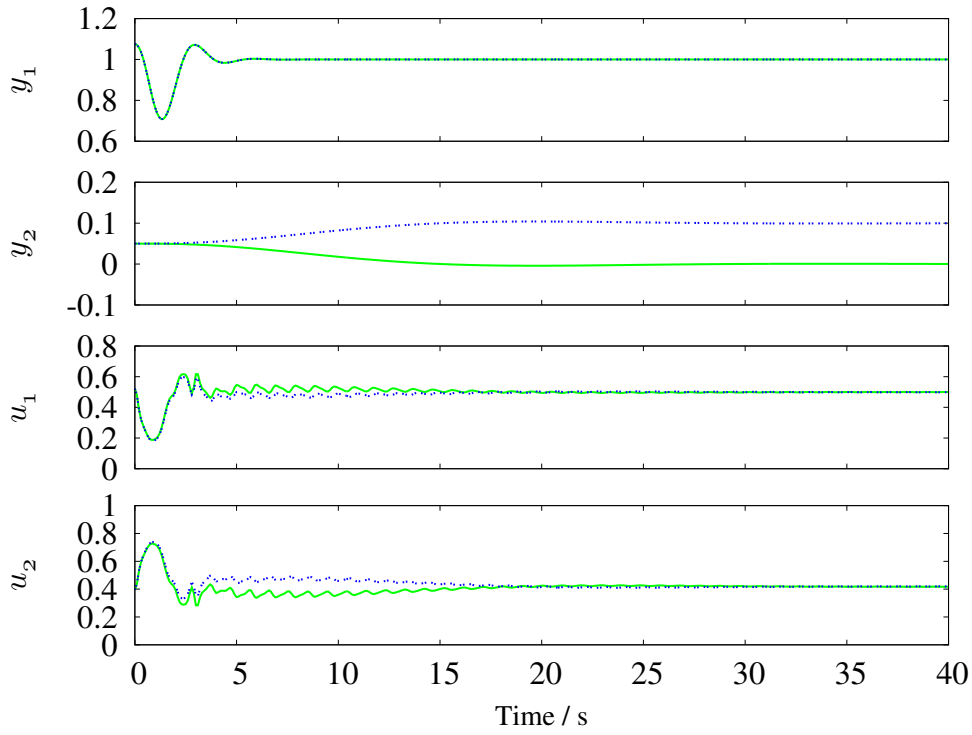

Figure 4.4: Time responses of outputs y_1 and y_2 and inputs u_1 and u_2. The solid line shows the responses under $y_2^{\mathrm{ref}} = 0$, and the broken line under $y_2^{\mathrm{ref}} = 0.1$.

$\boldsymbol{x}(0)$ is set as follows:

$$\boldsymbol{x}(0) = \left[\boldsymbol{x}_{\mathrm{g}}^{*\top},\, \boldsymbol{x}_{\mathrm{e}}^{*\top} + [0.1,\, 0,\, 0,\, 0]^{\top},\, \boldsymbol{x}_{\mathrm{h}}^{*\top} + [0.1,\, 0,\, 0]^{\top}\right]^{\top}, \tag{4.56}$$

where $\boldsymbol{x}^* = [\boldsymbol{x}_{\mathrm{g}}^{*\top},\, \boldsymbol{x}_{\mathrm{e}}^{*\top},\, \boldsymbol{x}_{\mathrm{h}}^{*\top}]^{\top}$ stands for the equilibrium point under $(P_{\mathrm{e}\infty}^{\mathrm{ref}},\, p^{\mathrm{ref}}) = (1.0,\, 0)$. The coefficients $\alpha_{\mathrm{e}1},\, \ldots \alpha_{\mathrm{h}5}$ of the control law (4.47) are chosen as follows:

$$s^5 + \alpha_{\mathrm{e}5}s^4 + \alpha_{\mathrm{e}4}s^3 + \alpha_{\mathrm{e}3}s^2 + \alpha_{\mathrm{e}2}s + \alpha_{\mathrm{e}1} = (s^2 + 2.5^s + 2.5^2)^2(s + 2.5), \tag{4.57}$$

$$s^3 + \alpha_{\mathrm{h}3}s^2 + \alpha_{\mathrm{h}2}s + \alpha_{\mathrm{h}1} = (s^2 + 0.25^s + 0.25^2)(s + 0.25). \tag{4.58}$$

From Fig. 4.4, it is confirmed that the controller asymptotically stabilizes the corresponding equilibrium point according to the references of the outputs $(P_{\mathrm{e}\infty}^{\mathrm{ref}},\, p^{\mathrm{ref}})$. Since the electric power y_1 and the averaged pressure y_2 converge to constants, the energy balance in the two-site system is maintained. Also, the inputs u_1 and u_2 satisfy $u_i \in [0,\, 1]$, and thus the synthesized controller is feasible.

4.6 Summary

This chapter addressed a basic stabilization problem of the state-space model of the two-site system. We synthesized a controller that determines the signals of fuel inputs to the CHP plants for a given set of time-invariant references of the outputs of the state-space model. The outputs stand for the electric power flow to the infinite bus and the averaged pressure level. With this choice of the outputs, the state-space model becomes a minimum phase system under suitably chosen references of the outputs. We showed that the condition providing the minimum phase property was simplified due to the existence of the NHIM clarified in Chapter 3. Since the model is a minimum phase system, a standard stabilizing controller based on input-output linearization is applicable to render an equilibrium point of the model (exponentially) asymptotically stable.

Appendix 4.A Lie derivative of a function

The Lie derivative of a scalar function [1] provides a new function on the state space utilized for the structural analysis and controller synthesis in Chapters 4 and 5. Suppose $h : \mathbb{R}^n \supset X \to \mathbb{R}$ is a sufficiently smooth scalar function, and $\boldsymbol{f} : X \to \mathbb{R}^n$ a vector field, where X stands for the state space. Then, the Lie derivative $L_f h(\boldsymbol{x})$ is defined as

$$L_f h(\boldsymbol{x}) := \sum_{i=1}^{n} \frac{\partial h}{\partial x_i} f_i(\boldsymbol{x}) = \frac{\partial h}{\partial \boldsymbol{x}} \boldsymbol{f}(\boldsymbol{x}). \tag{4.59}$$

Thus, $L_f h(\boldsymbol{x})$ gives the rate of change of h along the flow of the vector field $\boldsymbol{f}$. For iterative calculation of Lie derivative, the following notations are utilized in this dissertation.

$$L_f^0 h(\boldsymbol{x}) := h(\boldsymbol{x}), \tag{4.60}$$

$$L_f^k h(\boldsymbol{x}) := L_f(L_f^{k-1} h)(\boldsymbol{x}) = \frac{\partial L_f^{k-1} h}{\partial \boldsymbol{x}} \boldsymbol{f}(\boldsymbol{x}), \quad k \geq 1, \tag{4.61}$$

$$L_g L_f^k h(\boldsymbol{x}) := L_g(L_f^k h)(\boldsymbol{x}) = \frac{\partial L_f^k h}{\partial \boldsymbol{x}} \boldsymbol{g}(\boldsymbol{x}), \tag{4.62}$$

where $\boldsymbol{g} : X \to \mathbb{R}^n$ is a vector field. Note that the Lie derivatives are obtained with symbolic computation by using e.g. Mathematica® [132].

Appendix 4.B Choice of the variable η

As mentioned in Sec. 4.1, the variable $\boldsymbol{\eta}$ is chosen so that the mapping $\boldsymbol{\Phi} : \boldsymbol{x} \to (\boldsymbol{\xi}, \boldsymbol{\eta})$ is a diffeomorphism to provide a coordinate transformation. For this, some of the original state variables $x_1, \ldots, x_n$ and their functions are chosen so that they are independent of the variable $\boldsymbol{\xi}$. Table 4.1 shows the dependency of the state variables appearing in the process of input-output linearization in Lemma 4.4. It is confirmed from Tab. 4.1 that two state variables appear in each step and that $x_{\mathrm{g}1}$, $x_{\mathrm{g}2}$, $x_{\mathrm{g}4}$, $x_{\mathrm{g}5}$ appear in the derivatives of both h_1 and h_2. Since the variable $x_{\mathrm{h}3}$ does not appear in Tab. 4.1, it should be chosen as one of the $\boldsymbol{\eta}$ variables. Because the dimension of the state space is thirteen, and the vector relative degree is $\{5, 3\}$, we need to choose four variables other than $x_{\mathrm{h}3}$. For this, it is implied from Tab. 4.1 to choose one variable using $(x_{\mathrm{g}3}, x_{\mathrm{g}6})$, two variables using $(x_{\mathrm{e}1}\, x_{\mathrm{e}2}, x_{\mathrm{e}3}, x_{\mathrm{e}4})$, and one variable using $(x_{\mathrm{h}1}, x_{\mathrm{h}2})$. Consequently, in this chapter, we take the variable $\boldsymbol{\eta}$ as follows:

$$\boldsymbol{\eta} := \left[x_{\mathrm{g}3}\ x_{\mathrm{e}1}\ x_{\mathrm{e}2}\ x_{\mathrm{h}1} - x_{\mathrm{h}2}\ x_{\mathrm{h}3}\right]^\top. \tag{4.63}$$

Table 4.1: Dependency of the original state variables $x_1 \ldots, x_n$ on the variables $\boldsymbol{\xi}_{\mathrm{e}}$, $\boldsymbol{\xi}_{\mathrm{h}}$. Two variables newly appear in each step of the input-output linearization in Lemma 4.4.

$\boldsymbol{\xi}_{\mathrm{e}}, \boldsymbol{\xi}_{\mathrm{h}}$	Dependency of x_i	New variables
$h_{\mathrm{e}}(\boldsymbol{x})$	$x_{\mathrm{e}1}$, $x_{\mathrm{e}3}$	
$L_f h_{\mathrm{e}}(\boldsymbol{x})$	$x_{\mathrm{e}1}$, $x_{\mathrm{e}2}$, $x_{\mathrm{e}3}$, $x_{\mathrm{e}4}$	$x_{\mathrm{e}2}$, $x_{\mathrm{e}4}$
$L_f^2 h_{\mathrm{e}}(\boldsymbol{x})$	$x_{\mathrm{g}3}$, $x_{\mathrm{g}6}$, $x_{\mathrm{e}1}$, $x_{\mathrm{e}2}$, $x_{\mathrm{e}3}$, $x_{\mathrm{e}4}$	$x_{\mathrm{g}3}$, $x_{\mathrm{g}6}$
$L_f^3 h_{\mathrm{e}}(\boldsymbol{x})$	$x_{\mathrm{g}2}$, $x_{\mathrm{g}3}$, $x_{\mathrm{g}5}$, $x_{\mathrm{g}6}$, $x_{\mathrm{e}1}$, $x_{\mathrm{e}2}$, $x_{\mathrm{e}3}$, $x_{\mathrm{e}4}$	$x_{\mathrm{g}2}$, $x_{\mathrm{g}5}$
$L_f^4 h_{\mathrm{e}}(\boldsymbol{x})$	$x_{\mathrm{g}1}$, $x_{\mathrm{g}2}$, $x_{\mathrm{g}3}$, $x_{\mathrm{g}4}$, $x_{\mathrm{g}5}$, $x_{\mathrm{g}6}$, $x_{\mathrm{e}1}$, $x_{\mathrm{e}2}$, $x_{\mathrm{e}3}$, $x_{\mathrm{e}4}$	$x_{\mathrm{g}1}$, $x_{\mathrm{g}4}$
$h_{\mathrm{h}}(\boldsymbol{x})$	$x_{\mathrm{h}1}$, $x_{\mathrm{h}2}$	
$L_f h_{\mathrm{h}}(\boldsymbol{x})$	$x_{\mathrm{g}2}$, $x_{\mathrm{g}5}$, $x_{\mathrm{h}1}$, $x_{\mathrm{h}2}$	$x_{\mathrm{g}2}$, $x_{\mathrm{g}5}$
$L_f^2 h_{\mathrm{h}}(\boldsymbol{x})$	$x_{\mathrm{g}1}$, $x_{\mathrm{g}2}$, $x_{\mathrm{g}4}$, $x_{\mathrm{g}5}$, $x_{\mathrm{h}1}$, $x_{\mathrm{h}2}$	$x_{\mathrm{g}1}$, $x_{\mathrm{g}4}$

Appendix 4.C Parameter setting

Table 4.2 lists the values of parameters used for the numerical simulations in Sec. 4.5. The values of parameter are based on [111, 31, 64] for the gas turbines, [9, 124] for the electric subsystem, and [18, 63] for the heat subsystem.

Table 4.2: Parameters for numerical simulation

Symbol	Meaning	Value
$T_{\mathrm{v}i}$	Valve positioner time constant	0.05 s
$T_{\mathrm{f}i}$	Fuel system time constant	0.4 s
$T_{\mathrm{CD}i}$	Compressor volume time constant	0.1 s
W_{oi}	Fuel valve lower limit	0.23 p.u.
$K_{\mathrm{e}1}$	Rated mechanical power #1	7.5 MW
$K_{\mathrm{e}2}$	Rated mechanical power #2	3.0 MW
$K_{\mathrm{h}i}$	Rated heat output	6.0 MJ/s
β_i	Coefficient for no fuel condition	0
ω_{s}	Synchronous speed	377 rad/s
H_i	Per-unit inertia time constant	10 s
D_i	Damping coefficient	0.05 p.u.
E_i	Voltage of the generator	1.0 p.u.
B_{i0}	Transfer susceptance to infinete bus	1.0 p.u.
B_{12}	Transfer susceptance	0.5 p.u.
G_{ij}	Transfer conductances	0
p_0	Nominal value of pressure	800 kPa
ρ_{s}	Density of saturated steam	4.161 kg/m^3
h_{s}	Specific enthalpy of steam	2768 kJ/kg
h_{w}	Specific enthalpy of water	721.0 kJ/kg
e_i	Coefficient of pressure variation	3073 J/Pa
d	Diameter of the steam pipe	0.2 m
L	Length of the pipe	200 m
λ	Friction coefficient	0.016
$Q'_{\mathrm{L}1}$	Heat consumption at site #1	2.0 MJ/s
$Q'_{\mathrm{L}2}$	Heat consumption at site #2	5.0 MJ/s

Chapter 5

Tracking control of energy flows

This chapter addresses an output tracking control problem for regulating the following two energy flows: the electric power flow to the infinite bus and the heat transfer rate between the two sites. The control problem is closely related to a hierarchical management architecture for flexible and reliable services of energy supply. As mentioned in Sec. 1.1, the frequency control of electric power systems [84] has been realized with a hierarchical architecture based on the time-scale separation principle: a high-level planner solves an optimization problem to generate a signal of optimal power flow, and a low-level controller regulates the electric powers of generators with the measurement of the system frequency. Recently, this hierarchical architecture has been reconsidered in the contexts of Smart grids and ESI. For example, an enhanced automatic generation control is proposed in [57] through a discussion on sensing, communication, and control architectures to manage temporal and spatial characteristics of power systems. In [7], a distributed frequency control is proposed for the integration of multiple asynchronous AC systems and a high-voltage direct current grid. In [46], a unified framework of hierarchical control is proposed to realize a given global desired state by local actions of measurement and control with applications to an integrated energy system.

Figure 5.1 shows the hierarchical architecture studied in this chapter. In the architecture, a high-level planner generates the signals of optimal flows of multiple types of energy, for which several studies are reported in e.g. [42, 80, 11, 79], and a low-level controller tracks the generated signal while keeping the state bounded. In Chapter 4, we synthesized a stabilizing controller for maintaining the steady energy balance. This is intended to resolve the energy imbalances between demand and supply, which is caused by short-term variations and prediction errors in loads and generations of renewable energy

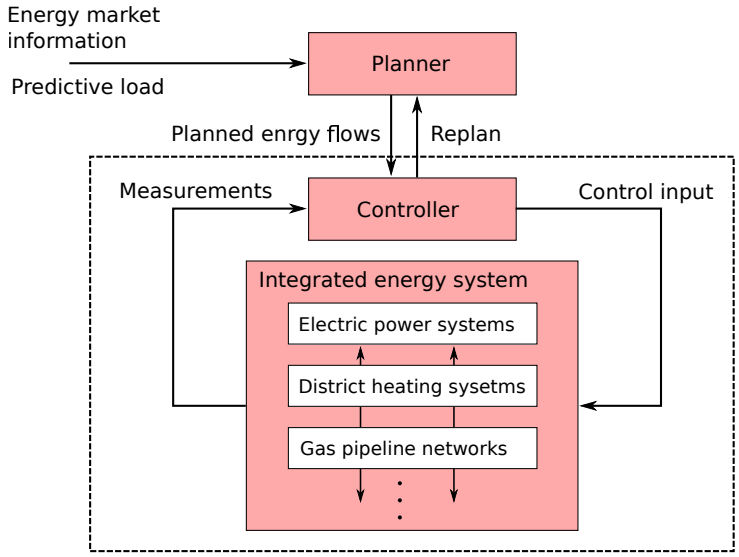

Figure 5.1: Hierarchical management architecture for integrated systems of different energy infrastructures

resources. If the variations and prediction errors are small, the stabilizing controller will track the planned signal. However, if this is not the case, as a result of the control, the actual values of energy flows deviate from their planned values. In the example of the two-site system, a planner will generate the signals of energy flows (the electric power to the infinite bus and the heat transfer rate) satisfying Eq. (1.5) by predictive values of the electric and heat loads. However, if there is a large prediction error, the energy flows will deviate from the planned values because the stabilizing controller regulates the heat transfer rate so as to satisfy Eq. (1.5) for the actual values of loads and the electric power to the infinite bus.

In this chapter, we synthesize an output tracking controller to regulate the two energy flows independently. For this, based on geometric nonlinear control theory, we firstly clarify the fundamental limitation for realizing the planned energy flows and resolving the energy imbalances. When the outputs of the state-space model of the two-site system are given as the two energy flows, the system becomes a *non-minimum phase* system: see Definition 4.3. Stability property of the zero dynamics is investigated and characterized by the NHIM in Chapter 3. It is then shown that the tracking control can be achieved with the outputs in Eq. (4.29) by considering a slowly time varying reference of the outputs. While the derived controller does not guarantee the stability of an equilibrium point, it achieves a transient energy supply driven by market or energy-efficiency policies.

Since the tracking controller is synthesized with the same outputs as those used in Chapter 4, the two different objectives (stabilization and tracking) are achieved by a single control scheme. Thus, it is possible for the high-level planner to select a control objective (stabilization or tracking) without changing the control structure so that it achieves flexible and reliable services of energy supply. A similar hierarchical management architecture is proposed in [74, 75] for operation of a helicopter based unmanned aerial vehicle. The management architecture consists of several layers including strategic planning, trajectory generation, and regulation layers in order to accomplish the missions of searching, investigating, and locating objects in an unknown environment by switching the missions during a flight. The controller synthesized in this chapter is expected to become a key component in such a hierarchical management architecture.

5.1 Structural analysis

This section performs a structural analysis of the state-space model of the two-site system with the following choice of the outputs:

$$y_1 = h_{\mathrm{e}}(\boldsymbol{x}) := P_{\mathrm{e}\infty}(x_{\mathrm{e}1},\, x_{\mathrm{e}3}), \tag{5.1a}$$

$$\hat{y}_2 = \hat{h}_{\mathrm{h}}(\boldsymbol{x}) := Q'_{\mathrm{n}}(x_{\mathrm{h}3}), \tag{5.1b}$$

where y_1 stands for the electric power to the infinite bus, and $\hat{y}_2$ for the heat transfer rate between the two sites. The output y_1 is the same as Eq. (4.29), and $\hat{y}_2$ is different from Eq. (4.29). For the outputs, we derive the zero dynamics of the model in Sec. 5.1.1 and analyze the non-minimum phase property of the model in Sec. 5.1.2.

5.1.1 Derivation of zero dynamics

Here, as in Sec. 4.3, we perform input-output linearization to derived the zero dynamics with respect to the outputs in Eq. (5.1). The state-space model is given by

$$\underbrace{\begin{bmatrix}\dot{\boldsymbol{x}}_{\mathrm{g}}\\ \dot{\boldsymbol{x}}_{\mathrm{e}}\\ \dot{\boldsymbol{x}}_{\mathrm{h}}\end{bmatrix}}_{\dot{\boldsymbol{x}}} = \underbrace{\begin{bmatrix}\boldsymbol{f}_{\mathrm{g}}(\boldsymbol{x}_{\mathrm{g}})\\ \boldsymbol{f}_{\mathrm{e}}(\boldsymbol{x}_{\mathrm{g}}, \boldsymbol{x}_{\mathrm{e}})\\ \boldsymbol{f}_{\mathrm{h}}(\boldsymbol{x}_{\mathrm{g}}, \boldsymbol{x}_{\mathrm{h}})\end{bmatrix}}_{\boldsymbol{f}(\boldsymbol{x})} + \underbrace{\begin{bmatrix}\boldsymbol{g}_{\mathrm{g}1}(\boldsymbol{x}_{\mathrm{g}})\\ 0\\ 0\end{bmatrix}}_{\boldsymbol{g}_1(\boldsymbol{x})} u_1 + \underbrace{\begin{bmatrix}\boldsymbol{g}_{\mathrm{g}2}(\boldsymbol{x}_{\mathrm{g}})\\ 0\\ 0\end{bmatrix}}_{\boldsymbol{g}_2(\boldsymbol{x})} u_2, \tag{5.2a}$$

$$\boldsymbol{y} = \begin{bmatrix} y_1 & \hat{y}_2 \end{bmatrix}^\top = \underbrace{\begin{bmatrix} \boldsymbol{h}_{\mathrm{e}}(\boldsymbol{x}) & \hat{\boldsymbol{h}}_{\mathrm{h}}(\boldsymbol{x}) \end{bmatrix}^\top}_{\hat{\boldsymbol{h}}(\boldsymbol{x})}, \tag{5.2b}$$

where the functions $\boldsymbol{f}_{\mathrm{g}}$, $\boldsymbol{f}_{\mathrm{e}}$, $\boldsymbol{f}_{\mathrm{h}}$, $\boldsymbol{g}_{\mathrm{g1}}$, and $\boldsymbol{g}_{\mathrm{g2}}$ represent dynamic characteristics of the model and are given in Sec. 4.2. The result of the input-output linearization is summarized in the following lemma:

Lemma 5.1. *Consider the model (5.2) with the outputs in Eq. (5.1). Then, there exists an open set $\hat{D}$ of the state space X such that the model has vector relative degree $\{5, 4\}$ at $\boldsymbol{x} \in \hat{D}$, and the internal dynamics are described with the variable $\hat{\boldsymbol{\eta}}$ given by*[1]

$$\hat{\boldsymbol{\eta}} = \begin{bmatrix} x_{\mathrm{g3}} & x_{\mathrm{e1}} & x_{\mathrm{e2}} & \dfrac{T_{\mathrm{h1}}x_{\mathrm{h1}} + T_{\mathrm{h2}}x_{\mathrm{h2}}}{T_{\mathrm{h1}} + T_{\mathrm{h2}}} \end{bmatrix}^{\top} = \begin{bmatrix} w_{\mathrm{t1}} & \delta_1 & \omega_1 & \dfrac{T_{\mathrm{h1}}p_1 + T_{\mathrm{h2}}x_2}{T_{\mathrm{h1}} + T_{\mathrm{h2}}} \end{bmatrix}^{\top}. \tag{5.3}$$

Proof. The proof follows from direct application of the method of input-output linearization. For the chosen output, the decoupling matrix $\hat{\mathsf{A}}(\boldsymbol{x})$ is obtained by differentiating the outputs y_1 and y_2 in 5 and 4 times, respectively:

$$\hat{\mathsf{A}}(\boldsymbol{x}) := \begin{bmatrix} L_{g_1}L_f^4 h_{\mathrm{e}}(\boldsymbol{x}) & L_{g_2}L_f^4 h_{\mathrm{e}}(\boldsymbol{x}) \\ L_{g_1}L_f^3 \hat{h}_{\mathrm{h}}(\boldsymbol{x}) & L_{g_2}L_f^3 \hat{h}_{\mathrm{h}}(\boldsymbol{x}) \end{bmatrix}. \tag{5.4}$$

The matrix $\hat{\mathsf{A}}(\boldsymbol{x})$ depends only on $\boldsymbol{x}_{\mathrm{e}}$, and its determinant is given by

$$\det\hat{\mathsf{A}}(\boldsymbol{x}) = -\hat{A}_1 \frac{\mathrm{d}P_{\infty 1}}{\mathrm{d}x_{\mathrm{e1}}}(x_{\mathrm{e1}}) - \hat{A}_2 \frac{\mathrm{d}P_{2\infty}}{\mathrm{d}x_{\mathrm{e3}}}(x_{\mathrm{e3}}), \tag{5.5}$$

where $\hat{A}_1$ and $\hat{A}_2$ are positive constants. The functions $P_{\infty 1}$ and $P_{\infty 2}$ are given in Eq. (4.23), and thus it is possible to choose an open set $\hat{D}_1 \subset X$ such that $\det\hat{\mathsf{A}}(\boldsymbol{x}) \neq 0$. Thus, the model has vector relative degree $\{5, 4\}$ at $\boldsymbol{x} \in \hat{D}_1$. Then, the following coordinate transformation can be defined:

$$\hat{\boldsymbol{\Phi}} : \boldsymbol{x} \mapsto (\boldsymbol{\xi}_{\mathrm{e}},\ \hat{\boldsymbol{\xi}}_{\mathrm{h}},\ \hat{\boldsymbol{\eta}}), \tag{5.6}$$

with $\boldsymbol{\xi}_{\mathrm{e}}$ and $\hat{\boldsymbol{\xi}}_{\mathrm{h}}$ given by

$$\boldsymbol{\xi}_{\mathrm{e}} := \begin{bmatrix} h_{\mathrm{e}}(\boldsymbol{x}) & L_f h_{\mathrm{e}}(\boldsymbol{x}) & L_f^2 h_{\mathrm{e}}(\boldsymbol{x}) & L_f^3 h_{\mathrm{e}}(\boldsymbol{x}) & L_f^4 h_{\mathrm{e}}(\boldsymbol{x}) \end{bmatrix}^{\top}, \tag{5.7}$$

$$\hat{\boldsymbol{\xi}}_{\mathrm{h}} := \begin{bmatrix} \hat{h}_{\mathrm{h}}(\boldsymbol{x}) & L_f \hat{h}_{\mathrm{h}}(\boldsymbol{x}) & L_f^2 \hat{h}_{\mathrm{h}}(\boldsymbol{x}) & L_f^3 \hat{h}_{\mathrm{h}}(\boldsymbol{x}) \end{bmatrix}^{\top}. \tag{5.8}$$

With the variable $\hat{\boldsymbol{\eta}}$ chosen as in Eq. (5.3), the determinant $\det\mathrm{D}\hat{\boldsymbol{\Phi}}(\boldsymbol{x})$ of the Jacobian matrix $\mathrm{D}\hat{\boldsymbol{\Phi}}(\boldsymbol{x})$ is given by

$$\begin{aligned} \det\mathrm{D}\hat{\boldsymbol{\Phi}}(\boldsymbol{x}) = &- \hat{F}_0 \left\{ \frac{\mathrm{d}P_{\infty 2}}{\mathrm{d}x_{\mathrm{e3}}}(x_{\mathrm{e3}}) \right\}^3 \cdot \left\{ \hat{F}_1 \frac{\mathrm{d}P_{\infty 1}}{\mathrm{d}x_{\mathrm{e1}}}(x_{\mathrm{e1}}) + \hat{F}_2 \frac{\mathrm{d}P_{\infty 2}}{\mathrm{d}x_{\mathrm{e3}}}(x_{\mathrm{e3}}) \right\} \\ &\cdot \left\{ \boldsymbol{F}_3 \frac{\mathrm{d}P_{\infty 1}}{\mathrm{d}x_{\mathrm{e1}}}(x_{\mathrm{e1}}) + \hat{F}_4 \frac{\mathrm{d}P_{\infty 2}}{\mathrm{d}x_{\mathrm{e3}}}(x_{\mathrm{e3}}) \right\}, \end{aligned} \tag{5.9}$$

[1] As mentioned in Chapter 4, the choice of the variable $\hat{\boldsymbol{\eta}}$ is not unique.

where $\hat{F}_0, \ldots, \hat{F}_4$ are positive constants determined by the parameters of the model. Thus, there exists an open set $\hat{D}_2 \subset X$ such that $\mathrm{detD}\hat{\boldsymbol{\Phi}}(\boldsymbol{x}) \neq 0$ at $\boldsymbol{x} \in \hat{D}_2$. By choosing an open set $\hat{D}$ satisfying $\hat{D} := \hat{D}_1 \cap \hat{D}_2$, the internal dynamics with respect to the outputs in Eq. (5.1) are described by

$$\dot{\boldsymbol{\eta}} = \hat{\boldsymbol{q}}(\boldsymbol{\xi}_{\mathrm{e}}, \hat{\boldsymbol{\xi}}_{\mathrm{h}}, \hat{\boldsymbol{\eta}}) := \bar{\hat{\boldsymbol{q}}}(\hat{\boldsymbol{\Phi}}^{-1}(\boldsymbol{\xi}_{\mathrm{e}}, \hat{\boldsymbol{\xi}}_{\mathrm{h}}, \hat{\boldsymbol{\eta}})), \tag{5.10}$$

where $\bar{\hat{\boldsymbol{q}}}$ is given by

$$\bar{\hat{\boldsymbol{q}}}(\cdot) = \left[f_{\mathrm{g3}}(\cdot) \quad f_{\mathrm{e1}}(\cdot) \quad f_{\mathrm{e2}}(\cdot) \quad \frac{T_{\mathrm{h1}} f_{\mathrm{h1}}(\cdot) + T_{\mathrm{h2}} f_{\mathrm{h2}}(\cdot)}{T_{\mathrm{h1}} + T_{\mathrm{h2}}} \right]^{\top}. \tag{5.11}$$

Thus, the internal dynamics with respect to the outputs in Eq. (5.1) are described by the variable $\hat{\boldsymbol{\eta}}$ in Eq. (5.3). □

Thus, the zero dynamics of the model (5.2) are derived by considering the internal dynamics (5.10) with the outputs kept to zero for all time. Strictly speaking, as in Sec. 4.3, we consider the zero dynamics with respect to the following set-point error:

$$\hat{\boldsymbol{e}}_{\mathrm{s}} := \left[y_1 - Y_1^{\mathrm{ref}},\ \hat{y}_2 - \hat{Y}_2^{\mathrm{ref}} \right]^{\top}. \tag{5.12}$$

With respect to the set-point error (5.12), the zero dynamics are described by

$$\dot{\hat{\boldsymbol{\eta}}} = \hat{\boldsymbol{q}} \left([Y_1^{\mathrm{ref}}, 0, \ldots, 0]^{\top}, [\hat{Y}_2^{\mathrm{ref}}, 0, 0, 0]^{\top}, \hat{\boldsymbol{\eta}} \right). \tag{5.13}$$

5.1.2 Analysis of non-minimum phase property

Here, we analyze the zero dynamics described by Eq. (5.13) and investigate the non-minimum phase property of the model (5.2). First, we will show that the model (5.2) is a non-minimum phase system. If the model is a minimum phase system, there should exist an equilibrium point satisfying $\hat{\boldsymbol{e}}_{\mathrm{s}} = 0$. However, it is confirmed that the values of Y_1^{ref} and $\hat{Y}_2^{\mathrm{ref}}$ can not be chosen independently with the equilibrium condition of the model (5.2), i.e. there exists an algebraic constraint between Y_1^{ref} and $\hat{Y}_2^{\mathrm{ref}}$ under the equilibrium condition. The constraint is discussed for a simple model in Sec. 1.4 as Eq. (1.5), and precisely shown in Appendix 5.A for the model (5.2). If the constraint is not satisfied, the model is a non-minimum phase system due to the nonexistence of an equilibrium point of the zero dynamics.

Even if there exists an equilibrium point satisfying $\hat{\boldsymbol{e}}_{\mathrm{s}} = 0$, the model is shown to be a non-minimum phase system. For this, we consider the following $\boldsymbol{e}_{\mathrm{s}}$ by setting Y_1^{ref} and $\hat{Y}_2^{\mathrm{ref}}$ on an equilibrium point $\boldsymbol{x}^*$:

$$\hat{\boldsymbol{e}}_{\mathrm{s}} := \left[y_1 - P_{\mathrm{e}\infty}(x^*_{\mathrm{e}1}, x^*_{\mathrm{e}3}),\ \hat{y}_2 - Q'_{12}(x^*_{\mathrm{h}3})\right]^\top. \tag{5.14}$$

The following theorem states that the model is a non-minimum phase system due to the existence of a set of non-isolated equilibrium points in the zero dynamics:

Theorem 5.2. *Consider the zero dynamics of the model (5.2) with respect to the set-point error (5.14) with an equilibrium point $\boldsymbol{x}^*$. Suppose that Lemma 5.1 holds, and that $\boldsymbol{x}^*$ exists in the open set $\hat{D}$ stated by Lemma 5.1. Then, the associated equilibrium point $\hat{\boldsymbol{\eta}}^* = (x^*_{\mathrm{g}3}, x^*_{\mathrm{e}1}, x^*_{\mathrm{e}2}, (T_{\mathrm{h}1}x^*_{\mathrm{h}1} + T_{\mathrm{h}2}x^*_{\mathrm{h}2})/(T_{\mathrm{h}1} + T_{\mathrm{h}2}))^\top$ of the zero dynamics is not isolated, implying that the model is a non-minimum phase system.*

Proof. When the model (5.2) has an equilibrium point $\boldsymbol{x}^*$ under a certain constant input $(u_1^*,\ u_2^*)$, the following point $\boldsymbol{x}$ defined as

$$\boldsymbol{x} = \left[\boldsymbol{x}_{\mathrm{g}}^{*\top},\ \boldsymbol{x}_{\mathrm{e}}^{*\top},\ \left[x^*_{\mathrm{h}1} + a,\ x^*_{\mathrm{h}2} + a,\ x^*_{\mathrm{h}3}\right]^\top\right]^\top,\ \forall a \in \mathbb{R}, \tag{5.15}$$

becomes an equilibrium point of the model under the same input. This is verified by direct calculation of Eq. (4.26) and results from the property of the inner-limit of model of the heat subsystem in Sec. 3.2.3. Thus, any equilibrium point $\boldsymbol{x}^*$ of the model is not isolated, and all the equilibrium points form a connected set $\mathcal{I}(u_1^*, u_2^*)$, defined as

$$\mathcal{I}(u_1^*, u_2^*) := \left\{ \left[\boldsymbol{x}_{\mathrm{g}}^{*\top}, \boldsymbol{x}_{\mathrm{e}}^{*\top}, \left[x^*_{\mathrm{h}1} + a, x^*_{\mathrm{h}2} + a, x^*_{\mathrm{h}3}\right]^\top\right]^\top \in X \;\middle|\; a \in \mathbb{R} \right\}. \tag{5.16}$$

The equilibrium point $\hat{\boldsymbol{\eta}}^*$ of the zero dynamics is not isolated because $h_{\mathrm{e}}(\boldsymbol{x}) = h_{\mathrm{e}}(\boldsymbol{x}^*)$ and $\hat{h}_{\mathrm{h}}(\boldsymbol{x}) = \hat{h}_{\mathrm{h}}(\boldsymbol{x}^*)$ hold at any point $\boldsymbol{x}$ in $\mathcal{I}(u_1^*, u_2^*)$. These equilibrium points also form the following set of non-isolated equilibrium points:

$$\mathcal{Z} = \left\{ \left[x^*_{\mathrm{g}3},\ x^*_{\mathrm{e}1},\ x^*_{\mathrm{e}2},\ \frac{T_{\mathrm{h}1}x^*_{\mathrm{h}1} + T_{\mathrm{h}2}x^*_{\mathrm{h}2}}{T_{\mathrm{h}1} + T_{\mathrm{h}2}} + a\right]^\top \;\middle|\; a \in \mathbb{R} \right\}. \tag{5.17}$$

The proof is thus completed. □

The above theorem suggests that the stability property of the zero dynamics described by Eq. (5.13) can be characterized by the existence of an invariant manifold similar to

the NHIM in the heat subsystem clarified in Chapter 3. Here, we provide numerical simulations of the zero dynamics to illustrate the existence of the invariant manifold. The setting of the parameters is the same as that used in Sec. 4.5 and shown in Appendix 4.C. First, we provide a numerical result of the zero dynamics described by Eq. (5.13) with a setting of Y_1^{ref} and $\hat{Y}_2^{\mathrm{ref}}$ such that there exists an equilibrium point of the zero dynamics. Figure 5.2 shows several trajectories of the zero dynamics with the following values of Y_1^{ref} and $\hat{Y}_2^{\mathrm{ref}}$:

$$Y_1^{\mathrm{ref}} = 1.0, \quad \hat{Y}_2^{\mathrm{ref}} = 1.69. \tag{5.18}$$

The initial conditions of the trajectories are listed in Tab. 5.1. Figure 5.2a shows responses of $\hat{\boldsymbol{\eta}}$. In the figure, the *red* lines show the trajectories from the initial conditions with $\hat{\eta}_2 = 0.8$, the *green* lines with $\hat{\eta}_2 = 1.0$, and the *blue* lines with $\hat{\eta}_2 = 1.2$. To illustrate the existence of the invariant manifold mentioned above, Figs. 5.2b and 5.2c provide projections of the trajectories in the full four-dimensional phase space to lower-dimensional sub-spaces. In Fig. 5.2b, the trajectories from the initial conditions of Groups A, B, and C in Tab. 5.1 are projected to the $(\hat{\eta}_1, \hat{\eta}_2, \hat{\eta}_3)$ space. It is observed that the variables $\hat{\eta}_2$ and $\hat{\eta}_3$ exhibit oscillatory responses, and the trajectories from different $\hat{\eta}_1$ converge to a two-dimensional set in the projected space. In Fig. 5.2c, the trajectories of Groups A, D, and E are projected to the $(\hat{\eta}_2, \hat{\eta}_3, \hat{\eta}_4)$ space. From Fig. 5.2c together with Figs. 5.2a and 5.2b, it is confirmed that all the trajectories converge to a set of equilibrium points that form an invariant manifold given by Eq. (5.17).

Furthermore, a similar invariant manifold can be identified when no equilibrium point exists. Figure 5.3 shows the trajectories of the zero dynamics with the following values of

Table 5.1: List of the initial conditions of the trajectories in Figs. 5.2 and 5.3

Group	Initial Condition $(\hat{\eta}_1, \hat{\eta}_2, \hat{\eta}_3, \hat{\eta}_4)$	Group	Initial Condition $(\hat{\eta}_1, \hat{\eta}_2, \hat{\eta}_3, \hat{\eta}_4)$
A	(0.1, 0.8, 0, 0)	D	(0.1, 0.8, 0, 2)
	(0.1, 1.0, 0, 0)		(0.1, 1.0, 0, 2)
	(0.1, 1.2, 0, 0)		(0.1, 1.2, 0, 2)
B	(0.7, 0.8, 0, 0)	E	(0.1, 0.8, 0, −2)
	(0.7, 1.0, 0, 0)		(0.1, 1.0, 0, −2)
	(0.7, 1.2, 0, 0)		(0.1, 1.2, 0, −2)
C	(1.4, 0.8, 0, 0)		
	(1.4, 1.0, 0, 0)		
	(1.4, 1.2, 0, 0)		

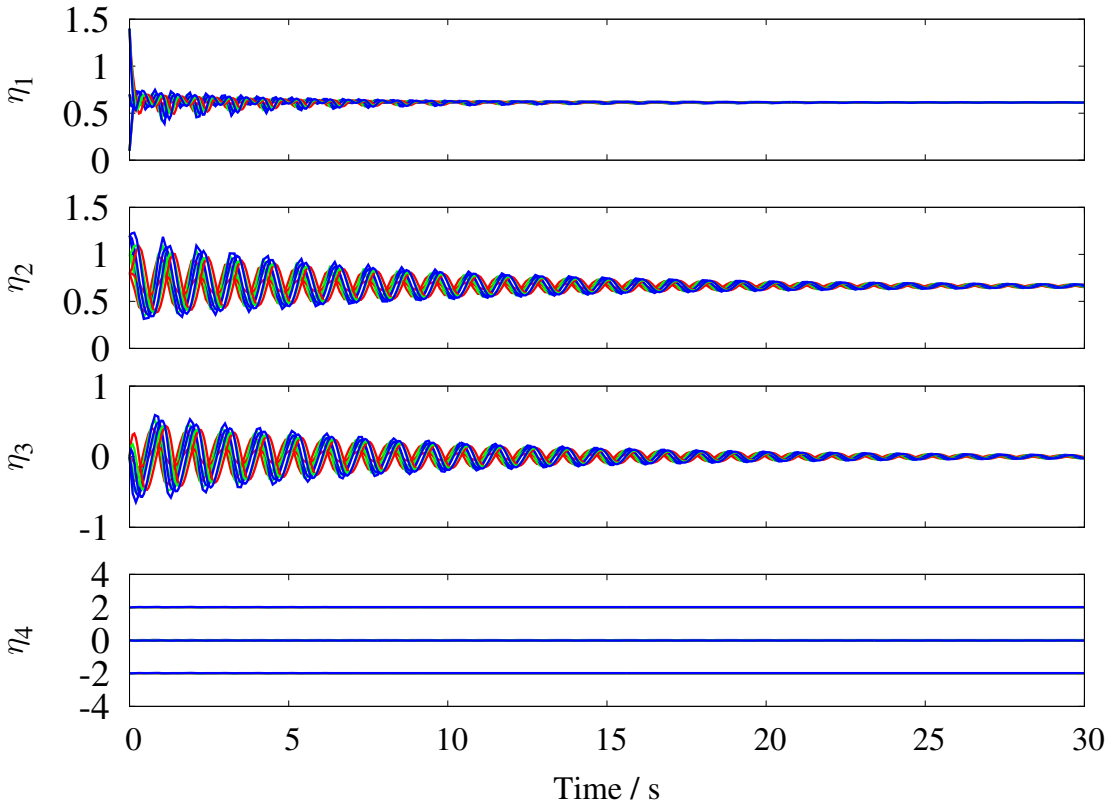

(a) Responses of the variables $\hat{\eta}_1$, $\hat{\eta}_2$, $\hat{\eta}_3$, $\hat{\eta}_4$

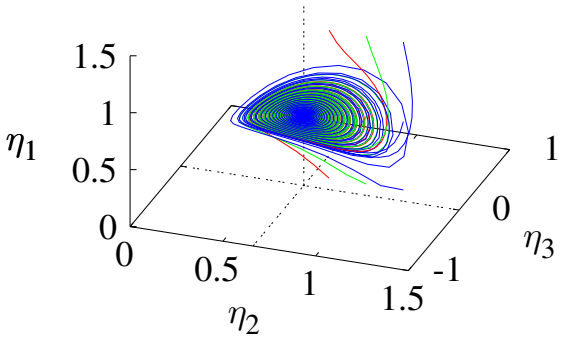

(b) Projection to $(\hat{\eta}_1, \hat{\eta}_2, \hat{\eta}_3)$ space

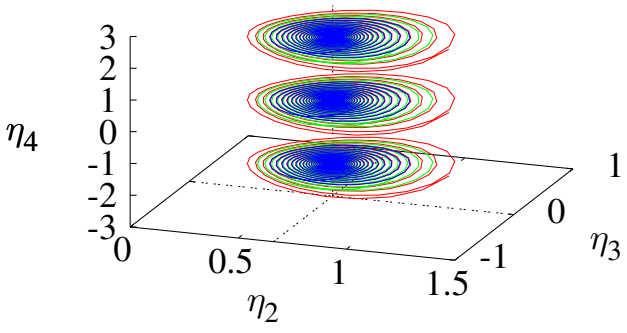

(c) Projection to $(\hat{\eta}_2, \hat{\eta}_3, \hat{\eta}_4)$ space

Figure 5.2: Trajectories of the zero dynamics described by Eq. (5.13) with a setting of Y_1^{ref} and $\hat{Y}_2^{\mathrm{ref}}$ such that there exists an equilibrium point: $Y_1^{\mathrm{ref}} = 1.0$ and $\hat{Y}_2^{\mathrm{ref}} = 1.69$.

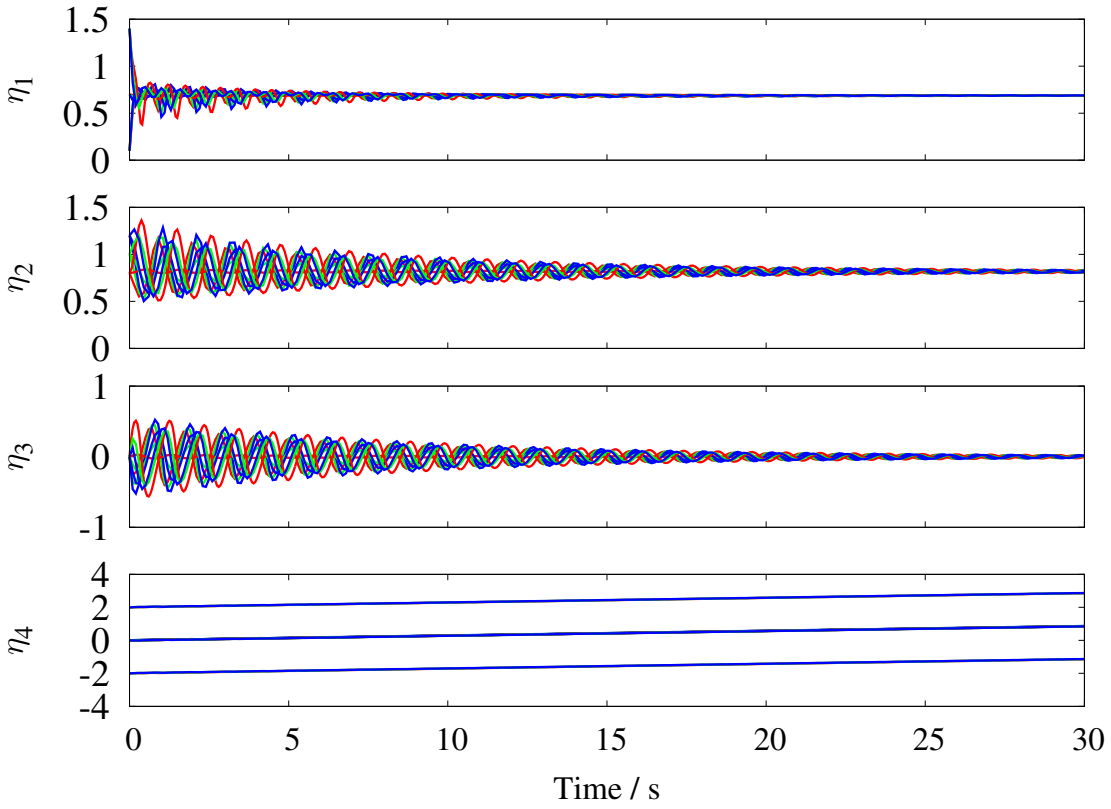

(a) Responses of the variables $\hat{\eta}_1$, $\hat{\eta}_2$, $\hat{\eta}_3$, $\hat{\eta}_4$

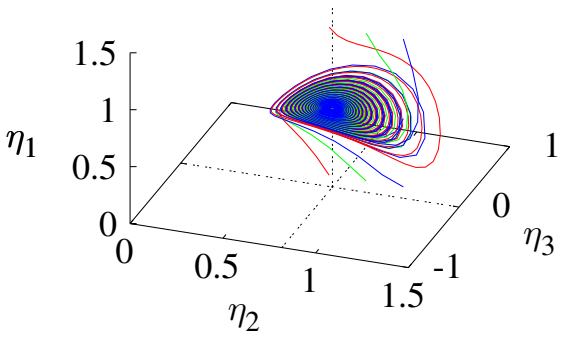

(b) Projection to ($\hat{\eta}_1$, $\hat{\eta}_2$, $\hat{\eta}_3$) space

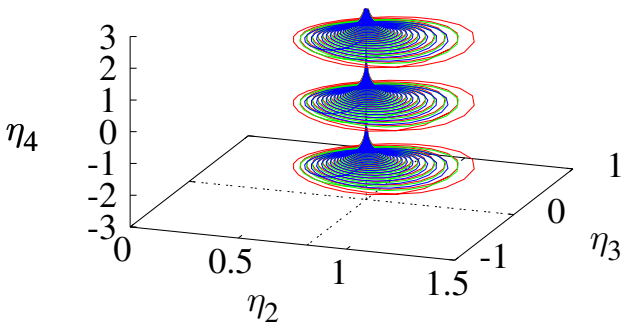

(c) Projection to ($\hat{\eta}_1$, $\hat{\eta}_2$, $\hat{\eta}_3$) space

Figure 5.3: Trajectories of the zero dynamics described by Eq. (5.13) with a setting of Y_1^{ref} and $\hat{Y}_2^{\mathrm{ref}}$ such that no equilibrium point: $Y_1^{\mathrm{ref}} = 1.2$ and $\hat{Y}_2^{\mathrm{ref}} = 1.69$.

Y_1^{ref} and $\hat{Y}_2^{\mathrm{ref}}$:

$$Y_1^{\mathrm{ref}} = 1.2, \quad \hat{Y}_2^{\mathrm{ref}} = 1.69. \tag{5.19}$$

As in Fig. 5.2, all the trajectories converge to an invariant manifold in the phase space of the zero dynamics. The invariant manifold is parallel to that in Fig. 5.2 consisting of the equilibrium points in Eq. (5.17). The value of $\hat{\eta}_4$ parametrizes the points on the invariant manifold and represent the dynamics along the manifold.

The above result clarifies the fundamental limitation for realizing the planned energy flows and resolving the energy balance in the two-site system. As mentioned before, the above two objectives are described by the output tracking control in terms of the outputs in Eq. (5.12) and the stabilizing control discussed in Chapter 4, respectively. Here, as stated in [32], if the zero dynamics of a system have no bounded solution, then it is impossible to achieve precision tracking with stability. Thus, the result of Fig. 5.3 implies that the tracking control of the energy flows is not feasible on the infinite time interval because the state variable is not bounded under the control. Furthermore, due to the above analysis, it is clarified that the boundedness of the state variable under the tracking control can be quantified by the value of $\hat{\eta}_4$ that parameterizes the dynamics along the invariant manifold parallel to the set $\mathcal{Z}$ given by Eq. (5.17).

5.2 Controller synthesis

This section synthesizes an output tracking controller for the energy flows in the two-site system. As shown in Sec. 5.1, to guarantee the boundedness of the state variable, it is required to manage the zero dynamics with respect to the outputs in Eq. (5.1). For this purpose, in this section, we utilize the outputs in Eq. (4.29) as virtual outputs:

$$y_1 = h_{\mathrm{e}}(\boldsymbol{x}) := P_{\mathrm{e}\infty}(x_{\mathrm{e}1},\, x_{\mathrm{e}3}), \tag{4.29a}$$

$$y_2 = h_{\mathrm{h}}(\boldsymbol{x}) := \frac{T_{\mathrm{h}1}x_{\mathrm{h}1} + T_{\mathrm{h}2}x_{\mathrm{h}2}}{T_{\mathrm{h}1} + T_{\mathrm{h}2}} = \hat{\eta}_4. \tag{4.29b}$$

Here, the strategy that we utilize is motivated by the so-called *output redefinition method* proposed in [40]. While various methods are proposed in e.g. [49, 14, 33] for controlling non-minimum phase systems, the above redefinition of the outputs enables us to directly manage the boundedness of the zero dynamics quantified by $\hat{\eta}_4$.

In the rest of this section, we show that the tracking of the original outputs in Eq. (5.1) is achievable by using suitable reference trajectories of the virtual outputs in Eq. (4.29).

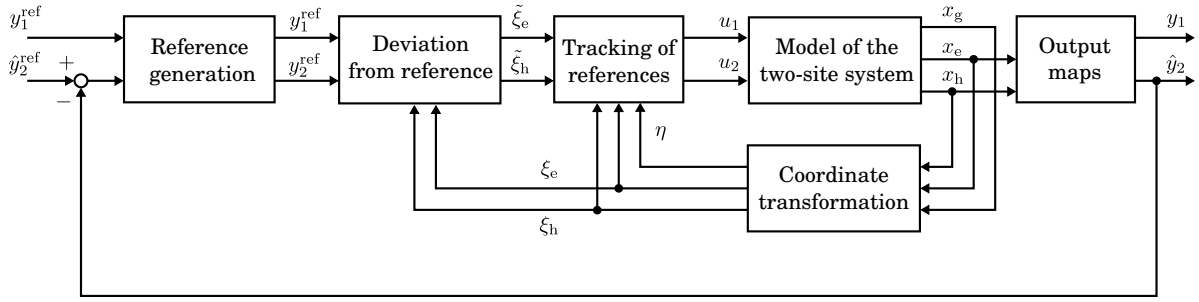

Figure 5.4: Block diagram of the controller synthesized in this section. The objective is to achieve output tracking of the outputs y_1 and $\hat{y}_2$ in Eq. (5.1) by utilizing time-varying references of the outputs y_1 and y_2 in Eq. (4.29).

Figure 5.4 shows the block diagram of the controller that will be synthesized. For given references $y_1^{\mathrm{ref}}(t)$ and $\hat{y}_2^{\mathrm{ref}}(t)$ of the outputs in Eq. (5.1), the part of reference generation calculates the reference trajectory $y_1^{\mathrm{ref}}(t)$ and $y_2^{\mathrm{ref}}(t)$ of the outputs in Eq. (4.29). For $y_1^{\mathrm{ref}}(t)$ and $y_2^{\mathrm{ref}}(t)$, a standard tracking controller as in [59, 113] is applicable:

$$\begin{bmatrix} u_1 \\ u_2 \end{bmatrix} = \mathsf{A}^{-1}(\boldsymbol{x}) \begin{bmatrix} y_1^{\mathrm{ref}(5)}(t) - L_f^5 h_1(\boldsymbol{x}) - \sum_{j=1}^{5} \alpha_{\mathrm{e}j} \tilde{\xi}_{\mathrm{e}i}(t) \\ y_2^{\mathrm{ref}(3)}(t) - L_f^3 h_2(\boldsymbol{x}) - \sum_{j=1}^{3} \alpha_{\mathrm{h}j} \tilde{\xi}_{\mathrm{h}i}(t) \end{bmatrix}, \tag{5.21}$$

where the coefficients $\alpha_{\mathrm{e}j}$ and $\alpha_{\mathrm{h}j}$ are chosen so that the polynomials $s^5 + \alpha_{\mathrm{e}5} s^4 + \cdots + \alpha_{\mathrm{e}1}$ and $s^3 + \alpha_{\mathrm{h}3} s^2 + \alpha_{\mathrm{h}2} s + \alpha_{\mathrm{h}1}$ are Hurwitz, and the error variables $\tilde{\boldsymbol{\xi}}_{\mathrm{e}}$ and $\tilde{\boldsymbol{\xi}}_{\mathrm{h}}$ are given by

$$\tilde{\boldsymbol{\xi}}_{\mathrm{e}} := \left[h_{\mathrm{e}}(x) - y_1^{\mathrm{ref}}(t),\ L_f h_{\mathrm{e}}(x) - \dot{y}_1^{\mathrm{ref}}(t),\ \ldots,\ L_f^4 h_{\mathrm{e}}(x) - y_1^{\mathrm{ref}(4)}(t) \right], \tag{5.22a}$$

$$\tilde{\boldsymbol{\xi}}_{\mathrm{h}} := \left[h_{\mathrm{h}}(x) - y_2^{\mathrm{ref}}(t),\ L_f h_{\mathrm{h}}(x) - \dot{y}_2^{\mathrm{ref}}(t),\ L_f^2 h_{\mathrm{h}}(x) - y_2^{\mathrm{ref}(2)}(t) \right]. \tag{5.22b}$$

In the following, we mainly discuss the generation of the references y_1^{ref} and y_2^{ref} to achieve the tracking control. In Sec. 5.2.1, it is shown that the control of energy flows is possible by using a ramp-wise reference in terms of the output y_2. Then, in Sec. 5.2.2, we synthesize a controller including the part of reference generation using integral control. For the controller synthesis, the structural analysis in Sec. 4.3 (particularly Lemma 4.5) as well as that in Sec. 5.1 plays a central role.

5.2.1 Control with time-varying references

First, we show that time-varying references effectively work for the control of energy flows in the two-site system. Particularly, from the result in Fig. 5.3, we consider the

following references of the outputs in Eq. (4.29):

$$y_1^{\mathrm{ref}}(t) := P_{\mathrm{e}\infty}^{\mathrm{ref}}, \tag{5.23a}$$

$$y_2^{\mathrm{ref}}(t) := p^{\mathrm{ref}} + t\Delta p^{\mathrm{ref}}. \tag{5.23b}$$

For the above references, the control law (5.21) becomes

$$\begin{bmatrix} u_1 \\ u_2 \end{bmatrix} = \mathsf{A}^{-1}(\boldsymbol{x})\cdot \begin{bmatrix} -L_f^5 h_1(\boldsymbol{x}) - \alpha_{\mathrm{e}5}\xi_{\mathrm{e}5} - \alpha_{\mathrm{e}4}\xi_{\mathrm{e}4} - \alpha_{\mathrm{e}3}\xi_{\mathrm{e}3} - \alpha_{\mathrm{e}2}\xi_{\mathrm{e}2} - \alpha_{\mathrm{e}1}(\xi_{\mathrm{e}1} - P_{\mathrm{e}\infty}^{\mathrm{ref}}) \\ -L_f^3 h_2(\boldsymbol{x}) - \alpha_{\mathrm{h}3}\xi_{\mathrm{h}3} - \alpha_{\mathrm{h}2}(\xi_{\mathrm{h}2} - \Delta p^{\mathrm{ref}}) - \alpha_{\mathrm{h}1}(\xi_{\mathrm{h}1} - p_{\mathrm{ref}} - t\Delta p^{\mathrm{ref}}) \end{bmatrix}, \tag{5.24}$$

The following theorem states that the controller (5.24) stabilizes a trajectory of the closed-loop system:

Theorem 5.3. *Consider the model (5.2) with the state-feedback control law (5.24). Suppose that for given $P_{\mathrm{e}\infty}^{\mathrm{ref}}$ and Δp^{ref}, there exist η^{ref} satisfying the following equation:*

$$\boldsymbol{q}\left([P_{\mathrm{e}\infty}^{\mathrm{ref}}, 0, \dots 0]^\top,\, [0, \Delta p^{\mathrm{ref}}, 0]^\top, \boldsymbol{\eta}^{\mathrm{ref}}\right) = 0. \tag{5.25}$$

Furthermore, suppose the point $(\boldsymbol{\xi}_{\mathrm{e}},\, \boldsymbol{\xi}_{\mathrm{h}},\, \boldsymbol{\eta}) = \left([P_{\mathrm{e}\infty}^{\mathrm{ref}}, 0, \dots 0]^\top,\, [0, \Delta p^{\mathrm{ref}}, 0]^\top, \boldsymbol{\eta}^{\mathrm{ref}}\right)$ exists in the open subset D stated in Lemma 4.4. Then, there exists a trajectory of the closed-loop system given by

$$(\boldsymbol{\xi}_{\mathrm{e}}(t),\, \boldsymbol{\xi}_{\mathrm{h}}(t),\, \boldsymbol{\eta}(t)) = \left([P_{\mathrm{e}\infty}^{\mathrm{ref}}, 0, \dots 0]^\top,\, [p^{\mathrm{ref}} + t\Delta p^{\mathrm{ref}},\, \Delta p^{\mathrm{ref}},\, 0]^\top,\, \boldsymbol{\eta}^{\mathrm{ref}}\right). \tag{5.26}$$

In addition to the existence, the trajectory is asymptotically stable if the polynomials $s^5 + \alpha_{\mathrm{e}5}s^4 + \cdots + \alpha_{\mathrm{e}1}$ and $s^3 + \alpha_{\mathrm{h}3}s^2 + \cdots + \alpha_{rmh1}$ are Hurwitz, and all of the eigenvalues of the matrix $\tilde{\mathsf{Q}}$ defined as

$$\tilde{\mathsf{Q}} := \frac{\partial \boldsymbol{q}}{\partial \boldsymbol{\eta}}\left([P_{\mathrm{e}\infty}^{\mathrm{ref}}, 0, \dots 0]^\top,\, [0, \Delta p^{\mathrm{ref}}, 0]^\top, \boldsymbol{\eta}^{\mathrm{ref}}\right) \tag{5.27}$$

has negative real parts.

Proof. By considering the system in the normal form (4.38) with the control law (5.24), the closed-loop system has the following form:

$$\dot{\tilde{\boldsymbol{\xi}}}_{\mathrm{e}} = \mathsf{A}_{\mathrm{e}}\tilde{\boldsymbol{\xi}}_{\mathrm{e}}, \tag{5.28a}$$

$$\dot{\tilde{\boldsymbol{\xi}}}_{\mathrm{h}} = \mathsf{A}_{\mathrm{h}}\tilde{\boldsymbol{\xi}}_{\mathrm{h}}, \tag{5.28b}$$

$$\dot{\boldsymbol{\eta}} = \boldsymbol{q}\left(\tilde{\boldsymbol{\xi}}_{\mathrm{e}} + [P_{\mathrm{e}\infty}^{\mathrm{ref}},\, 0, \dots,\, 0]^\top,\, \tilde{\boldsymbol{\xi}}_{\mathrm{h}} + [p^{\mathrm{ref}} + t\Delta p^{\mathrm{ref}},\, \Delta p^{\mathrm{ref}},\, 0]^\top,\, \boldsymbol{\eta}\right), \tag{5.28c}$$

with

$$\mathsf{A}_{\mathrm{e}} := \begin{bmatrix} 0 & 1 & 0 & 0 & 0 \\ 0 & 0 & 1 & 0 & 0 \\ 0 & 0 & 0 & 1 & 0 \\ 0 & 0 & 0 & 0 & 1 \\ -\alpha_{\mathrm{e}1} & -\alpha_{\mathrm{e}2} & -\alpha_{\mathrm{e}3} & -\alpha_{\mathrm{e}4} & -\alpha_{\mathrm{e}5} \end{bmatrix}, \tag{5.29a}$$

$$\mathsf{A}_{\mathrm{h}} := \begin{bmatrix} 0 & 1 & 0 \\ 0 & 0 & 1 \\ -\alpha_{\mathrm{h}1} & -\alpha_{\mathrm{h}2} & -\alpha_{\mathrm{h}3} \end{bmatrix}. \tag{5.29b}$$

Thus, Eq. (5.26) is a trajectory of the system (5.2). From Lemma 4.5, Eq. (5.28c) is rewritten as follows:

$$\dot{\boldsymbol{\eta}} = \boldsymbol{q}\left(\tilde{\boldsymbol{\xi}}_{\mathrm{e}} + [P^{\mathrm{ref}}_{\mathrm{e}\infty}, 0, \ldots, 0]^{\top}, \tilde{\boldsymbol{\xi}}_{\mathrm{h}} + [0, \Delta p^{\mathrm{ref}}, 0]^{\top}, \boldsymbol{\eta}\right). \tag{5.30}$$

Thus, $(\tilde{\boldsymbol{\xi}}_{\mathrm{e}}(t), \tilde{\boldsymbol{\xi}}_{\mathrm{h}}(t), \boldsymbol{\eta}(t)) = (0, 0, \boldsymbol{\eta}^{\mathrm{ref}})$ is an equilibrium point of the closed-loop system. The stability of the equilibrium is determined by the eigenvalues of the following matrix

$$\begin{bmatrix} \mathsf{A}_{\mathrm{e}} & 0 & 0 \\ 0 & \mathsf{A}_{\mathrm{h}} & 0 \\ * & * & \tilde{\mathsf{Q}} \end{bmatrix} \tag{5.31}$$

By assumption, the eigenvalues of $\tilde{\mathsf{Q}}$ have negative real parts, and the eigenvalues of A_{e} and A_{h} are the zeros of the Hurwitz polynomials. The proof is thus completed. □

In the above controller, the rate of the ramp-wise change Δp^{ref} should be determined suitably in order to achieve desired values of the energy flows of electricity and heat. In Sec. 5.2.2, we consider an integral control for this. Here, it should be noted that, the same controller is effective for regulating the electricity and gas flows through the two-site system: see Fig. 5.5. For this, the following physical insight can be utilized for selecting the value of Δp^{ref}: If the fuel gas supply exceeds the amount required for the heat demand, the pressures of boilers will increase, and vise versa. Thus, it is expected that the gas flows can be increased by using a reference with $\Delta p^{\mathrm{ref}} > 0$ and decreased with $\Delta p^{\mathrm{ref}} < 0$. The control of electricity and gas flows will be demonstrated in Sec. 5.3.1. For this, since the value of $\Phi_{\mathrm{ge}}(\boldsymbol{x}_{\mathrm{g}}, \boldsymbol{x}_{\mathrm{e}})$ converges under Theorem 5.3, and hence $\dot{\boldsymbol{x}}_{\mathrm{g}} = \dot{\boldsymbol{x}}_{\mathrm{e}} = 0$ holds, we have the following corollary:

Corollary 5.4. *Consider the model (5.2) with the feedback low (5.24). Suppose that for given Y_1^{ref} and Y_2^{ref}, the assumptions of Theorem 5.3 hold. Then, along the trajectory*

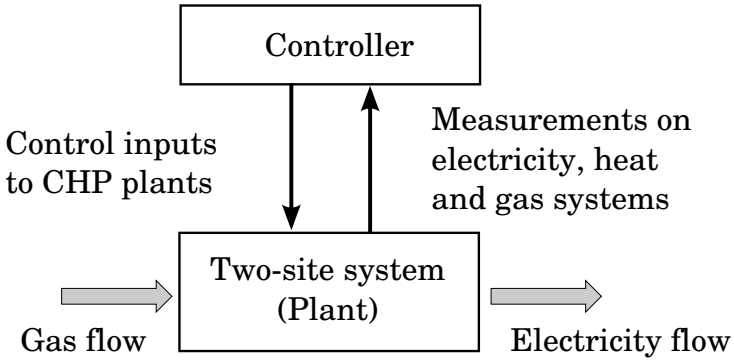

Figure 5.5: Schematic diagram of regulation of electricity and gas flows

given by Eq. (5.26), all the state variables except for $x_{\mathrm{h}1}$ *and* $x_{\mathrm{h}2}$ *become constants, and the electric power* $P_{\mathrm{e}\infty}$ *and the gas flow rate* P_{gas} *are given by*

$$P_{\mathrm{e}\infty} = P_{\mathrm{e}\infty}^{\mathrm{ref}}, \tag{5.32}$$

$$P_{\mathrm{gas}} = P_{\mathrm{m}1}^{-1}(P_{\mathrm{e}1}(x_{\mathrm{e}1}^{\mathrm{ref}}, x_{\mathrm{e}3}^{\mathrm{ref}})) + P_{\mathrm{m}2}^{-1}(P_{\mathrm{e}2}(x_{\mathrm{e}1}^{\mathrm{ref}}, x_{\mathrm{e}3}^{\mathrm{ref}})), \tag{5.33}$$

where $x_{\mathrm{e}1}^{\mathrm{ref}}$ *and* $x_{\mathrm{e}3}^{\mathrm{ref}}$ *are given for* $j = 1, 3$ *as*

$$x_{\mathrm{e}j}^{\mathrm{ref}} := \Phi_{j+6}^{\prime -1}([P_{\mathrm{e}\infty}^{\mathrm{ref}}, 0 \ldots, 0]^{\top}, [\Delta p^{\mathrm{ref}}, 0]^{\top}, [\eta_1^{\mathrm{ref}}, \eta_2^{\mathrm{ref}}, \eta_3^{\mathrm{ref}}]^{\top}). \tag{5.34}$$

5.2.2 Control with reference generation

Here, we synthesize the controller including the reference generation in Fig. 5.4. Since the ramp-wise reference of y_2 is effective for the control of energy flows, we consider the following system for the reference generation[2]:

$$\dot{\sigma}_1 = \sigma_2, \tag{5.35a}$$

$$\dot{\sigma}_2 = K(\hat{h}_{\mathrm{h}}(\boldsymbol{\eta}) - \hat{Y}_2^{\mathrm{ref}}), \tag{5.35b}$$

where K is a feedback gain, and the function $\hat{h}_{\mathrm{h}}$ stands for the heat transfer rate as given by Eq. (5.1). Here, we abuse the notation of $\hat{h}_{\mathrm{h}}$ and regard it as a function of the variable η describing the internal dynamics of the system with respect to the (redefined) outputs given by Eq. (4.29). This is consistent with the output redefinition method in [40] in that

[2]The form of Eq. (5.35) is intended as an integral control while it is rather simple compared with a standard one (see [68]) in order to facilitate the following stability analysis.

the regulated output is converted into a state trajectory of new zero dynamics. By using the system (5.35), the reference y_2^{ref} is given as

$$y_2^{\mathrm{ref}}(t) = \sigma_1(t). \tag{5.36}$$

Thus, for constant references of the outputs $y_1^{\mathrm{ref}}(t) = Y_1^{\mathrm{ref}}$ and $\hat{y}_2^{\mathrm{ref}}(t) = \hat{Y}_2^{\mathrm{ref}}$, the control law (5.21) becomes

$$\begin{bmatrix} u_1 \\ u_2 \end{bmatrix} = \mathsf{A}^{-1}(\boldsymbol{x}) \begin{bmatrix} -L_f^5 h_1(\boldsymbol{x}) \\ -L_f^3 h_2(\boldsymbol{x}) \\ \quad -\alpha_{\mathrm{e}5}\xi_{\mathrm{e}5} - \alpha_{\mathrm{e}4}\xi_{\mathrm{e}4} - \alpha_{\mathrm{e}3}\xi_{\mathrm{e}3} - \alpha_{\mathrm{e}2}\xi_{\mathrm{e}2} - \alpha_{\mathrm{e}1}(\xi_{\mathrm{e}1} - Y_1^{\mathrm{ref}}) \\ \quad -\alpha_{\mathrm{h}3}(\xi_{\mathrm{h}3} - \sigma_1) - \alpha_{\mathrm{h}2}(\xi_{\mathrm{h}2} - \sigma_2) - \alpha_{\mathrm{h}1}(\xi_{\mathrm{h}1} - K(\hat{h}_{\mathrm{h}}(\boldsymbol{\eta}) - \hat{Y}_2^{\mathrm{ref}})) \end{bmatrix}, \tag{5.37}$$

The following theorem states that the precision tracking is achieved for the constant references:

Theorem 5.5. *Consider the model (5.2) with the state-feedback control law (5.37). Suppose that for given (constant) references Y_1^{ref} and $\hat{Y}_2^{\mathrm{ref}}$, there exist a constant Δp^{ref} satisfying the assumptions in Theorem 5.3, and the following equation holds for $\boldsymbol{\eta}^{\mathrm{ref}}$ stated in Theorem 5.3:*

$$h_{\mathrm{h}}(\boldsymbol{\eta}^{\mathrm{ref}}) - \hat{Y}_2^{\mathrm{ref}} = 0. \tag{5.38}$$

Then, there exists a trajectory of the close-loop system satisfying $y_1 = Y_1^{\mathrm{ref}}$ and $\hat{y}_2 = \hat{Y}_2^{\mathrm{ref}}$ for all time. In addition to the existence, the trajectory is asymptotically stable if the polynomials $s^5 + \alpha_{\mathrm{e}5}s^4 + \cdots + \alpha_{\mathrm{e}1}$ and $s^3 + \alpha_{\mathrm{h}3}s^2 + \cdots + \alpha_{\mathrm{h}1}$ are Hurwitz, and all of the eigenvalues of the matrix given by

$$\begin{bmatrix} \tilde{\mathsf{Q}} + K\boldsymbol{B}_3\boldsymbol{C}^\top & K\boldsymbol{B}_2 \\ \boldsymbol{C}^\top & 0 \end{bmatrix} \tag{5.39}$$

have negative real parts, where $\tilde{\mathsf{Q}}$, $\boldsymbol{B}_2$, $\boldsymbol{B}_3$, $\boldsymbol{C}$ are given by

$$\tilde{\mathsf{Q}} := \frac{\partial \boldsymbol{q}}{\partial \boldsymbol{\eta}} \left([Y_1^{\mathrm{ref}}, 0, \ldots, 0]^\top, [0, \Delta p^{\mathrm{ref}}, 0]^\top, \boldsymbol{\eta}^{\mathrm{ref}} \right), \tag{5.40}$$

$$\boldsymbol{B}_2 := \frac{\partial \boldsymbol{q}}{\partial \xi_{\mathrm{h}2}} \left([Y_1^{\mathrm{ref}}, 0, \ldots, 0]^\top, [0, \Delta p^{\mathrm{ref}}, 0]^\top, \boldsymbol{\eta}^{\mathrm{ref}} \right), \tag{5.41}$$

$$\boldsymbol{B}_3 := \frac{\partial \boldsymbol{q}}{\partial \xi_{\mathrm{h}3}} \left([Y_1^{\mathrm{ref}}, 0, \ldots, 0]^\top, [0, \Delta p^{\mathrm{ref}}, 0]^\top, \boldsymbol{\eta}^{\mathrm{ref}} \right), \tag{5.42}$$

$$\boldsymbol{C} := \frac{\partial y_{\mathrm{h}}}{\partial \boldsymbol{\eta}} \left([Y_1^{\mathrm{ref}}, 0, \ldots, 0]^\top, [0, \Delta p^{\mathrm{ref}}, 0]^\top, \boldsymbol{\eta}^{\mathrm{ref}} \right)^\top. \tag{5.43}$$

Proof. The error variables $\tilde{\boldsymbol{\xi}}_{\mathrm{e}}$ and $\tilde{\boldsymbol{\xi}}_{\mathrm{h}}$ are given by

$$\tilde{\boldsymbol{\xi}}_{\mathrm{e}} := \left[\xi_{\mathrm{e}1} - y_{\mathrm{e}}^{\mathrm{ref}}(t),\, \ldots,\, \xi_{\mathrm{e}5} - y_{\mathrm{e}}^{\mathrm{ref}(4)}(t)\right]^{\top} \tag{5.44a}$$

$$\tilde{\boldsymbol{\xi}}_{\mathrm{h}} := \begin{bmatrix} \xi_{\mathrm{h}1} - \sigma_1 \\ \xi_{\mathrm{h}2} - \sigma_2 \\ \xi_{\mathrm{h}3} - K(\hat{h}_{\mathrm{h}}(\boldsymbol{\eta}) - \hat{y}_2^{\mathrm{ref}}(t)) \end{bmatrix}. \tag{5.44b}$$

For the given constant references $y_1^{\mathrm{ref}}(t) = Y_1^{\mathrm{ref}}$ and $\hat{y}_2^{\mathrm{ref}}(t) = \hat{Y}_2^{\mathrm{ref}}$, the closed-loop system is rewritten as follows:

$$\dot{\tilde{\boldsymbol{\xi}}}_{\mathrm{e}} = \mathsf{A}_{\mathrm{e}}\tilde{\boldsymbol{\xi}}_{\mathrm{e}}, \tag{5.45a}$$

$$\dot{\tilde{\boldsymbol{\xi}}}_{\mathrm{h}} = \mathsf{A}_{\mathrm{h}}\tilde{\boldsymbol{\xi}}_{\mathrm{h}}, \tag{5.45b}$$

$$\dot{\boldsymbol{\eta}} = \boldsymbol{q}\left(\tilde{\boldsymbol{\xi}}_{\mathrm{e}} + [Y_1^{\mathrm{ref}},\, 0, \ldots,\, 0]^{\top},\, \tilde{\boldsymbol{\xi}}_{\mathrm{h}} + [\sigma_1,\, \sigma_2,\, K(\hat{h}_{\mathrm{h}}(\boldsymbol{\eta}) - \hat{Y}_2^{\mathrm{ref}})]^{\top},\, \boldsymbol{\eta}\right). \tag{5.45c}$$

$$\dot{\sigma}_1 = \sigma_2, \tag{5.45d}$$

$$\dot{\sigma}_2 = K(\hat{h}_{\mathrm{h}}(\boldsymbol{\eta}) - \hat{Y}_2^{\mathrm{ref}}), \tag{5.45e}$$

From Lemma 4.5, the dynamics of σ_1 can be separated from the rest of the system because σ_1 appears only in Eq. (5.45d) and $\xi_{\mathrm{h}1}$ in Eq. (5.45c): see Fig. 5.6. Thus, we have

$$\dot{\tilde{\boldsymbol{\xi}}}_{\mathrm{e}} = \mathsf{A}_{\mathrm{e}}\tilde{\boldsymbol{\xi}}_{\mathrm{e}}, \tag{5.46a}$$

$$\dot{\tilde{\boldsymbol{\xi}}}_{\mathrm{h}} = \mathsf{A}_{\mathrm{h}}\tilde{\boldsymbol{\xi}}_{\mathrm{h}}, \tag{5.46b}$$

$$\dot{\boldsymbol{\eta}} = \boldsymbol{q}(\tilde{\boldsymbol{\xi}}_{\mathrm{e}} + [Y_{\mathrm{e}}^{\mathrm{ref}},\, 0, \ldots,\, 0]^{\top},\, \tilde{\boldsymbol{\xi}}_{\mathrm{h}} + [0,\, \sigma_2,\, K(\hat{h}_{\mathrm{h}}(\boldsymbol{\eta}) - \hat{Y}_2^{\mathrm{ref}})]^{\top},\, \boldsymbol{\eta}), \tag{5.46c}$$

$$\dot{\sigma}_2 = K(\hat{h}_{\mathrm{h}}(\boldsymbol{\eta}) - \hat{Y}_2^{\mathrm{ref}}). \tag{5.46d}$$

For the above system, the trajectory $(\sigma_2(t), \tilde{\boldsymbol{\xi}}_{\mathrm{e}}(t), \tilde{\boldsymbol{\xi}}_{\mathrm{h}}(t), \boldsymbol{\eta}(t)) = (\Delta p^{\mathrm{ref}}, 0, 0, \boldsymbol{\eta}^{\mathrm{ref}})$ is an equilibrium point of the system. The stability of the equilibrium point is determined by

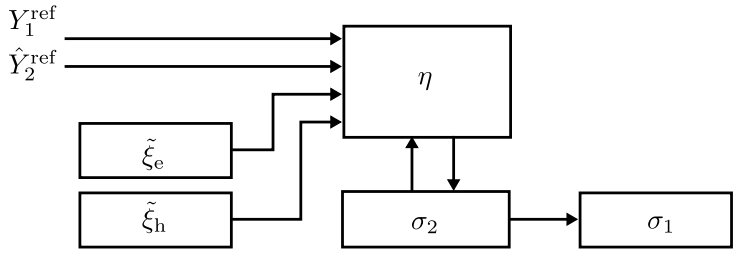

Figure 5.6: Schematic diagram of the structure of the closed-loop system

the following matrix:

$$\begin{bmatrix} \mathsf{A}_{\mathrm{e}} & 0 & 0 & 0 \\ 0 & \mathsf{A}_{\mathrm{h}} & 0 & 0 \\ * & * & \tilde{\mathsf{Q}} + K\boldsymbol{B}_3\boldsymbol{C}^\top & K\boldsymbol{B}_2 \\ * & * & \boldsymbol{C}^\top & 0 \end{bmatrix}. \tag{5.47}$$

From the assumption, all of the eigenvalues of the above matrix have negative real parts. □

5.3 Numerical simulation

This section demonstrates the effectiveness of the controllers synthesized in Sec. 5.2 under a practical setting of parameters. The setting of parameters is the same as that used in Chapter 4, and shown in Appendix 4.C. In Sec. 5.3.1, we firstly consider the controller with time-varying references derived in Sec. 5.2.1. As mentioned in the end of Sec. 5.2.1 the controller can be utilized for regulating the electricity and gas flows. Then, in Sec. 5.3.2, we consider the controller derived in Sec. 5.2.2 for regulating the electricity and heat flows.

5.3.1 Regulation of electricity and gas flows

First, we confirm the assumptions of Theorem 5.3 and demonstrate that the electricity and gas flows can be regulated by the control law (5.24). In order to verify the condition of the existence of the trajectory given by Eq. (5.26), Fig. 5.7 shows the open set D stated in Lemma 4.4. As in the case considered in Sec. 4.5, the *solid* lines show the condition $\det\mathsf{A}(\boldsymbol{x}) = 0$ and the *broken* lines $\det\mathrm{D}\boldsymbol{\Phi}(\boldsymbol{x}) = 0$. By defining the set D_{e} representing the inside of these lines containing $(x_{\mathrm{e}1},\, x_{\mathrm{e}3}) = (0,\, 0)$, the set D is given as follows:

$$D = \left\{ \left[\boldsymbol{x}_{\mathrm{g}}^\top,\, \boldsymbol{x}_{\mathrm{e}}^\top,\, \boldsymbol{x}_{\mathrm{h}}^\top\right]^\top \in X \mid (x_{\mathrm{e}1}, x_{\mathrm{e}3}) \in D_{\mathrm{e}} \right\}. \tag{5.48}$$

In the figure, the points ($\circ$) show the values of $(x_{\mathrm{e}1},\, x_{\mathrm{e}3})$ for various Δp^{ref} with $P_{\mathrm{e}\infty}^{\mathrm{ref}} = 1.0$. It is confirmed that the points exist in the open set D when $\Delta p^{\mathrm{ref}} \in [-0.068,\, 0.1]$. Thus, the trajectory given by Eq. (5.26) exists on the above interval of Δp^{ref}. For each trajectory, its stability is given by the matrix $\tilde{\mathsf{Q}}$. It is confirmed that $\tilde{\mathsf{Q}}$ has one real eigenvalue around -10, and the real parts of the other eigenvalues are shown in Fig. 5.8. As shown in the figure, if $\Delta p^{\mathrm{ref}} > 0.046$, a pair of complex conjugate eigenvalues have positive real parts. Thus, the assumptions of Theorem 5.3 is satisfied under $\Delta p^{\mathrm{ref}} \in [-0.068,\, 0.046]$.

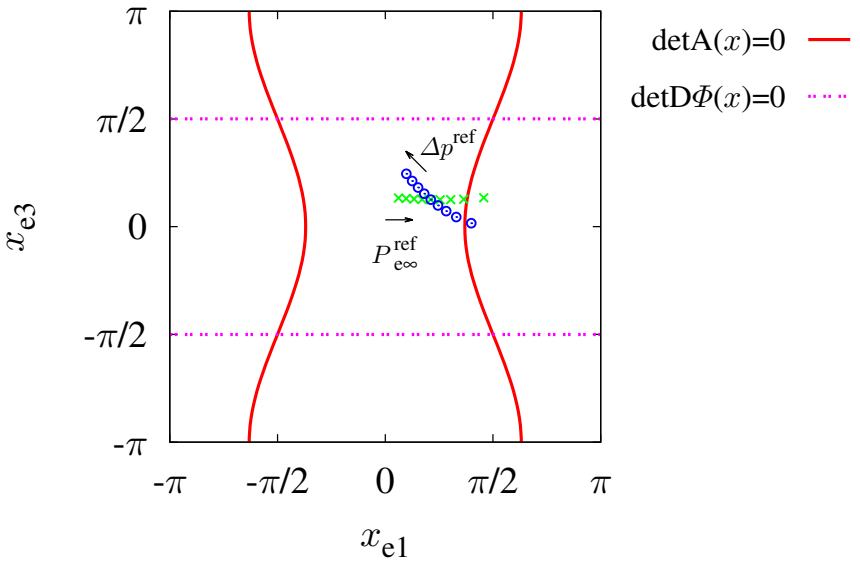

Figure 5.7: Singularity condition of $\mathsf{A}(x)$ and $\mathrm{D}\Phi(x)$

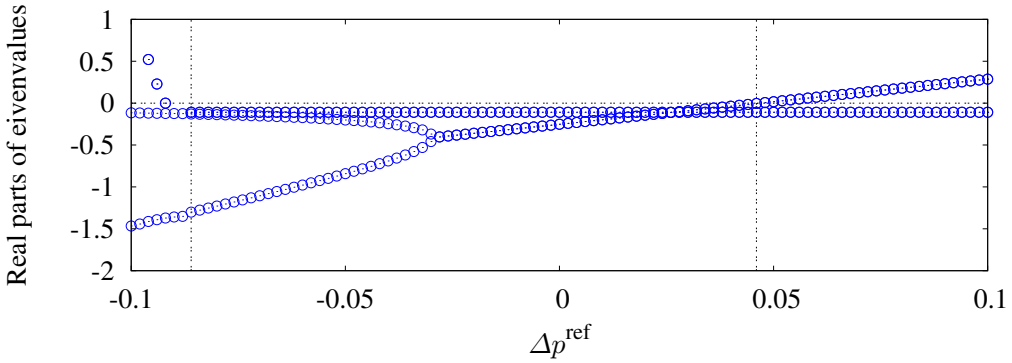

Figure 5.8: Real parts of eigenvalues of $\tilde{\mathsf{Q}}$ for various Δp^{ref}

By changing the value of Δp^{ref}, the gas flow rate P_{gas} changes as shown in Fig. 5.9. The figure shows that the gas flow rate can be change from 0.7 to 1.4. Here, to demonstrate the effectiveness of the control law (5.24), Fig. 5.10 shows the responses of the outputs y_1, y_2 and the gas flow rate P_{gas} under the following references:

$$y_1^{\mathrm{ref}}(t) = P_{\mathrm{e}\infty}^{\mathrm{ref}} = 1.0, \quad y_2^{\mathrm{ref}}(t) = p^{\mathrm{ref}} + t\Delta p^{\mathrm{ref}} = -0.02\,t. \tag{5.49}$$

The initial condition $\boldsymbol{x}(0)$ and the coefficients $\alpha_{\mathrm{e1}}, \ldots, \alpha_{\mathrm{h3}}$ of the control law (5.24) are the same as those used in Sec. 4.5. In Fig. 5.10, both the electric power y_1 and the

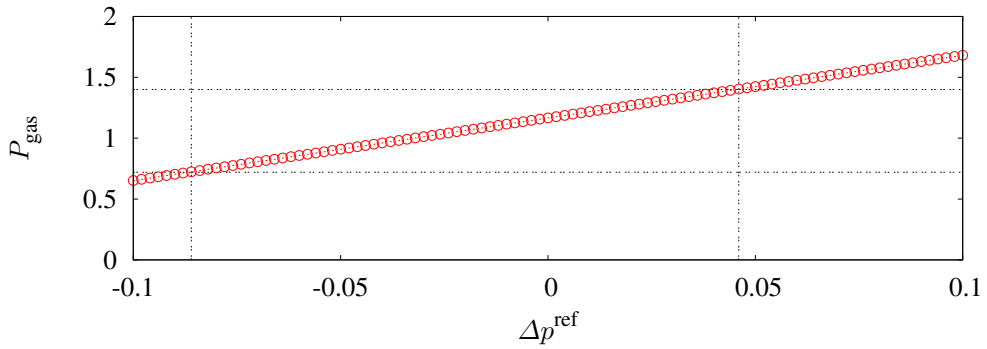

Figure 5.9: Relation between Δp^{ref} and the final value of P_{gas}

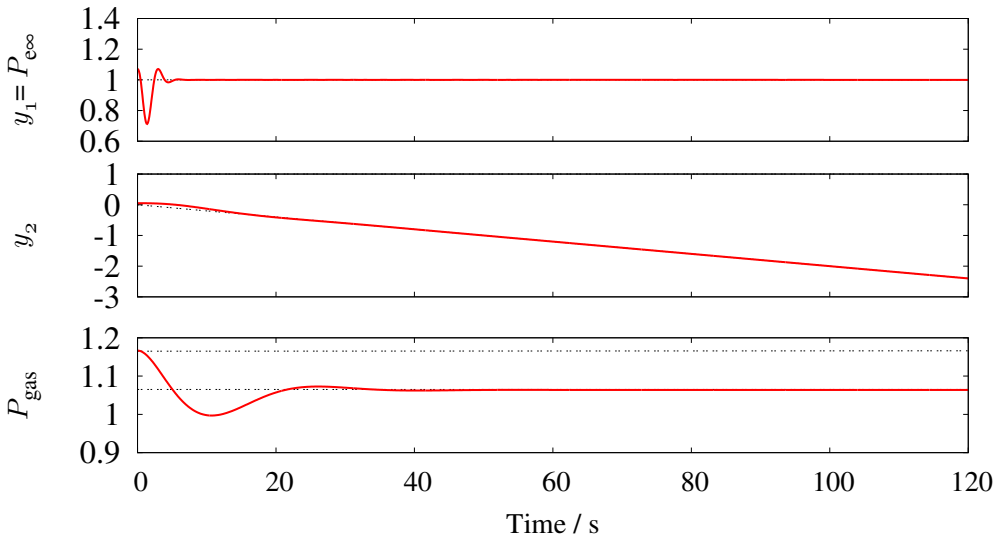

Figure 5.10: Time responses of output variables and gas flow under the control law (5.24) with $P_{\mathrm{e}\infty}^{\mathrm{ref}} = 1.0$ and $\Delta p^{\mathrm{ref}} = -0.02$. Due to the setting of ramp-wise reference of y_2, the gas flow rate P_{gas} is reduced compared to the value at the equilibrium point.

pressure y_2 track their references. As mentioned before, the relationship between Δp^{ref} in the reference y_2^{ref} and the gas flow rate P_{gas} can be understood by the following physical insight: If the fuel gas supply exceeds the amount required for the heat demand, the pressures of boilers will increase, and vise versa. Thus, it is expected that the gas flows can be increased by using a reference with $\Delta p^{\mathrm{ref}} > 0$ and decreased with $\Delta p^{\mathrm{ref}} < 0$. In the case of Fig. 5.10, $\Delta p^{\mathrm{ref}} = -0.02$, and it is observed that the gas flow rate P_{gas} is reduced compared to the value at the equilibrium point.

5.3.2 Regulation of electricity and heat flows

Finally, we consider the control law (5.37) for regulating of the electricity and heat flows. The assumptions of Theorem 5.5 can be checked as conducted in Sec. 5.3.1. Here we provide a numerical simulation of the closed-loop system. The coefficients $\alpha_{\mathrm{e}1}, \ldots, \alpha_{\mathrm{h}3}$ of the control law (5.24) are the same as before, and the initial condition $\boldsymbol{x}(0)$ is given by the equilibrium point $\boldsymbol{x}^*$ under $(P_{\mathrm{e}\infty}^{\mathrm{ref}}, p^{\mathrm{ref}}) = (1.0, 0)$. Figure 5.11 shows the responses of the outputs y_1, $\hat{y}_2$ in Eq. (5.1) and y_2 in Eq. (4.29) under the following Y_1^{ref} and $\hat{Y}_2^{\mathrm{ref}}$:

$$Y_1^{\mathrm{ref}} = 1.2, \quad \hat{Y}_2^{\mathrm{ref}} = 1.69. \tag{5.50}$$

As shown in Sec. 5.1, there exists no equilibrium point under the above references. In Fig. 5.11, it is observed that the outputs y_1, $\hat{y}_2$ track their references implying that the controller achieves the regulation of the electric power $P_{\mathrm{e}\infty}$ and heat flow rate Q'_{n}.

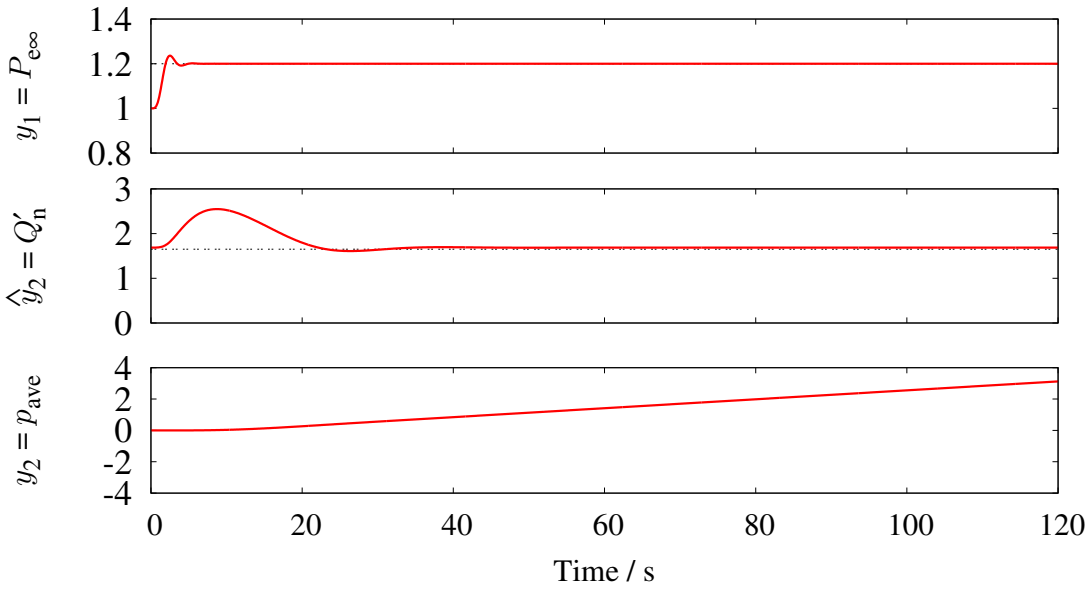

Figure 5.11: Time responses of output variables under the control law (5.37) for regulating of the electricity and heat flows. The outputs y_1, $\hat{y}_2$ track their references implying that the controller achieves the regulation of the electric power $P_{\mathrm{e}\infty}$ and heat flow rate Q'_{n}.

5.4 Summary

In this chapter, we addressed an output tracking control problem in a hierarchical management architecture of the two-site system: a high-level planner generates a signal of optimal flows of multiple types of energy, and a low-level controller tracks the signal. In the control problem, the outputs of the state-space model of the two-site system are given as the following two energy flows: the electric power to the infinite bus and the heat transfer rate between the two sites. To clarify the fundamental limitation for realizing the planned energy flows and maintaining the steady energy balance from the perspective on nonlinear control theory, we firstly conducted the structural analysis based on the input-output linearization introduced in Chapter 4. With the given outputs, it is shown that the model becomes a non-minimum phase system. The non-minimum phase property is characterized by the existence of an invariant manifold in the zero dynamics of the model and clarifies the fact that it is in general impossible to achieve the two control objectives in Chapters 4 and 5 (stabilization and tracking) simultaneously. Then, based on the structural analysis, we synthesized a tracking controller for the energy flows by utilizing a slowly time-varying reference of the outputs used in Chapter 4: the electric power to the infinite bus and the averaged pressure of the boilers. The strategy we took here can be regarded as the so-called output redefinition method for non-minimum phase systems. As a result of the output redefinition, the tracking controller in this chapter and the stabilizing controller in Chapter 4 were synthesized with the same outputs. Thus, the two control objectives can be achieved by a single control scheme without changing its structure. By managing the control scheme with a high-level planner, a hierarchical control structure can be considered to facilitate the control of multiscale dynamics in the two-site system.

Appendix 5.A Equilibrium analysis

In the hierarchical management architecture in Fig. 5.1, a high-level planner determines a set of desired energy flows y_1^{ref} and $\hat{y}_2^{\mathrm{ref}}$ as well as the fuel flows u_1^{ref} and u_2^{ref} under constraints on the energy balance. Thus, there should exists an equilibrium point $\boldsymbol{x}^*$ where the energy flows y_1^* and $\hat{y}_2^*$ are close to their planned values. However, due to the load-prediction errors, short-term load variations, and schedule changes, it is not possible to achieve the exact values of the planned energy flows. The equilibrium condition for

the model (5.2) is checked by direct calculation of Eqs. (4.18), (4.21), and (4.26). From $\dot{\boldsymbol{x}}_{\rm g} = 0$, we have

$$x^*_{\rm g3} = x^*_{\rm g2} = x^*_{\rm g1} = W_{\rm o1} + (1 - W_{\rm o1})u^*_1, \tag{5.51a}$$
$$x^*_{\rm g6} = x^*_{\rm g5} = x^*_{\rm g4} = W_{\rm o2} + (1 - W_{\rm o2})u^*_2, \tag{5.51b}$$

from $\dot{\boldsymbol{x}}_{\rm e} = 0$,

$$x^*_{\rm e1} = x^*_{\rm e3} = 0, \tag{5.52a}$$
$$P_{\rm e1}(x^*_{\rm e1},\, x^*_{\rm e3}) - P_{\rm m1}(x^*_{\rm g3}) = 0, \tag{5.52b}$$
$$P_{\rm e2}(x^*_{\rm e1},\, x^*_{\rm e3}) - P_{\rm m2}(x^*_{\rm g6}) = 0, \tag{5.52c}$$

and from $\dot{\boldsymbol{x}}_{\rm h} = 0$,

$$Q'_{\rm a1}(x^*_{\rm g3}) - Q'_{\rm L1} - Q'_{12}(x^*_{\rm h3}) = 0, \tag{5.53a}$$
$$Q'_{\rm a2}(x^*_{\rm g6}) - Q'_{\rm L2} + Q'_{12}(x^*_{\rm h3}) = 0, \tag{5.53b}$$
$$\frac{1}{\rho_{\rm s}}(x^*_{\rm h1} - x^*_{\rm h2}) - \frac{\lambda L}{2d}x^{*2}_{\rm h3} = 0, \tag{5.53c}$$

where the symbol $*$ represents the value at an equilibrium point. In order to realize a given $y^{\rm ref}_1$, the values of $x^*_{\rm e1}$ and $x^*_{\rm e3}$ should satisfy $y^{\rm ref}_1 = P_{\rm e\infty}(x^*_{\rm e1}, x^*_{\rm e3})$. Also, there should exist $x^*_{\rm g3}$ and $x^*_{\rm g6}$ satisfying Eqs. (5.52b), (5.52c), (5.53a), and (5.53b). Consequently, it is confirmed that there exists an equilibrium point $\boldsymbol{x}^*$ realizing the energy flow $y^{\rm ref}_1$ if and only if there exist $x^*_{\rm e1}$ and $x^*_{\rm e3}$ satisfying

$$y^{\rm ref}_1 - P_{\rm e\infty}(x^*_{\rm e1},\, x^*_{\rm e3}) = 0, \tag{5.54a}$$
$$Q'_{\rm a1}(P^{-1}_{\rm m1}(P_{\rm e1}(x^*_{\rm e1},\, x^*_{\rm e3}))) - Q'_{\rm L1} + Q'_2(P^{-1}_{\rm m2}(P_{\rm e2}(x^*_{\rm e1},\, x^*_{\rm e3}))) - Q'_{\rm L2} = 0. \tag{5.54b}$$

For these $x^*_{\rm e1}$ and $x^*_{\rm e3}$, the actual output $\hat{y}_2$ and inputs u_1 and u_2 are given as follows:

$$\hat{y}^*_2 = Q'_{\rm a1}(P^{-1}_{\rm m1}(P_{\rm e1}(x^*_{\rm e1},\, x^*_{\rm e3}))) - Q'_{\rm L1}, \tag{5.55}$$
$$u^*_1 = P_{\rm e1}(x^*_{\rm e1},\, x^*_{\rm e3}), \quad u^*_2 = P_{\rm e2}(x^*_{\rm e1},\, x^*_{\rm e3}). \tag{5.56}$$

Thus, the values of $\hat{y}_2$, u_1, and u_2 are in general different from their planned values $\hat{y}^{\rm ref}_2$, $u^{\rm ref}_1$, and $u^{\rm ref}_2$.

Chapter 6

Conclusions and future directions

This dissertation addressed multiscale dynamics occurring in a rudimentary model of Energy Systems Integration (ESI) [43, 100]. In this integration, multiple types of energy such as electricity, heat and natural gas are managed together to satisfy specifications of stability, reliability, and efficiency of energy supply. While electricity has been managed with the so-called scale separation of power system dynamics [114, 84], no dynamical principle has been discussed and understood in literature for managing multiple types of energy. This dissertation took a bottom-up approach to the problem and focused on multiscale dynamics occurring in regional electricity and heat supply systems. We introduced a rudimentary two-site system to discuss the dynamic interaction between electromechanical and thermodynamic phenomena appearing due to fast operations of CHP plants proposed in e.g. [118, 41, 135]. Based on this, we conducted analysis and control of multiscale dynamics of simultaneous supply of electricity and heat. This chapter summarizes the results of this dissertation and discusses future directions.

6.1 Conclusions

This dissertation addressed multiscale dynamics occurring in a rudimentary two-site system, which was introduced in Chapter 1 based on a brief technical review of regional electricity and heat supply systems. The two-site system comprises two CHP plants connected to a commercial power grid (modeled as an infinite bus) through a transmission network and interconnected by a pipeline of steam or hot water. For the purpose of analysis and control, two subsystems were defined based on their physical characteristics: the electric subsystem and the heat subsystem.

In Chapter 2, we revisited the conventional scale separation of power system dynamics through stability analysis of the electric subsystem unidirectionally affected by the heat subsystem. The classical swing equation model [77, 114, 84] was generalized by modifying the description of the mechanical power transmitted to the generators in the electric subsystem. Based on the derived model, the conventional methods of stability analysis such as energy function method [24] are applicable for evaluating the effect of the heat subsystem if the dynamics of the heat subsystem are negligible due to scale separation. If this is not the case, the dynamic interaction between the two subsystems needs to be taken into account. In this direction, we analyzed the basins of attraction [124, 125, 47] of equilibrium points representing steady operating conditions of the generators in the electric subsystem. The analysis suggests that the generators in the electric subsystem are possibly destabilized due to transient dynamics of the heat subsystem.

Chapter 3 studied a problem of mathematical modeling for dynamics occurring in general steam supply networks, in which multiple boilers (including the heat recovery boiler within a CHP plant) were connected via a steam pipe network. The dynamics of interest were originally described by a distributed-parameter model for fast steam flows over a pipe network coupled with a lumped-parameter model for slow internal dynamics of boilers. In this chapter, through physically relevant approximations, we derived a simple lumped-parameter model representing the system-wide dynamics of interest. The correctness of the derived model was verified by theoretical and numerical analyses in terms of multi-scale property of steam supply. Specifically, we discussed structural stability of the model based on the concept of Normally Hyperbolic Invariant Manifold (NHIM) [129, 97, 76]. The existence of the NHIM suggests a separation principle for steam supply systems, which is analogue to that for electric power systems.

In Chapters 4 and 5, we synthesized control systems with a state-space model of the two-site system. Two basic control objectives were considered for regional energy supply. One is to maintain the steady energy balance between demand and supply for providing reliable services of energy supply. The other is to regulate energy flows in the system for achieving temporal energy supply, which is driven by market and energy-efficiency policies. For both the objectives, we performed structural analyses of the state-space model based on geometric nonlinear control theory [59, 113, 68]. The existence of the NHIM in Chapter 3 played an essential role in the structural analyses.

Chapter 4 synthesized a state-feedback controller for maintaining the energy balance.

The controller determines the signals of fuel inputs to the CHP plants to render an equilibrium point of the state-space model asymptotically (exponentially) stable. The structural analysis and controller synthesis were conducted with the method of input-output linearization [59, 113]. The state-space model becomes a minimum phase system when the outputs are given as the electric power flow interchanged with the infinite bus and the averaged pressure level, which parameterizes the slow dynamics along the NHIM. Thus, a standard stabilizing controller can be obtained based on the input-output linearization.

Chapter 5 addressed an output tracking control problem for the energy flows in the two-site system. When the outputs are given as the energy flows, the model becomes a non-minimum phase system. The non-minimum phase property was characterized by the existence of an invariant manifold in the zero dynamics of the model associated with the NHIM in Chapter 3. Then, based on the structural analysis, we synthesized a tracking controller for the energy flows by redefining the outputs and utilizing a slowly time-varying reference of the outputs used in Chapter 4. As a result, the different control objectives in Chapters 4 and 5 are achieved by a single control scheme without changing its structure. By managing this control scheme with a high-level planner, a hierarchical management architecture can be considered for shaping the multiscale dynamics in the two-site system.

6.2 Future directions

The ideas and implications presented in this dissertation are not restricted to the particular example of the two-site system. This section summarizes several future directions.

The first direction is to apply the ideas to other types of integrated energy systems. For example, the current analysis in Chapter 3 is restricted to steam supply systems. As mentioned there, the scale separation characterized by the NHIM is analog to the concept of COI (Center of Inertia) [77] in the field of power system engineering. Also, it would be expected that similar results are obtained for other types energy systems because the lumped-parameter model derived in Chapter 3 is similar to those proposed in [104, 103] for hot-water supply systems and in [137, 138] for natural gas infrastructures. This direction is important for the purpose of analyzing stability and reliability of energy systems in the context of ESI. As mentioned in Sec. 1.2, several approaches have been proposed for the analysis. Particularly, topological (graph theoretic) methods [96] have been extensively

applied. Although several studies [34, 91] successfully identified relationships between the physical characteristics of energy systems and topological properties, it is stated in e.g. [35, 51] that the value of topological models is not well-established, and the approach does not always capture the mechanisms of relevant behavior of the system. Here, in this dissertation, we derived a reduced-order model that explicitly contains the graph theoretic property of the system as well as multiscale property of the dynamics based on the concept of normally hyperbolic invariant manifold (NHIM). Thus, it is expected to clarify the relationship between topological and physical properties of energy systems under ESI based on the concept of NHIM.

The second direction is to propose a hierarchical management architecture for ESI. As mentioned in Chapters 4 and 5, for the next-generation energy systems, it is expected for a controller to achieve several different objectives[1]. Thus, in the architecture, a high-level planner selects the control objective of a low-level controller. Here, with the approach taken in this dissertation, there exists an NHIM associated with each control objective. For switching control objectives, the operating condition of the controlled system needs to be changed from the vicinity of a NHIM to another. Since the stability property of an NHIM describes local behavior near the manifold, an instability phenomenon as demonstrated in Chapter 2 possibly occurs due to the switching. It is thus important to explore the dynamics distant from the NHIM clarified in this dissertation[2]. Furthermore, it is suggested that the normal state[3] of a current energy system is maintained by the underlying scale-separation principle. Thus, exploring the dynamics is also important to understand instabilities leading to the emergency state. Indeed, in [119, 120], a collective instability phenomenon of synchronous generators is reported based on the coupled oscillator model with no scale separation in [89, 122]. Also, for steam supply (hydraulic) networks, the lumped-parameter modeling and the scale separation in Chapter 3 are no longer valid when fast pressure transients occur due to steam (water) hammer [44]. For reliable services of energy supply, it is expected to propose a hierarchical management architecture with taking these phenomena into account.

[1] For a "device-level" controller, this is a common idea. For example, in the field of process control, several selective control are normally considered by e.g. override control and auctioneering control [48].

[2] In general, it is well-known that dynamics distant from a NHIM induce rich variety of phenomena such as relaxation oscillations [76], mixed-mode oscillations [76], and self-replicating and self-similar spatio-temporal patterns [97].

[3] Here, by the term *normal state*, we intend the operating states [77] utilized in the field of power system engineering [77]. In the field, *normal, alert, emergency, in extremis, and restorative states* are defined for the purpose of analyzing power system security and designing appropriate control systems.

Bibliography

[1] R. Abraham, J. E. Marsden, and T. Ratiu, *Manifolds, Tensor Analysis, and Applications*, 2nd edition (Splinger-Verlog, 1988).

[2] ACEJ, Shibaura district heating and cooling center, A.C.E.J. NEWS, **3**(5), 13–18 (2013). [Online]. Available: `http://www.ace.or.jp/web/introductory/images/20130613081840_2.pdf`. [Accessed: 13-Jan-2017].

[3] N. Alamoodi and P. Daoutidis, Nonlinear decoupling control with deadtime compensation for multirange operation of steam power plants, *IEEE Transactions on Control Systems Technology*, **24**(1), 341–348 (2016).

[4] F. Alobaid, R. Postler, J. Ströhle, B. Epple, and H.-G. Kim, Modeling and investigation start-up procedures of a combined cycle power plant, *Applied Energy*, **85**(12), 1173–1189 (2008).

[5] S. An, Q. Li, and T. W. Gedra, Natural gas and electricity optimal power flow, In *Proc. the 2013 IEEE PES Transmission and Distribution Conference and Exposition*, pp. 138–143, 2003.

[6] G. Andersson, *Dynamics and Control of Electric Power Systems*, Lecture note 227-0528-00, ITET ETH, 2012.

[7] M. Andreasson, R. Wiget, D. V. Dimarogonas, K. H. Johansson, and G. Andersson, Distributed secondary frequency control through MTDC transmission systems, In *Proc. the 54th IEEE Conference on Decision and Control*, pp. 2627–2634, 2015.

[8] A. Arapostathis, S. Sastry, and P. Varaiya, Analysis of power-flow equation, *International Journal of Electrical Power & Energy Systems*, **3**(3), 115–126 (1981).

[9] A. Arapostathis and P. Varaiya, Behaviour of three-node power networks, *International Journal of Electrical Power & Energy Systems*, **5**(1), 22–30 (1983).

[10] A. Arapostathis, S. Sastry, and P. Varaiya, Global analysis of swing dynamics, *IEEE Transactions on Circuits and Systems*, **29**(10), 673–679 (1982).

[11] M. Arnold, R. R. Negenborn, G. Andersson, and B. D. Schutter, Model-based predictive control applied to multi-carrier energy systems, In *Proc. IEEE Power Energy Society General Meeting*, pp. 1–8, 2009.

[12] K. J. Åström and R. D. Bell, Drum-boiler dynamics, *Automatica*, **36**(3), 363–378 (2000).

[13] B. Avramovic, P. V. Kokotovic, J. R. Winkelman, and J. H. Chow, Area decomposition for electromechanical models of power systems, *Automatica*, **16**(6), 637–648 (1980).

[14] L. Benvenuti, M. D. di Benedetto, and J. W. Grizzle, Approximate output tracking for nonlinear non-minimum phase systems with an application to flight control, *International Journal of Robust and Nonlinear Control*, **4**(3), 397–414 (1994).

[15] T. Bergman, A. Lavine, F. Incropera, and D. Dewitt, *Fundamentals of Heat and Mass Transfer*, 7th edition (John Wiley & Sons, 2011).

[16] R. K. Brayton and J. K. Moser, A theory of nonlinear networks–i, *Quarterly of Applied Mathematics*, **22**(1), 1–33 (1964).

[17] N. G. Bretas and L. F. C. Alberto, Lyapunov function for power systems with transfer conductances: extension of the invariance principle, *IEEE Transactions on Power Systems*, **18**(2), 769–777 (2003).

[18] J. Bujak, Optimal control of energy losses in multi-boiler steam systems, *Energy*, **34**(9), 1260–1270 (2009).

[19] S. V. Buldyrev, R. Parshani, G. Paul, H. E. Stanley, and S. Havlin, Catastrophic cascade of failures in interdependent networks, *Nature*, **464**(7291), 1025–1028 (2010).

[20] A. Chakrabortty and M. D. Ilić, editors, *Control and Optimization Methods for Electric Smart Grids* (Springer-Verlog, 2012).

[21] M. Chaudry, N. Jenkins, and G. Strbac, Multi-time period combined gas and electricity network optimisation, *Electric Power Systems Research*, **78**(7), 1265–1279 (2008).

[22] H.-D. Chiang, Study of the existence of energy functions for power systems with losses, *IEEE Transactions on Circuits and Systems*, **36**(11), 1423–1429 (1989).

[23] H.-D. Chiang, *Direct Methods for Stability Analysis of Electric Power Systems: Theoretical Foundation, BCU Methodologies, and Applications* (John Wiley & Sons, 2010).

[24] H.-D. Chiang, F. Wu, and P. Varaiya, Foundation of direct methods for power system transient stability analysis, *IEEE Transactions on Circuits and Systems*, **34**(2), 160–173 (1987).

[25] G. Chicco and P. Mancarella, Distributed multi-generation: A comprehensive view, *Renewable and Sustainable Energy Reviews*, **13**(3), 535–551 (2009).

[26] J. H. Chow, editor, *Time-Scale Modeling of Dynamic Networks with Applications to Power Systems* (Springer-Verlog, 1982).

[27] J. H. Chow, editor, *Power System Coherency and Model Reduction* (Springer-Verlog, 2013).

[28] CHPA, *Integrated Energy: The Role of CHP and District Heating in Our Energy Future*, 2010, [Online]. Available: `http://www.theade.co.uk/integrated-energy_199.html`. [Accessed: 13-Jan-2017].

[29] K. J. Chua, S. K. Chou, and W. M. Yang, Advances in heat pump systems: A review, *Applied Energy*, **87**(12), 3611–3624 (2010).

[30] COMSOL, Comsol multiphysics, Avaiable: `http://www.comsol.com/`. [Accessed: 10-Feb-2017].

[31] F. P. de Mello and D. Ahner, Dynamic models for combined cycle plants in power system studies, *IEEE Transactions on Power Systems*, **9**(3), 1698–1708 (1994).

[32] S. Devasia, Approximated stable inversion for nonlinear systems with nonhyperbolic internal dynamics, *IEEE Transactions on Automatic Control*, **44**(7), 1419–1425 (1999).

[33] S. Devasia, D. Chen, and B. Paden, Nonlinear inversion-based output tracking, *IEEE Transactions on Automatic Control*, **41**(7), 930–942 (1996).

[34] I. Dobson, B. A. Carreras, V. E. Lynch, and D. E. Newman, Complex systems analysis of series of blackouts: Cascading failure, critical points, and self-organization, *Chaos: An Interdisciplinary Journal of Nonlinear Science*, **17**(2), 026103 (2007).

[35] I. Eusgeld, W. Kröger, G. Sansavini, M. Schläfer, and E. Zio, The role of network theory and object-oriented modeling within a framework for the vulnerability analysis of critical infrastructures, *Reliability Engineering & System Safety*, **94**(5), 954–963 (2009).

[36] H. Farhangi, The path of the smart grid, *IEEE Power & Energy Magazine*, **8**(1), 18–28 (2010).

[37] E. Felaco and I. Gasser, Modelling, asymptotic analysis and simulation of the gas dynamics in a chimney, *Journal of Mathematics in Industry*, **3**, 1–20 (2013).

[38] N. Fenichel, Persistence and smoothness of invariant manifolds for flows, *Indiana University Mathematics Journal*, **21**(3), 193–226 (1971).

[39] N. Fenichel, Geometric singular perturbation theory for ordinary differential equations, *Journal of Differential Equations*, **31**(1), 53–98 (1979).

[40] L. Fiorentini and A. Serrani, Adaptive restricted trajectory tracking for a non-minimum phase hypersonic vehicle model, *Automatica*, **48**(7), 1248–1261 (2012).

[41] M. D. Galus, S. Koch, and G. Andersson, Provision of load frequency control by phevs, controllable loads, and a cogeneration unit, *IEEE Transactions on Industrial Electronics*, **58**(10), 4568–4582 (2011).

[42] M. Geidl and G. Andersson, Optimal power flow of multiple energy carriers, *IEEE Transactions on Power Systems*, **22**(1), 145–155 (2007).

[43] M. Geidl, G. Koeppel, P. Favre-Perrod, B. Klöckl, G. Andersson, and K. Fröhlich, Energy hubs for the future, *IEEE Power & Energy Magazine*, **5**(1), 24–30 (2007).

[44] M. S. Ghidaoui, M. Zhao, D. A. Mclnnis, and D. H. Axworthy, A review of water hammer: Theory and practice, *Applied Mechanics Reviews*, **58**(1), 49–76 (2005).

[45] H.-M. Groscurth, T. Bruckner, and R. Kümmel, Modeling of energy-services supply systems, *Energy*, **20**(9), 941–958 (1995).

[46] S. Hara, Glocal control viewpoint for integrated energy system, In *the 52nd IEEE Conference on Decision and Control Workshop*, 2013.

[47] Y. Hasegawa and Y. Ueda, Global basin structure of attraction of two degrees of freedom swing equation system, *International Journal of Bifurcation and Chaos*, **9**(8), 1549–1569 (1999).

[48] I. Hashimoto, S. Hasebe, and M. Kano, *Process Control Engineering* (Asakura Shoten, 2002) (in Japanese).

[49] J. Hauser, S. Sastry, and G. Meyer, Nonlinear control design for slightly non-minimum phase systems: Application to V/STOL aircraft, *Automatica*, **28**(4), 665–679 (1992).

[50] A. Helseth and A. T. Holen, Structural vulnerability of energy distribution systems: Incorporating infrastructural dependencies, *International Journal of Electrical Power & Energy Systems*, **31**(9), 531–537 (2009).

[51] P. Hines, E. Cotilla-Sanchez, and S. Blumsack, Do topological models provide good information about electricity infrastructure vulnerability?, *Chaos: An Interdisciplinary Journal of Nonlinear Science*, **20**(3), 033122 (2010).

[52] M. W. Hirsch, C. C. Pugh, and M. Shub, Invariant manifolds, *Bulletin of the American Mathematical Society*, **76**(5), 1015–1019 (1970).

[53] M. Holmgren, Xsteam for matlab, [Online]. Available: `http://www.x-eng.com`. [Accessed: 11-Jan-2014].

[54] C. S. Hsu, *Cell-to-Cell Mapping: A Method of Global Analysis for Nonlinear Systems* (Splinger-Verlog, 1987).

[55] J. Huang, *Nonlinear Output Regulation* (Society for Industrial and Applied Mathematics, 2004).

[56] IEA, *Co-generation and Renewables: Solutions for a Low-carbon Energy Future*, 2011, [Online]. Available: `http://www.iea.org/publications/freepublications/publication/` [Accessed: 13-Jan-2017].

[57] M. D. Ilić and Q. Liu, Toward sensing, communications and control architectures for frequency regulation in systems with highly variable resources, In A. Chakrabortty and M. D. Ilić, editors, *Control and Optimization Methods for Electric Smart Grids* (Springer-Verlog, 2012).

[58] M. Iri, *Network Flow, Transportation and Scheduling: Theory and Algorithms* (Academic Press, 1969).

[59] A. Isidori, *Nonlinear Control Systems*, 3rd edition (Springer-Verlag, 1995).

[60] K. Ito, R. Yokoyama, and T. Shiba, Optimal operation of a diesel engine cogeneration plant including a heat storage tank, *Journal of Engineering for Gas Turbines and Power*, **114**(4), 687–694 (1992).

[61] J. Johansson, H. Hassel, and E. Zio, Reliability and vulnerability analyses of critical infrastructures: Comparing two approaches in the context of power systems, *Reliability Engineering & System Safety*, **120**, 27–38 (2013).

[62] J. Johansson and H. Hassel, An approach for modelling interdependent infrastructures in the context of vulnerability analysis, *Reliability Engineering & System Safety*, **95**(12), 1335–1344 (2010).

[63] JSME, *Hydraulic Losses in Pipes and Ducts* (Maruzen, 1979) (in Japanese).

[64] N. Kakimoto and K. Baba, Performance of gas turbine-based plants during frequency drops, *IEEE Transactions on Power Systems*, **18**(3), 1110–1115 (2003).

[65] K. Kavvadias, A. Tosios, and Z. Maroulis, Design of a combined heating, cooling and power system: Sizing, operation strategy selection and parametric analysis, *Energy Conversion and Management*, **51**(4), 833–845 (2010).

[66] J. K. Kevorkian and J. D. Cole, *Multiple Scale and Singular Perturbation Methods* (Springer-Verlag, 1996).

[67] M. Kezunovic, S. Meliopoulos, V. Venkatasubramanian, and V. Vittal, *Application of Time-Synchronized Measurements in Power System Transmission Networks* (Springer-Verlog, 2014).

[68] H. K. Khalil, *Nonlinear Systems*, 3rd edition (Prentice Hall, 2002).

[69] T. S. Kim, D. K. Lee, and S. T. Ro, Dynamic behavior analysis of a heat recovery steam generator during start-up, *International Journal of Energy Research*, **24**(2), 137–149 (2000).

[70] D. Kirschen and G. Strbac, *Fundamentals of Power System Economics* (John Wiley & Sons, 2004).

[71] Y. Kitapbayev, J. Moriarty, and P. Mancarella, Stochastic control and real options valuation of thermal storage-enabled demand response from flexible district energy systems, *Applied Energy*, **137**, 823–831 (2015).

[72] P. Kokotović, H. K. Khalil, and J. O'Reilly, *Singular Perturbation Methods in Control: Analysis and Design* (Society for Industrial and Applied Mathematics, 1999).

[73] P. V. Kokotovic, Subsystems, time scales and multimodeling, *Automatica*, **17**(6), 789–795 (1981).

[74] T. J. Koo, F. Hoffmann, H. Shim, B. Sinopoli, and S. Sastry, Hybrid control of an autonomous helicopter, In *Proc. IFAC Workshop on Motion Control*, pp. 285–290, 1998.

[75] T. J. Koo and S. Sastry, Output tracking control design of a helicopter model based on approximate linearization, In *Proc. the 37th IEEE Conference on Decision and Control*, volume 4, pp. 3635–3640, 1998.

[76] C. Kuehn, *Multiple Time Scale Dynamics* (Springer International Publishing, 2015).

[77] P. Kundur, *Power System Stability and Control* (McGraw-Hill, New York, 1994).

[78] L. D. Landau and E. M. Lifshitz, *Fluid Mechanics* (Pergamon, 1959).

[79] G. K. H. Larsen, N. D. van Foreest, and J. M. A. Scherpen, Distributed mpc applied to a network of households with micro-chp and heat storage, *IEEE Transactions on Smart Grid*, **5**(4), 2106–2114 (2014).

[80] C. Liu, M. Shahidehpour, and J. Wang, Coordinated scheduling of electricity and natural gas infrastructures with a transient model for natural gas flow, *Chaos: An Interdisciplinary Journal of Nonlinear Science*, **21**(2), 025102 (2011).

[81] Q. Liu, Z. Zhang, J. Pan, and J. Guo, A coupled thermo-hydraulic model for steam flow in pipe networks, *Journal of Hydrodynamics, Ser. B*, **21**(6), 861–866 (2009).

[82] X. Liu, J. Wu, N. Jenkins, and A. Bagdanavicius, Combined analysis of electricity and heat networks, *Applied Energy*, **162**, 1238–1250 (2016).

[83] H. Lund, A. N. Andersen, P. A. Østergaard, B. V. Mathiesen, and D. Connolly, From electricity smart grids to smart energy systems: A market operation based approach and understanding, *Energy*, **42**(1), 96–102 (2012).

[84] J. Machowski, J. W. Bialek, and J. R. Bumby, *Power System Dynamics: Stability and Control*, 2nd edition (John Wiley & Sons, 2008).

[85] P. Mancarella and G. Chicco, Real-time demand response from energy shifting in distributed multi-generation, *IEEE Transactions on Smart Grid*, **4**(4), 1928–1938 (2013).

[86] P. Mancarella, Cogeneration systems with electric heat pumps: Energy-shifting properties and equivalent plant modelling, *Energy Conversion and Management*, **50**(8), 1991–1999 (2009).

[87] P. Mancarella, MES (multi-energy systems): An overview of concepts and evaluation models, *Energy*, **65**, 1–17 (2014).

[88] D. R. Merkin, *Introduction to the Theory of Stability* (Springer-Verlag, 1997).

[89] I. Mezić, On the dynamics of molecular conformation, *Proceedings of the National Academy of Sciences*, **103**(20), 7542–7547 (2006).

[90] M. S. Morais and J. W. M. Lima, Natural gas network pricing and its influence on electricity and gas markets, In *Proc. the 2003 IEEE Bologna Power Tech Conference*, volume 3, 2003.

[91] A. E. Motter, S. A. Myers, M. Anghel, and T. Nishikawa, Spontaneous synchrony in power-grid networks, *Nature Physics*, **9**, 191–197 (2013).

[92] S. Mueller, R. Tuth, D. Fischer, B. Wille-Haussmann, and C. Wittwer, Balancing fluctuating renewable energy generation using cogeneration and heat pump systems, *Energy Technology*, **2**(1), 83–89 (2014).

[93] B. Müller, Low-mach-number asymptotics of the navier-stokes equations, *Journal of Engineering Mathematics*, **34**(1), 97–109 (1998).

[94] J. Munoz, N. Jimenez-Redondo, J. Perez-Ruiz, and J. Barquin, Natural gas network modeling for power systems reliability studies, In *Proc. the 2003 IEEE Bologna Power Tech Conference*, volume 4, 2003.

[95] M. Münster, P. E. Morthorst, H. V. Larsen, L. Bregnbæk, J. Werling, H. H. Lindboe, and H. Ravn, The role of district heating in the future danish energy system, *Energy*, **48**(1), 47–55 (2012).

[96] M. E. J. Newman, The structure and function of complex networks, *SIAM Review*, **45**(2), 167–256 (2003).

[97] Y. Nishiura, *Far-from-Equilibrium Dyanamics* (American Mathematical Society, 2002).

[98] H. Noda, Y. Seki, and Y. Iino, Next-generation bems technologies realizing comprehensive energy management of groups of buildings, *Toshiba Review*, **67**(9), 7–10 (2012) (in Japanese).

[99] K. Ogawa, K. Ishikawa, A. Yokoyama, T. Shinji, , Y. Watanabe, and K. Suzawa, Optimal equipment capacity and operation of district heating and cooling system for lfc regulating capacity, In *Proc. 2013 Annual Conference of IEEJ*, pp. 123–124, 2013 (in Japanese).

[100] M. O'Malley and B. Kroposki, Energy comes together: The integration of all systems, *IEEE Power & Energy Magazine*, **11**(5), 18–23 (2013).

[101] A. J. Osiadacz, *Simulation and Analysis of Gas Networks* (E. F. N. Spon, 1987).

[102] T. S. Pedersen, P. Andersen, K. M. Nielsen, H. L. Starmose, and P. D. Pedersen, Using heat pump energy storages in the power grid, In *Proc. the 2011 IEEE International Conference on Control Applications*, pp. 1106–1111, 2011.

[103] C. D. Persis, T. N. Jensen, R. Ortega, and R. Wisniewski, Output regulation of large-scale hydraulic networks, *IEEE Transactions on Control Systems Technology*, **22**(1), 238–245 (2014).

[104] C. D. Persis and C. S. Kallesoe, Pressure regulation in nonlinear hydraulic networks by positive and quantized controls, *IEEE Transactions on Control Systems Technology*, **19**(6), 1371–1383 (2011).

[105] M. Pirouti, *Modelling and Analysis of a District Heating Network* (PhD thesis, Cardiff University, 2013).

[106] R. Podmore, Identification of coherent generators for dynamic equivalents, *IEEE Transactions on Power Apparatus and Systems*, **PAS-97**(4), 1344–1354 (1978).

[107] C. Pozrikidis, *An Introduction to Grids, Graphs, and Networks* (Oxford University Press, 2014).

[108] J. Principe and R. Codina, Mathematical models for thermally coupled low speed flows, *Advances in Theoretical and Applied Mechanics*, **2**, 93–112 (2009).

[109] Y. G. Rebours, D. S. Kirschen, M. Trotignon, and S. Rossignol, A survey of frequency and voltage control ancillary services—part I: Technical features, *IEEE Transactions on Power Systems*, **22**(1), 350–357 (2007).

[110] B. Rezaie and M. A. Rosen, District heating and cooling: Review of technology and potential enhancements, *Applied Energy*, **93**, 2–10 (2012).

[111] W. I. Rowen, Simplified mathematical representations of heavy-duty gas turbines, *Journal of Engineering for Power*, **105**(4), 865–869 (1983).

[112] S. Sanaye, M. A. Meybodi, and S. Shokrollahi, Selecting the prime movers and nominal powers in combined heat and power systems, *Applied Thermal Engineering*, **28**(10), 1177–1188 (2008).

[113] S. Sastry, *Nonlinear Systems: Analysis, Stability, and Control* (Springer-Verlag, 1999).

[114] P. W. Sauer and M. A. Pai, *Power System Dynamics and Stability* (Prentice-Hall, 1997).

[115] R. Sepulchre, M. Janković, and P. K. Kokotović, *Constructive Nonlinear Control* (Springer-Verlag, 1997).

[116] M. Shahidehpour, Y. Fu, and T. Wideman, Impact of natural gas inflastracture of electric power systems, *Proceedings of the IEEE*, **93**(5), 1042–1056 (2005).

[117] SHASE, *Planning, Design, and Operation of City-Gas Cogeneration* (Maruzen, 2015) (in Japanese).

[118] T. Shinji, T. Sekine, A. Akisawa, T. Kashiwagi, G. Fujita, and M. Matsubara, Reduction of power fluctuation by distributed generation in micro grid, *Electrical Engineering in Japan*, **163**(2), 22–29 (2008).

[119] Y. Susuki, I. Mezić, and T. Hikihara, Global swing instability of multimachine power systems, In *Proc. the 47th IEEE Conference on Decision and Control*, pp. 2487–2492, 2008.

[120] Y. Susuki, I. Mezić, and T. Hikihara, Coherent swing instability of power grids, *Journal of Nonlinear Science*, **21**(3), 403–439 (2011).

[121] TGESC, Shibaura district heating and cooling center, [Online]. Available: `http://www.energy-advance.co.jp/business/smartenergy/area/shibaura.html`. [Accessed: 13-Jan-2017].

[122] P. D. Toit, I. Mezić, and J. Marsden, Coupled oscillator models with no scale separation, *Physica D: Nonlinear Phenomena*, **238**(5), 490–501 (2009).

[123] D. P. Traviss, A. G. Baron, and W. M. Rohsenow, Forced-convection condensation inside tubes, Technical Report 74, Massachusetts Institute of Technology, Heat Transfer Laboratory, 1971.

[124] Y. Ueda, T. Enomoto, and H. B. Stewart, Chaotic transients and fractal structures governing coupled swing dynamics, In J. H. Kim and J. Stringer, editors, *Applied Chaos*, pp. 207–218 (John Wiley & Sons, 1992).

[125] Y. Ueda, Y. Ueda, H. B. Stewart, and R. H. Abraham, Nonlinear resonance in basin portraits of two coupled swings under periodic forcing, *International Journal of Bifurcation and Chaos*, **8**(6), 1183–1197 (1998).

[126] M. P. Verma, Steam transport simulation in a geothermal pipeline network constrained by internally consistent thermodynamic properties of water, *Revista Mexicana de Ciencias Geológicas*, **30**(1), 210–221 (2013).

[127] C. Wen and B. Ydstie, Passivity based control of drum boiler, In *Proc. the 2009 American Control Conference*, pp. 1586–1591, 2009.

[128] S. Wiggins, *Introduction to Applied Nonlinear Dynamical Systems and Chaos*, 2nd edition (Springer-Verlag, 2003).

[129] S. Wiggins, *Normally Hyperbolic Invariant Manifolds in Dynamical Systems* (Springer-Verlag, 1994).

[130] J. R. Winkelman, J. H. Chow, B. C. Bowler, B. Avramovic, and P. V. Kokotovic, An analysis of interarea dynamics of multi-machine systems, *IEEE Transactions on Power Apparatus and Systems*, **PAS-100**(2), 754–763 (1981).

[131] J. R. Winkelman, J. H. Chow, J. J. Allemong, and P. V. Kokotovic, Multi-time-scale analysis of a power system, *Automatica*, **16**(1), 35–43 (1980).

[132] Wolfram, Mathematica, Avaiable: `http://www.wolfram.com/mathematica/`. [Accessed: 10-Feb-2017].

[133] A. J. Wood, B. F. Wollenberg, and G. B. Sheblé, *Power Generation, Operation, and Control*, 3rd edition (John Wiley & Sons, 2014).

[134] Y. Xing, A. Bagdanavicius, S. Lannon, M. Pirouti, and T. Bassett, Low temperature district heating network planning with focus on distribution energy losses, In *Proc. International Conference on Applied Energy*, pp. 1–10, 2012.

[135] Y. Yamasaki, D. Kobayashi, K. Ushijima, and S. Kaneko, Application of gas engines to compensation of power fluctuation from renewable energy generations, *Transactions of the JSME, Ser. B*, **79**(806), 264–274 (2013) (in Japanese).

[136] R. Yokoyama, K. Ito, and Y. Matsumoto, Optimal sizing of a gas turbine cogeneration plant in consideration of its operational strategy, *Journal of Engineering for Gas Turbines and Power*, **116**(1), 32–38 (1994).

[137] A. Zlotnik, M. Chertkov, and S. Backhaus, Optimal control of transient flow in natural gas networks, In *Proc. the 54th IEEE Conference on Decision and Control*, pp. 4563–4570, 2015.

[138] A. Zlotnik, L. Roald, S. Backhaus, M. Chertkov, and G. Andersson, Coordinated scheduling for interdependent electric power and natural gas infrastructures, *IEEE Transactions on Power Systems*, **32**(1), 600–610 (2017).

List of Publications

Journal articles

- H. Hoshino, Y. Susuki, and T. Hikihara, Stability of two-sites regional power and heat supply system: Numerical simulations under step change of heat transfer reference, *Transactions of ISCIE*, **27**(11), 452–460 (2014) (in Japanese).

- H. Hoshino, Y. Susuki, and T. Hikihara, A lumped-parameter model of multiscale dynamics in steam supply systems, *Journal of Computational and Nonlinear Dynamics*, **11**(6), 061018 (2016).

- H. Hoshino, Y. Susuki, T. J. Koo, and T. Hikihara, Nonlinear control of combined heat and power plants in a two-site regional energy system: Simultaneous regulation of electricity and gas flows, *Transactions of ISCIE*, **30**(5) (2017) (to appear).

- H. Hoshino, Y. Susuki, T. J. Koo, and T. Hikihara, Feedback stabilization and tracking of energy flows in two-site electricity and heat supply system (in preparation).

International conference proceedings

- H. Hoshino, Y. Susuki, and T. Hikihara, A nonlinear dynamical model of two-sites electricity and heat supply system, In *Proceedings of the 2014 International Symposium on Nonlinear Theory and its Applications*, pp.482–485, Luzern, Switzerland, September 14-18, 2014.

- H. Hoshino and Y. Susuki, Graph-based modeling and analysis of dynamic flows in steam supply networks, In *Proceedings of the 54th IEEE Conference on Decision and Control*, pp.1358-1363, Osaka, Japan, December 15–18, 2015.

- H. Hoshino, Y. Susuki, and T. Hikihara, Basins of attraction of steady operating conditions in a two-site electricity and heat supply system, In *Proceedings of the 2016 International Symposium on Nonlinear Theory and its Applications*, pp.675–678, Yugawara, Japan, November 27–30, 2016.

Conference presentations

- H. Hoshino and Y.Susuki, A dynamical analysis of steam supply network based on invariant manifold, In *the 2015 SIAM Conference on Applications of Dynamical Systems*, Part of PP1, Snowbird, Uta, USA, May 17-21, 2015.

Domestic conference proceedings

- H. Hoshino, Y. Susuki, and T. Hikihara, A study on dynamic model of heat transfer in power and heat supply system, In *Proceedings of the 13th SICE Annual Conference on Control Systems*, PS-025, Fukuoka, March 6, 2013 (in Japanese).

- H. Hoshino, Y. Susuki, and T. Hikihara, Numerical studies on dynamical model of regional power and heat supply system, *Technical Report of IEICE*, NLP2013-04, Aichi, April 25, 2013 (in Japanese).

- H. Hoshino, Y. Susuki, and T. Hikihara, Stability analysis of regional power and heat supply system with dynamic model of gas turbine, In *Proceedings of the 2013 Annual Conference of Power and Energy Society, IEEJ*, P13, Nigata, August 27, 2013 (in Japanese).

- H. Hoshino, Y. Susuki, and T. Hikihara, A study on dynamic model of heat transfer in power and heat supply system, In *Proceedings of the 1st Multi-symposium on Control Systems*, 5B2-5, Tokyo, March 5, 2014 (in Japanese).

- H. Hoshino, Y. Susuki, and T. Hikihara, A numerical study on regional supply of electricity and heat using dynamic model of heat transfer, In *Proceedings of the 58th Annual Conference of the ISCIE*, 324-3, Kyoto, May 23, 2014 (in Japanese).

- H. Hoshino, Y. Susuki, and T. Hikihara, A dynamical analysis of heat transfer in electricity and heat supply system, *Technical Report of IEICE*, NLP2014-39, Hokkaido, July 22, 2014.

- H. Hoshino and Y. Susuki, A study on stability of steam supply networks by graph-based representation, *Technical Report of IEICE*, NLP2014-120, Oita, January 26, 2015 (in Japanese).

- H. Hoshino, Y. Susuki, and T. Hikihara, A verification study of lumped-parameter model for steam flows between multiple boilers, In *Proceedings of the 2015 Annual Conference of JSME*, G0800303, Hokkaido, September 15, 2015 (in Japanese).

- H. Hoshino, Y. Susuki, T. J. Koo, and T. Hikihara, On the zero dynamics of a two-site electricity and heat supply system, In *Proceedings of the 58th Japan Joint Automatic Control Conference*, 2E2-1, Hyogo, November 15, 2015.

- H. Hoshino, Y. Susuki, T. J. Koo, and T. Hikihara, A controller design of a two-site electricity and heat supply system, In *Proceedings of the 60th Annual Conference of the ISCIE*, 141-4, Kyoto, May 25, 2016.

- H. Hoshino, Y. Susuki, T. J. Koo, and T. Hikihara, A study on tracking control of energy flows in two-site electricity and heat supply system, In *Proceedings of the 58th Japan Joint Automatic Control Conference*, SaA2-4, Fukuoka, November 12, 2016 (in Japanese).

- H. Hoshino, Y. Susuki, T. J. Koo, and T. Hikihara, Simultaneous regulation of electricity and heat flows in two-site electricity and heat supply system, In *Proceedings of the 2016 SICE Annual Conference on Systems and Information*, SS12-1, Shiga, December 6, 2016 (in Japanese).